TOUGHENING OF EPOXIES BASED ON SELF-ASSEMBLY OF NANO-SIZED AMPHIPHILIC BLOCK COPOLYMER MICELLES

A Dissertation

by

JIA LIU

Submitted to the Office of Graduate Studies of
Texas A&M University
in partial fulfillment of the requirements for the degree of

DOCTOR OF PHILOSOPHY

May 2009

Major Subject: Materials Science and Engineering

TOUGHENING OF EPOXIES BASED ON SELF-ASSEMBLY OF NANO-SIZED AMPHIPHILIC BLOCK COPOLYMER MICELLES

A Dissertation

by

JIA LIU

Submitted to the Office of Graduate Studies of
Texas A&M University
in partial fulfillment of the requirements for the degree of

DOCTOR OF PHILOSOPHY

Approved by:

Chair of Committee,	Hung-Jue Sue
Committee Members,	Abraham Clearfield
	Terry S. Creasy
	Hong Liang
Chair of Interdisciplinary Faculty,	Tahir Cagin

May 2009

Major Subject: Materials Science and Engineering

ABSTRACT

Toughening of Epoxies Based on Self-Assembly of Nano-Sized Amphiphilic Block Copolymer Micelles. (May 2009)

Jia Liu, B.S., Fudan University;

M.Phil., The Hong Kong University of Science and Technology

Chair of Advisory Committee: Dr. Hung-Jue Sue

As a part of a larger effort towards the fundamental understanding of mechanical behaviors of polymers toughened by nanoparticles, this dissertation focuses on the structure-property relationship of epoxies modified with nano-sized poly(ethylene-*alt*-propylene)-*b*-poly(ethylene oxide) (PEP-PEO) block copolymer (BCP) micelle particles. The amphiphilic BCP toughener was incorporated into a liquid epoxy resin and self-assembled into well-dispersed 15 nm spherical micelle particles. The nano-sized BCP, at 5 wt% loading, can significantly improve the fracture toughness of epoxy (ca. 180% improvement) without reducing modulus at room temperature and exhibits only a slight drop (ca. 5 °C) in glass transition temperature (T_g). The toughening mechanisms were found to be BCP micelle nanoparticle cavitation, followed by matrix shear banding, which mainly accounted for the observed remarkable toughening effect. The unexpected "nano-cavitation" phenomenon cannot be predicted by existing physical models. The plausible causes for the observed nano-scale cavitation and other mechanical behaviors may include the unique structural characteristics of BCP micelles and the influence from the surrounding epoxy network, which is significantly modified by the epoxy-miscible PEO block. Other mechanisms, such as crack tip blunting, may also play a role in the

toughening. Structure-property relationships of this nano-domain modified polymer are discussed. In addition, other important factors, such as strain rate dependence and matrix crosslink density effect on toughening, have been investigated. This BCP toughening approach and conventional rubber toughening techniques are compared. Insights on the decoupling of modulus, toughness, and T_g for designing high performance thermosetting materials with desirable physical and mechanical properties are discussed.

To
my mother Yuqin Jiang
姜玉琴
and
my father Yinglong Liu
劉應龍

ACKNOWLEDGEMENTS

First of all, I would like to give my greatest gratitude to my advisor, Prof. Hung-Jue Sue, for his inspiration, guidance and encouragement over the entire course of my Ph.D. program. His endless energy and enthusiasm for research create an excellent environment that leads me to work independently and productively on many interesting topics. I also thank my committee members, Profs. Abraham Clearfield, Terry Creasy and Hong Liang, for their valuable advice and support.

This research project is also a good example of teamwork. I am really grateful to the people that I have collaborated with, without whom my dissertation would not have been possible. They are Prof. Frank Bates at Department of Chemical Engineering and Materials Science at University of Minnesota, and his Ph.D. student Mr. Zach Thompson. We also worked closely with the research scientists and engineers from the Epoxy R&D Group at The Dow Chemical Company, including Drs. Marv Dettloff, George Jacob, Nikhil Verghese and Ha Pham. I have enjoyed working with each one of you.

Special acknowledgements are given to Prof. Andreas Holzenburg and Ms. Ann Ellis from the Microscopy and Imaging Center at Texas A&M University, for their tremendous help in the use of their microscopy equipment.

I also would like to thank many former and current colleagues in our group, including Drs. Jong-Il Weon, Woong-Jae Boo and Luyi Sun, Mr. Han Jiang, Mr. Dazhi Sun, Mr. Ehsan Moghbelli and Mr. Chaochen Wei. It has been an enjoyable and unforgettable experience working together with these people. I really appreciate the professional and personal friendship formed with them.

Last but not least, I want to express my sincere thankfulness to my beloved parents for their long-term support and unconditional love throughout my life. I dedicate this dissertation to you and I hope I will merit your faith in me in my future career.

TABLE OF CONTENTS

Page

ABSTRACT iii

DEDICATION v

ACKNOWLEDGEMENTS vi

TABLE OF CONTENTS viii

LIST OF TABLES xi

LIST OF FIGURES xii

CHAPTER

I INTRODUCTION 1

1.1 Background 1
1.2 Epoxies Modified with Self-Assembled BCP Micelles 1
1.3 Research Objectives and Significance 2
1.4 Dissertation Layout 4

II LITERATURE REVIEW 6

2.1 Polymer Toughening Principles 6
2.2 Self-Assembly of BCP for Epoxy Toughening 15

III TOUGHENING MECHANISMS IN EPOXIES CONTAINING NANO-SIZED BLOCK COPOLYMER MICELLES 26

3.1 Introduction 26
3.2 Experimental 27
3.2.1 Materials 27
3.2.2 Preparation of BCP-Modified Epoxy 28
3.2.3 Morphology Characterization 30
3.2.4 Density Measurements 30
3.2.5 Mechanical Property Measurements 31
3.2.6 Investigation of Fracture Mechanisms 32
3.3 Results 35
3.3.1 Morphology of BCP-Toughened Epoxy 35
3.3.2 Dynamic Mechanical Behavior 35
3.3.3 Tensile Behavior 40

CHAPTER Page

3.3.4 Fracture Toughness Measurements 41
3.3.5 Toughening Mechanisms Studies 43
3.4 Discussion 51
3.4.1 Criterion for Rubber Particle Cavitation 51
3.4.2 Nano-Cavitation Phenomenon in BCP-Toughened Epoxy 56
3.4.3 Other Toughening Mechanisms 61
3.4.4 Implication of the Present Findings 61
3.5 Summary 64

IV CROSSLINK DENSITY EFFECT ON FRACTURE BEHAVIOR OF EPOXIES CONTAINING NANO-SIZED BLOCK COPOLYMER MICELLES 65

4.1 Introduction 65
4.2 Experimental 67
4.2.1 Materials 67
4.2.2 Preparation of BCP-Modified Epoxy Resin 69
4.2.3 Density Measurement 71
4.2.4 Dynamic Mechanical Analysis (DMA) 71
4.2.5 Fracture Toughness Measurement 72
4.2.6 Toughening Mechanisms Investigation 72
4.3 Results and Discussion 73
4.3.1 Dynamic Mechanical Behavior 73
4.3.2 Determination of Crosslink Density 78
4.3.3 Fracture Toughness Measurement 82
4.3.4 Crosslink Density Effect on Toughening Mechanisms 84
4.3.5 Implications of the Present Work 92
4.4 Summary 93

V STRAIN RATE EFFECT ON MECHANICAL PROPERTIES OF EPOXIES CONTAINING NANO-SIZED BLOCK COPOLYMER MICELLES 95

5.1 Introduction 95
5.2 Experimental 97
5.2.1 Materials 97
5.2.2 Preparation of BCP-Modified Epoxy 98
5.2.3 Dynamic Mechanical Analysis (DMA) 98
5.2.4 Transmission Electron Microscopy (TEM) 99
5.2.5 Fracture Toughness Measurements 99
5.2.6 Scanning Electron Microscopy (SEM) 100
5.2.7 Double-Notch Four-Point-Bending (DN-4PB) Test 100
5.2.8 Tensile Tests 101
5.3 Results and Discussion 102
5.3.1 Morphology of BCP-Toughened Epoxy 102

CHAPTER Page

5.3.2 Viscoelastic Damping Characteristics 103
5.3.3 Fracture Behavior 104
5.3.4 Strain Rate Effect on Mechanical Properties and Toughening Mechanisms 116
5.3.5 Effect of PEO Block on Epoxy Properties 131
5.4 Summary 133

VI CONCLUSIONS AND RECOMMENDATIONS 135

6.1 Concluding Remarks 135
6.1.1 Epoxy Toughening with Nano-Sized Block Copolymer (BCP) Micelles 135
6.1.2 Toughening Mechanisms in Epoxies Containing Nano-Sized BCP Micelles 135
6.1.3 Crosslink Density Effect on Fracture Behavior of Epoxies Containing Nano-Sized BCP Micelles 136
6.1.4 Strain Rate Effect on Mechanical Properties of Epoxies Containing Nano-Sized BCP Micelles 137
6.2 Recommendations and Challenges for Future Work 138
6.2.1 Other Important Factors in Epoxy Toughening 138
6.2.2 Localized Interactions at Interface/Interphase 139
6.2.3 Mechanics in Nanometer Scales 140
6.2.4 Applications of Nano-Toughening Technique in Other Matrices 141

REFERENCES 142

VITA 154

LIST OF TABLES

TABLE Page

2.1 Examples of available toughening mechanisms in polymers 7

3.1 Storage modulus, T_g and fracture toughness values of neat epoxy and BCP-toughened epoxy 36

3.2 Young's modulus and yield stress values of neat epoxy and BCP-toughened epoxy 40

4.1 Chemical structures of epoxy resin, chain extender, crosslinker and block copolymer used in this investigation 68

4.2 Storage modulus (E'), glass transition temperature (T_g) and fracture toughness (K_{IC}) of the samples 76

4.3 Density and molecular weight between crosslinks (M_c) of the model epoxy systems 80

5.1 Fracture toughness (MPa•m$^{1/2}$) of neat epoxy and BCP-toughened epoxy at different test rates 105

5.2 Young's modulus and yield stress values of BCP-toughened epoxy specimens at different tensile test rates 128

LIST OF FIGURES

FIGURE Page

2.1 Crack toughening mechanisms in rubber-filled epoxies: (1) shear band formation near rubber particles; (2) fracture of rubber particles after cavitation; (3) stretching, (4) debonding and (5) tearing of rubber particles; (6) transparticle fracture; (7) debonding of hard particles; (8) crack deflection by hard particles; (9) voided/ cavitated rubber particles; (10) crazing; (11) plastic zone at craze tip; (12) diffuse shear yielding; (13) shear band/craze interaction 14

2.2 Illustrations of (a) structure of BCP and (b) phase separation of amphiphilic BCP in solutions or homopolymer blends..... 17

2.3 Phase morphologies of ordered BCP in the neat state 19

2.4 TEM image of epoxy/PEO-PEP (52 wt%) blend. The inset provides an interpretation of the morphology: cylindrical PEP cores surrounded by PEO shells, enclosed by the epoxy matrix..... 19

2.5 Disordered morphologies of self-assembled BCP in epoxy: spherical micelles, wormlike micelles, and vesicles..... 20

2.6 TEM images of epoxy/PBO-PEO (5 wt%) blends with three disordered morphologies: (a) vesicles, (b) wormlike micelles, and (c) spherical micelles 20

2.7 Schematics of proposed fracture process associated with the epoxies modified by (a) spherical micelles, (b) wormlike micelles, and (c) vesicles..... 24

3.1 Schematics of (a) a DN-4PB specimen and (b) microscopy study on a DN-4PB specimen. The arrested subcritical crack tip damage zone from the core region was examined by OM and TEM 33

3.2 Nano-structured morphology of BCP-toughened epoxy: TEM micrographs at (a) low magnification and (b) high magnification, and a schematic illustration (c). The amphiphilic BCP consists of an epoxy-miscible PEO block and an epoxy-immiscible PEP block and forms as spherical micelles with an average diameter of 15 nm. The BCP phase was stained by RuO_4 prior to the TEM observation and shows a darker color in the micrographs 37

3.3 DMA plots of neat epoxy and BCP-toughened epoxy. Storage modulus (*E'*) and tan δ curves are presented. The temperature maximum peak in the tan δ curve is recorded as glass transition temperature (T_g). The storage modulus and T_g values are summarized in Table 3.1 38

FIGURE Page

3.4 Engineering stress-strain curves of neat epoxy and BCP-toughened epoxy. The Young's modulus and yield stress values are summarized in Table 3.2 41

3.5 Fracture surfaces of (a) neat epoxy and (b) BCP-toughened epoxy after SEN-3PB tests. A stress-whitening zone was clearly observed in front of the initial crack, as seen in (b). The red dashed lines represent the initial crack marks 42

3.6 OM images of the BCP-toughened epoxy DN-4PB specimen with the subcritical crack tip damage zone at (a) bright field and (b) cross-polarized light field. The crack propagates from left to right. The images were taken at the same location ... 43

3.7 TEM micrographs of the BCP-toughened epoxy DN-4PB specimen at different locations: (a) adjacent to the crack wake, (b) some distance (in a range of 0.8-1.6 μm) from the crack wake, and (c) further away (more than 1.6 μm) from the crack wake. Insets demonstrate the spots where TEM micrographs were taken for each case. The BCP phase was stained by RuO_4 prior to the TEM observation 47

3.8 An illustration of the sequence of cavitation-induced shear banding process as one of the toughening mechanisms in BCP-toughened epoxy. (a) initiation of a starting crack; (b) formation of a BCP cavitation zone at the crack tip when the specimen is loaded; (c) expansion of the cavitation zone and initiation of a matrix shear banding zone at the crack tip when the hydrostatic stress is relieved by the cavitation; (d) crack propagates when the shear strain energy builds up to a critical value, with a damage zone surrounding the crack. The sizes of the crack, cavitation and shear banding zone are not drawn to scale 50

3.9 Calculated potential energy of a cavitated rubber particle as a function of the reduced radius of cavity, *r/R*, based on Lazzeri and Bucknall's energy balance model, at rubber particle volume strains of Δ_{V0} = (a) 0.004, (b) 0.03, and (c) 0.2, respectively. The curves were generated using Equation 10 with various particle radii *R* (in μm) and *G* = 0.4 MPa, *K* = 2000 MPa, $\Gamma = 0.03$ Nm^{-1}, $\rho = 1.0$ and $F(\lambda_f) = 1.0$ 53

3.10 Schematic illustration of the cavitation processes based on (a) Lazzeri and Bucknall's model[71] and (b) the present work. Lazzeri and Bucknall neglected the energy contribution from the pre-existence of transient nanovoids within rubber particles, while that part has to be considered when dealing with nanometer-sized particles 58

3.11 Schematic illustration of the two different expansion processes in (a) an ideal rubber particle and (b) a BCP micelle particle. The size expansion of the voids and the particles are not drawn to scale 60

FIGURE Page

4.1 Scheme of chain extension and crosslinking reactions in the present epoxy curing process 70

4.2 DMA spectra of (a) neat epoxies and (b) BCP-modified epoxies with different crosslink densities. The storage modulus (E') and glass transition temperature (T_g) values are summarized in Table 4.2 74

4.3 Correlations of theoretical M_c and experimental M_c estimated using (a) rubber elasticity equation and (b) Nielsen and Timm's equation, for the neat and modified epoxies in this study 81

4.4 Fracture toughness, K_{IC}, plotted against the matrix M_c for two sets of neat and modified epoxy resins: the ones in the present work (□ unmodified and ■ 5 wt% BCP-modified) and in the work done by Sue et al.[17] (△ unmodified and ▲ 5 wt% CSR-modified). The experimental estimated M_c data of the CSR system were reprocessed using Equation (4.1) from the rubber elasticity theory 83

4.5 OM images of subcritical crack tip regions in CET900/BCP (a,b), CET1550/ BCP (c,d) and CET2870/BCP (e,f), respectively. All the cracks propagate from left to right. The images were taken under both bright (a,c,e) and cross-polarized (b,d,f) fields at same location for each example 85

4.6 TEM micrographs taken in the vicinity of subcritical crack tips in (a) CET900/ BCP, (b) CET1550/BCP and (c) CET2870/BCP, respectively. The specimen thin-sections were stained using 0.5% RuO_4 aqueous solution prior to TEM imaging. The crack propagating directions are indicated in the images. In the CET2870/BCP image, the arrows point to the BCP nanoparticles that are severely stretched 89

5.1 TEM micrograph showing the spherical micellar morphology of BCP phase in epoxy matrix 102

5.2 Tan δ traces of neat epoxy and BCP-toughened epoxy in a region leading up to their T_g 104

5.3 Fracture surfaces of BCP-toughened epoxy specimens after the SEN-3PB tests at test rates of (a) 0.51 mm/min, (b) 15.24 mm/min, and (c) 508 mm/min, respectively. The red dashed lines represent the initial crack fronts and the crack propagated from top to bottom 106

5.4 SEM micrographs showing the fracture surface of BCP-toughened epoxy fractured at 0.51 mm/min at a magnification of (a) 150× and (b) 600×. The insets show the spots where the micrographs were taken. The blue dashed lines represent the initial crack fronts and the crack propagates from left to right 108

FIGURE Page

5.5 SEM micrographs showing the fracture surface of BCP-toughened epoxy fractured at 15.24 mm/min at a magnification of (a) 150× and (b) 600×. The insets show the spots where the micrographs were taken. The blue dashed lines represent the initial crack fronts and the crack propagates from left to right..... 110

5.6 SEM micrographs showing the fracture surface of BCP-toughened epoxy fractured at 508 mm/min at a magnification of (a) 150× and (b) 600×. The insets show the spots where the micrographs were taken. The blue dashed lines represent the initial crack fronts and the crack propagates from left to right..... 112

5.7 SEM micrographs showing the fracture surface of neat epoxy fractured at 0.51 mm/min at a magnification of (a) 150× and (b) 600×. The insets show the spots where the micrographs were taken. The red dashed lines represent the initial crack fronts and the crack propagates from left to right..... 114

5.8 OM images showing the subcritical crack tip damage zones of BCP-toughened epoxy specimens after the DN-4PB tests at different rates of (a) 0.51 mm/min, (b) 15.24 mm/min, and (c) 508 mm/min. The crack propagates from left to right in each case..... 117

5.9 TEM micrographs of BCP-toughened epoxy after DN-4PB test at 0.51 mm/min at locations (a) close to the crack tip and (b) some distance away from the crack. The insets show the spots where the micrographs were taken. The arrows indicate the crack propagation direction 120

5.10 TEM micrographs of BCP-toughened epoxy after DN-4PB test at 15.24 mm/min at locations (a) close to the crack tip and (b) some distance away from the crack. The insets show the spots where the micrographs were taken. The arrows indicate the crack propagation direction 122

5.11 TEM micrographs of BCP-toughened epoxy after DN-4PB test at 508 mm/min at locations (a) close to the crack tip and (b) some distance away from the crack. The insets show the spots where the micrographs were taken. The arrows indicate the crack propagation direction 124

5.12 Stress-strain curves of BCP-toughened epoxy specimens at tensile test rates of 0.51, 5.08, 50.8 and 508 mm/min..... 127

5.13 Schematic of stable-unstable transitions in mechanical behavior of toughened plastics as test rate increases 129

5.14 Fracture toughness, K_{IC}, plotted against loading rate for two sets of neat and toughened epoxies: the ones in the present work (■ unmodified and ■ 5 wt% BCP-modified), and in Ref. 50 (△ unmodified and △ 12.5 wt% CTBN-modified) 131

FIGURE Page

6.1 (a) Illustration of swelling-induced change in the interfacial curvature for PEP-PEO and epoxy blends. PEO blocks extend from the neat PEO/PEP interface as a “dry brush”. Epoxy selectively swells the PEO brush, creating a “wet brush” and the PEO/PEP interface curves to accommodate this change within the constraint of constant density while minimizing PEP and PEO chain distortions. (b) Illustration of PEO block expulsion as the epoxy matrix crosslinks and its molecular weight diverges. The system initially has a curved interface due to selective swelling of the PEO blocks by the epoxy. As the epoxy cures, the PEO blocks are expelled, transforming the “wet brush” to a “dry brush”, thereby reducing the interfacial curvature..... 140

CHAPTER I

INTRODUCTION

1.1. Background

Nanotechnologies present tremendous potential for the polymer industry. Among the several possibilities, polymer nanocomposites that contain either inorganic nano-particles, organic nano-domains, or both, exhibit many promising properties that are suitable for various engineering and microelectronic applications.[1] However, fundamental knowledge regarding the "nano-scale" phenomena is still lacking. Significant efforts are still needed. This dissertation focuses on epoxies containing amphiphilic block copolymer (BCP) nanoparticles as a model system to understand their structure-property relationship.

1.2. Epoxies Modified with Self-Assembled BCP Micelles

Epoxies are one of the most versatile classes of polymers with diverse applications.[2] However, one serious flaw of epoxies is their inherent brittleness which can greatly limit their commercial applications. Epoxy toughening has been an interesting and challenging topic for over four decades. Significant efforts have been undertaken on epoxies toughened with micrometer-sized liquid rubbers,[3-8] core-shell

---

The dissertation follows the style of *Macromolecules*.

rubber (CSR) particles,[9-20] and thermoplastic particles.[21-31]

In recent years, a new epoxy toughening approach using self-assembled amphiphilic BCP has drawn significant attention.[32-41] Bates and coworkers[32-34, 38, 42-48] discovered that amphiphilic BCPs that self assemble into micellar structures are effective as nano-domain tougheners for epoxy resins. The BCPs usually consist of an epoxy-miscible block and an epoxy-immiscible block. In epoxy resins BCPs can self-assemble into well-defined micro/nano-structures in the form of spherical micelles, worm-like micelles, or vesicles, depending on their molecular weight, block length, and composition. Adding a small amount ($\leq$ 5 wt%) of such BCPs has been shown to give remarkable improvement in fracture toughness. Mechanisms like debonding, cavitation, crack deflection were proposed to account for the toughening, but no direct experimental evidence was reported.[38] Similar work on triblock copolymer toughened epoxies has also been reported recently.[36, 41] However, the toughening mechanisms responsible for such toughening effect are still unknown.

1.3. Research Objectives and Significance

The objective of this research is to fundamentally investigate the structure-property relationships of nano-domain modified polymer systems *via* the studies of toughened epoxies based on amphiphilic nano-sized BCP micelle particles. The goal of the research is to gain an understanding of the following:

(a) The structural/physical/mechanical characteristics of the materials using transmission electron microscopy (TEM), dynamic mechanical analysis (DMA), tensile test, and fracture toughness measurement;

(b) The fracture and toughening mechanisms of the materials *via* double-notch four-point bending (DN-4PB) technique;

(c) The effects from other important factors, such as strain rate dependence and matrix crosslink density effect, etc.;

(d) Implications of the present findings for designing high performance toughened polymers and comparisons with conventional toughening methods.

It is expected that the present work will contribute significantly to the fundamental understanding of the structure-property relationship of polymers containing nano-domains, including the understanding of nano-structure characteristics, interface/interphase, etc. In addition, significant insights will be given to the fundamental understanding of polymer toughening, including novel nano-toughening technique, toughening mechanism study, matrix effect, strain rate effect, etc.

1.4. Dissertation Layout

To further introduce the background of this research, two compendious literature reviews of self-assembly of amphiphilic BCPs in epoxy and toughening principles for polymers are included in Chapter II.

A new epoxy toughening method based on self-assembly of nano-sized BCP micelle particles is laid out in Chapter III. The structural, physical**,** and mechanical characteristics of the materials, and more importantly, their fracture and toughening mechanisms, are discussed in this chapter. An explanation of possible reasons responsible for remarkable mechanical property improvements and a unique "nano-cavitation" phenomenon is also given.

In Chapter IV, the emphasis is placed on the effect of matrix crosslink density on toughening. Specifically, the crosslink density of epoxy resins is varied *via* a controlled epoxy thermoset technology to study their mechanical behaviors. It is found that the "toughenability" of epoxy resins is strongly dependent on the intrinsic ductility of the matrix.

Another important factor, the strain rate effect on mechanical properties, is addressed in Chapter V. It is found that BCP-modified epoxies exhibit a stronger rate dependence than the neat epoxy and epoxies toughened by other toughening agents. The effects of strain rate on toughening mechanisms are discussed in this chapter based on unambiguous experimental findings. Extreme care is suggested for the application of this material if high rate performance is of primary concern.

Finally, an overall conclusion of this research is made in Chapter VI. Additionally, recommendations of possible directions and approaches for future work are given based on the current findings. Meanwhile, challenges and concerns are pointed out.

CHAPTER II

LITERATURE REVIEW

2.1. Polymer Toughening Principles

Glassy polymers are inherently brittle if not toughened, which can greatly limit their engineering applications. Toughening of brittle polymers *via* incorporation of a dispersed elastomeric phase is well known as an effective method to improve fracture resistance and impact strength.[3-6, 8-10, 12, 13, 17, 19, 49-74] Rubber modification has been reported as an effective approach for toughening brittle epoxy thermosets since the beginning of the 1970s.[53, 75] Since then, significant work has been done to gain a better understanding of the structure-property relationship between the polymer matrix and the toughening agents for designing epoxy thermoset systems with desired properties.[3, 4, 6-10, 12, 21, 23-25, 31, 76-79]

Depending on various nature of toughening agents and host polymers, and different stress conditions materials experience, different toughening mechanism(s) may operate in a toughened system, and the toughening effects those mechanisms give may vary. Some popular polymer toughening mechanisms and their general toughening effects are summarized in Table 2.1.[80]

Table 2.1. Examples of available toughening mechanisms in polymers.[80]

Toughening Mechanism	**Toughening Effect**	**Example**
Shear banding/ yielding	Up to *an order of magnitude* improvement in fracture toughness	
Croiding	Up to *an order of magnitude* improvement in fracture toughness	
Crazing	Up to *several folds* improvement in fracture toughness	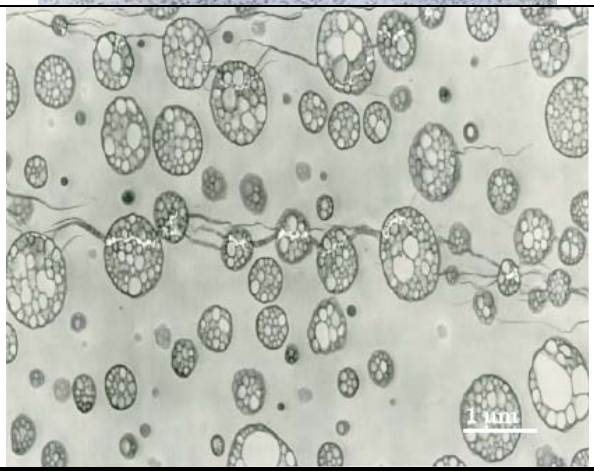

Table 2.1. Continued.

Toughening Mechanism	**Toughening Effect**	**Example**
Crack deflection/ multiple cracking	Up to *double* improvement in fracture toughness	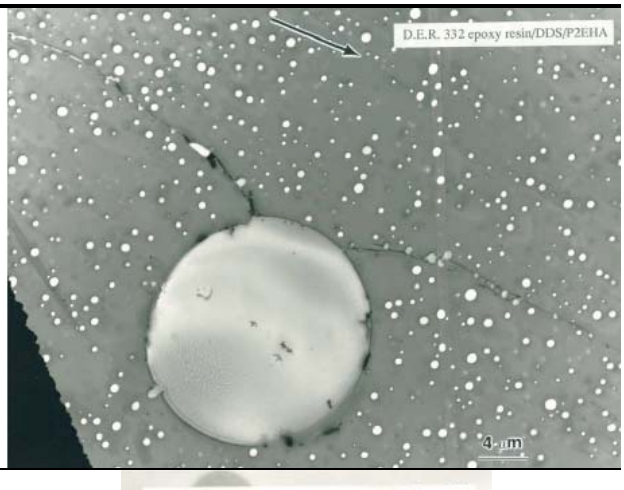
Crack bridging	*Incremental* improvement in fracture toughness	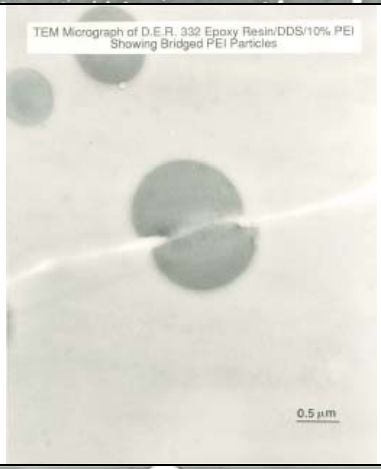
Crack bifurcation	*Fractional* improvement in fracture toughness	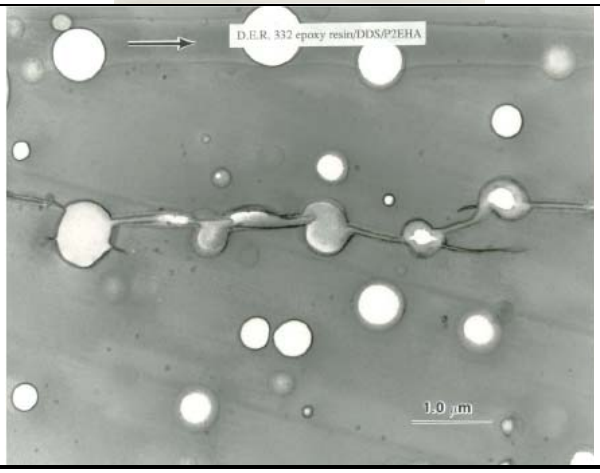

Table 2.1. Continued.

Toughening Mechanism	**Toughening Effect**	**Example**
Crack pinning	*Fractional* improvement in fracture toughness	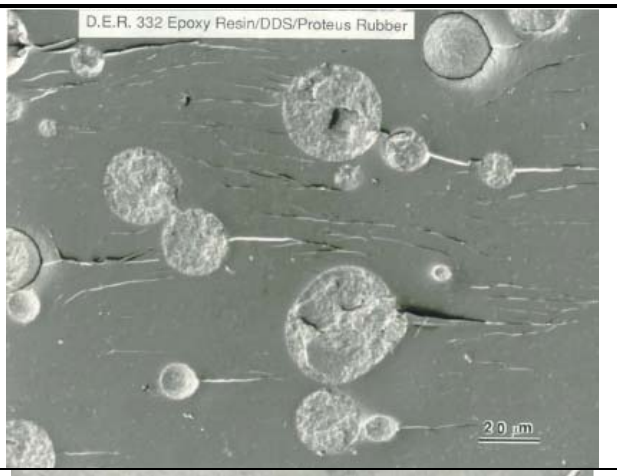
Segmental crack growth	*Fractional* improvement in fracture toughness	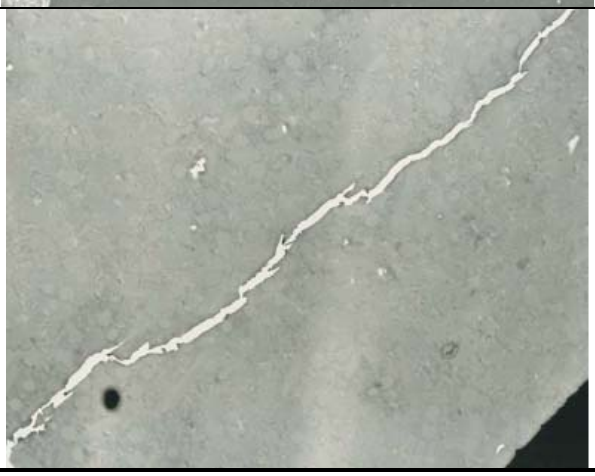

In a toughened polymer system, the roles of the toughening agent (or toughener phase) is to provide numerous effective stress concentration sites or alter the stress state the matrix experiences, and to promote one or more of those toughening mechanisms mentioned in Table 2.1, especially the most effective ones. Meanwhile, the toughener

phase has to maintain the basic physical and mechanical characteristics of the matrix. The selection of suitable toughening agents requires several considerations:

(a) The type of the rubbery phase (including cavitational strength, bulk modulus, glass transition temperature, etc.);

(b) The size of rubber particles which has to scale with the crack tip radius and the craze band width;

(c) Interface/interphase (e.g., chemical and physical bonding);

(d) The dispersion level (e.g., random *vs.* clustered);

(e) The phase morphology in matrix (e.g., continuous *vs.* co-continuous *vs.* phase inversion).

It is also necessary to note that the nature of the polymer matrix plays at least an equally important role in toughening. The considerations of the matrix properties include:

(a) Yield/brittle stress;

(b) Toughenability (e.g., shear banding *vs.* crazing, or crazing *vs.* cracking, etc.);

(c) Molecular mobility;

(d) Crosslink density and distribution for thermosets;

(e) Natural crack tip radius;

(f) Other properties such as molecular weight & molecular weight distribution, crystallinity, morphology, etc.;

(g) Stress state, rate and temperature dependence.

As one of the most effective toughening mechanisms, cavitation of the elastomeric phase has long been recognized as critical in promoting shear banding in various thermosets and thermoplastics.[3-6, 8] Cavitation of rubber particles was first observed on the fracture surfaces of rubber-toughened epoxy resins more than 30 years ago.[52] Since then, many researchers have demonstrated that the major toughening mechanisms of many rubber-modified polymers are cavitation of rubber particles, followed by shear banding of the matrix.

In rubber-modified plastics, voiding can occur inside the rubber particles under hydrostatic tension. This can be manifested by a macroscopic phenomenon of stress-whitening. Once the rubber particles cavitate, the hydrostatic tension near the cavitation sites is relieved, especially at the crack tip region. The stress state of the matrix near the voids is then transformed from a triaxial stress state to a biaxial stress state, which favors the initiation of shear bands.[3-6, 8] Thus, although cavitation in itself cannot be regarded as a significant energy-absorbing process, the real role of cavitation is to relieve the triaxial stress, thereby facilitating the matrix shear banding. Quite a number of examples in the open literature support the above concept, which include the rubber toughening of epoxy,[3-6, 8-10, 12, 17, 19, 52-57] nylon,[58-61] polycarbonate,[62-65] poly(vinyl chloride),[66-68] poly(butylene terephthalate),[69] etc.

Sultan and McGarry[53] investigated the rubber particle size effect on the fracture toughness of rubber-modified epoxies. Since then, many researchers have studied the importance of rubber particle size on toughening for a variety of polymers.[6, 13, 70-74] In the case of large particles, Pearson and Yee[6] found that particles $\geq$ 20 μm in diameter are

ineffective for toughening ductile epoxy matrices. Azimi et al.[70] later indicated that lack of interaction with the crack tip process zone is the main reason for the ineffectiveness of large rubber particles for toughening. On the other hand, for small particle sizes, Bucknall and coworkers[71-73] have proposed a model based on an energy balance concept, showing that the cavitation process in the rubber particles cannot occur with particles less than 250 nm in diameter. Experimentally, some researchers have reported that 200 nm is the lower limit of rubber particle size for effective toughening.[13, 74] On the contrary, the smallest rubber particle size that has been shown to cavitate is 100 nm based on core-shell rubber (CSR)-modified epoxy systems.[9, 10, 12, 17, 19, 55-57]

For the particular case of epoxy toughening, a summary of possible toughening events in rubber-filled epoxies is sketched in a review by Garg et al.[78] (shown in Figure 2.1). Significant efforts have been undertaken on epoxies toughened with micrometer-sized liquid rubbers,[3-8] CSR particles,[9-20] and thermoplastic particles.[21-31] The addition of rubbery toughening agents usually leads to an impressive toughening effect, but tends to cause severe deterioration in glass transition temperature (T_g), modulus, strength, and other desirable properties, such as processability due to high viscosity. One approach to improve the epoxy fracture toughness is *via* the incorporation of reactive rubber particles,[3-8] such as carboxyl-terminated butadiene acrylonitrile (CTBN), which can react with the surrounding epoxy matrix. This can improve the fracture toughness, but also sacrifices the strength and T_g. A second approach is to include non-reactive toughening modifiers, such as CSR[9-20] or thermoplastic particles.[21-31] The problem with using CSR particles is usually the difficulty in achieving a uniform dispersion in some epoxy

systems,[81] because the highly crosslinked cores usually hinder their dissolution in epoxy resins. In the case of thermoplastic particles, they typically give a moderate toughening effect and cannot produce satisfactory results for low temperatures or high rate test conditions.[21, 24] Due to this poor efficiency, high concentrations of thermoplastic particles are often used, which may have a detrimental effect on the processability because of high viscosity. Other than the use of toughening agents, another approach is through flexibilization or lowering the crosslink density of the matrix by directly reacting some monofunctional or high molecular weight difunctional molecules with epoxy monomers. Again, this method can toughen the epoxy but with the trade-off in strength and thermal properties.

Considering the concerns and deficiencies aforementioned in the current epoxy toughening technologies, there is a significant need to develop alternative toughening approaches to greatly increase the fracture resistance of brittle epoxies without compromising other desirable physical and mechanical properties.

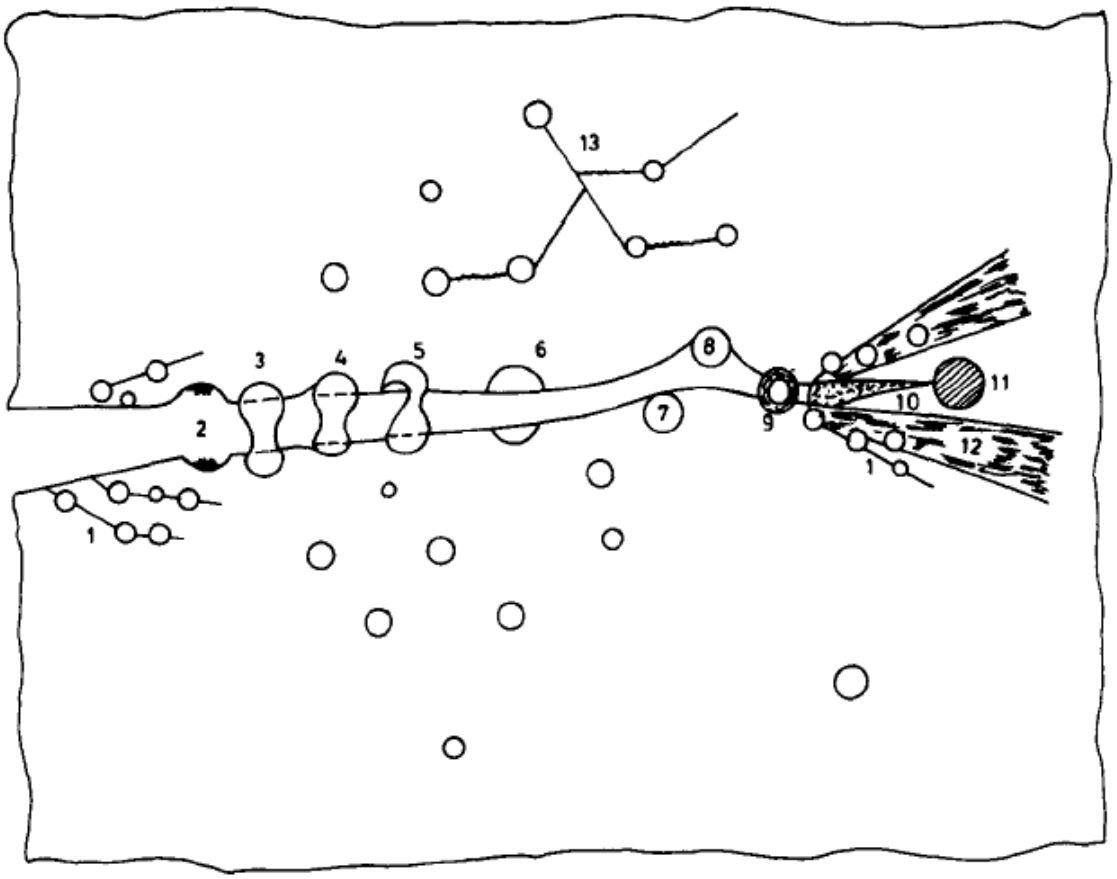

Figure 2.1. Crack toughening mechanisms in rubber-filled epoxies: (1) shear band formation near rubber particles; (2) fracture of rubber particles after cavitation; (3) stretching, (4) debonding and (5) tearing of rubber particles; (6) transparticle fracture; (7) debonding of hard particles; (8) crack deflection by hard particles; (9) voided/cavi tated rubber particles; (10) crazing; (11) plastic zone at craze tip; (12) diffuse shear yielding; (13) shear band/craze interaction. (After Garg et al.[78]).

2.2. Self-Assembly of BCP for Epoxy Toughening

Cutting-edge nano-technologies have been considered to have a tremendous impact on polymer industries. Among all ongoing nano-technologies that have potential in the future, the following bottom-up approaches have been recently introduced for polymer property modifications[1]:

(a) incorporation of well-dispersed nano-scale inorganic particles, e.g., exfoliated layered silicates;[82-85]

(b) self-assemblies of organic molecules forming various nano-structures, e.g., BCP micelles.[32-34, 38, 42-48]

The incorporation of nano-scale structures is believed to improve one or more aspects of the host polymer properties, including but not limited to, modulus, toughness, thermal stability, barrier property, etc.[86, 87] However, in some cases, the addition of nano-phase may on one hand improve some properties, yet, on the other hand, simultaneously deteriorate others. Fundamentals and mechanisms of the "nano" phenomena are not well understood because of the difficulties in available analytical techniques and lack of fundamental knowledge at nanometer size scales.

In the last decade, there have been a number of literature reports of novel morphologies of BCPs,[88-91] BCP and homopolymer blends,[92-96] and BCP in solution.[97-103] It has been a rising question whether those BCP morphologies can be duplicated in thermosetting polymers to give desirable properties. Thus, a new epoxy toughening approach using self-assembled BCP has drawn significant attention.[32-41]

It is well know that amphiphilic BCP molecules will self-assemble in a selected solvent (or homopolymer) with the solvent (or homopolymer)-immiscible block forming phase-separated domains in the solution (or blend), as shown in Figure 2.2. Recently, Bates and co-workers[32, 34, 43, 45] have found that the same morphologies seen in BCP and homopolymer blends can be duplicated in cured blends of epoxy and poly(ethylene oxide)-poly(ethylene-*alt*-propylene) (PEO-PEP) BCP. Similarly, epoxidized poly(isoprene)-poly(butadiene) (PI-PB)[44, 45] and methacrylic BCPs[45, 46] have also been shown to be effective. The morphological development during the curing process of the same epoxy resin containing poly(ethylene oxide)-poly(propylene oxide) (PEO-PPO) and PEO-PPO-PEO BCPs has also been studied by Mijovic et al.[104] and later by Guo et al.[105] Kosonen et al. have investigated the self-assembly and dynamic mechanical behavior of poly(2-vinylpyridine)-poly(isoprene) (P2VP-PI) BCPs blended with phenolic thermosets[106, 107] and then PEO-PPO-PEO blended with resol thermosets.[108]

–A–A–A–A–A–B–B–B–B–B–

(a)

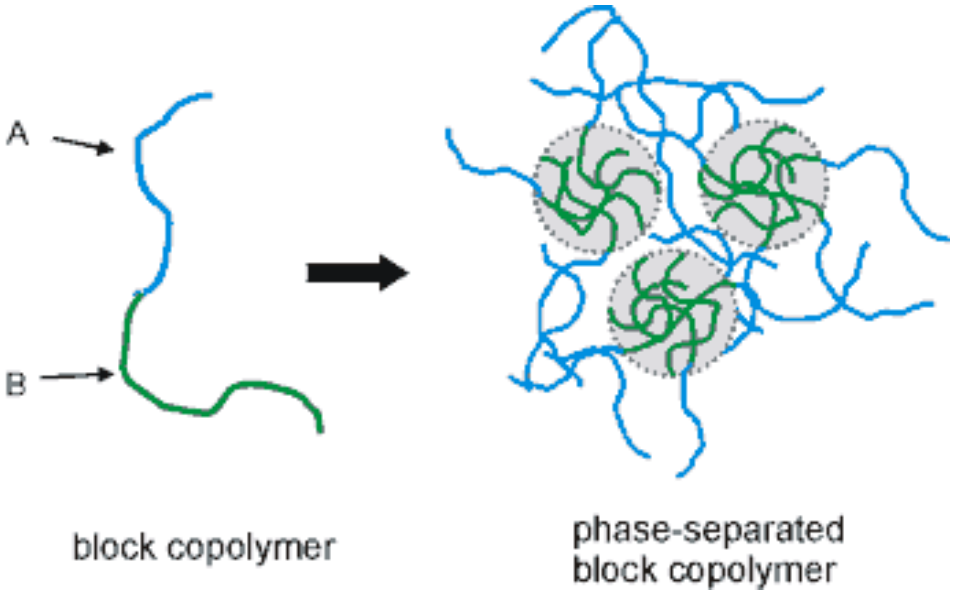

(b)

Figure 2.2. Illustrations of (a) structure of BCP and (b) phase separation of amphiphilic BCP in solutions or homopolymer blends.

With appropriate design of the molecular architecture, the BCPs can self-assemble to form ordered or disordered morphologies prior to curing and curing locks in the morphology that is already present.[42, 43] There may be some phase transitions taking place in ordered morphologies during curing, but not in the disordered scenarios. In addition, if the BCP and epoxy blend is on the transition point of macroscopic phase separation, curing can induce this transition. A proper BCP designed for epoxy modification consists of an epoxy-philic block and an epoxy-phobic block. The repulsion between the two blocks, measured by χ and the degree of polymerization, N, must be large enough so the product of χN is larger than approximately 10 where χ is proportional to the square of the difference in solubility parameters between the two blocks.[109] The BCP will micro-phase separate into an ordered morphology in the neat state and into ordered or disordered morphologies in blends depending on concentrations.[95] An illustration of phase morphologies of ordered BCP in the neat state is shown in Figure 2.3. An example of an ordered morphology of epoxy/BCP blend is presented in Figure 2.4. Illustrations and examples of disordered morphologies of epoxy/BCP blend are also shown in Figures 2.5 and 2.6.

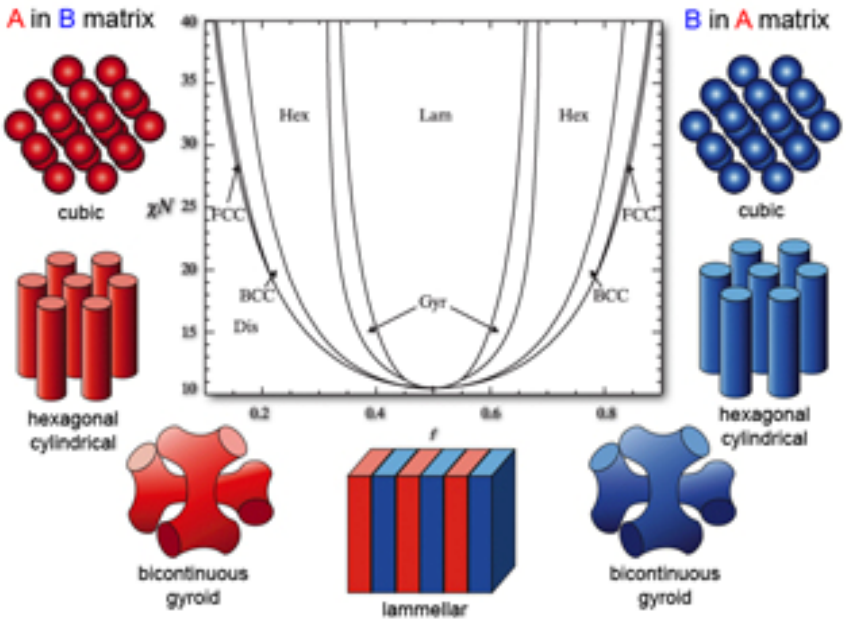

Figure 2.3. Phase morphologies of ordered BCP in the neat state.

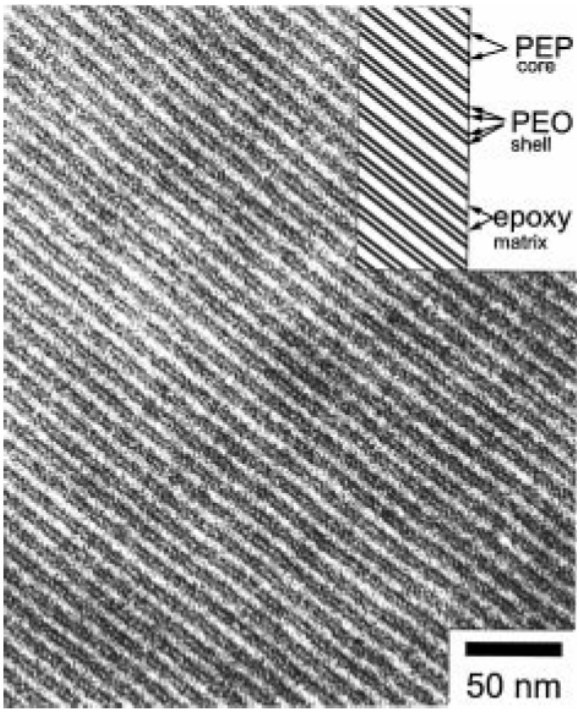

Figure 2.4. TEM image of epoxy/PEO-PEP (52 wt%) blend. The inset provides an interpretation of the morphology: cylindrical PEP cores surrounded by PEO shells, enclosed by the epoxy matrix. (After Lipic et al.[43]).

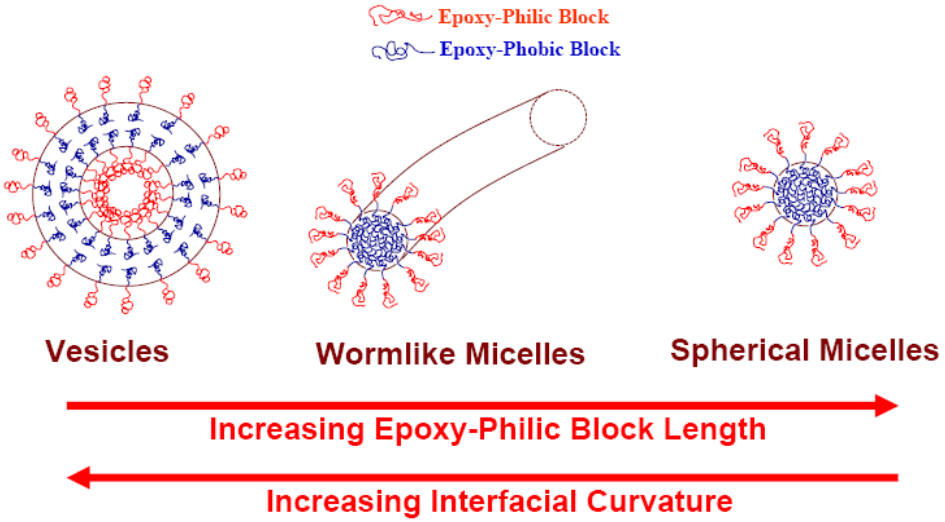

Figure 2.5. Disordered morphologies of self-assembled BCP in epoxy: spherical micelles, wormlike micelles, and vesicles.

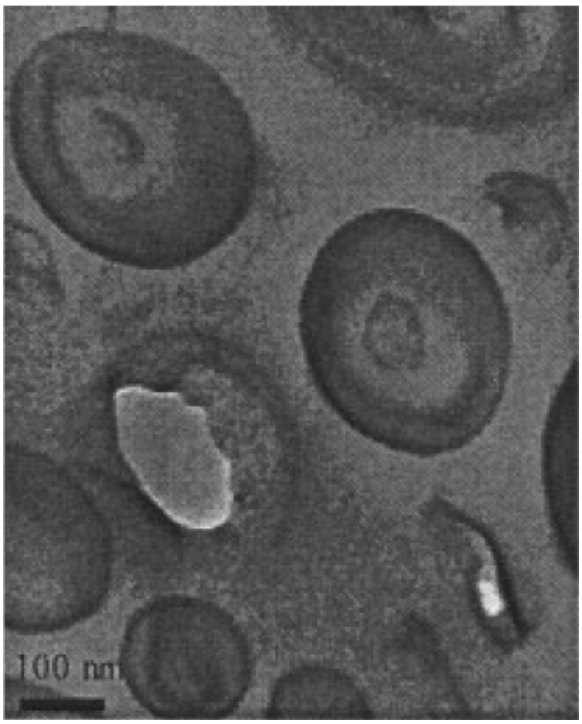

(a)

Figure 2.6. TEM images of epoxy/PBO-PEO (5 wt%) blends with three disordered morphologies: (a) vesicles, (b) wormlike micelles, and (c) spherical micelles. (After Wu et al.[38]).

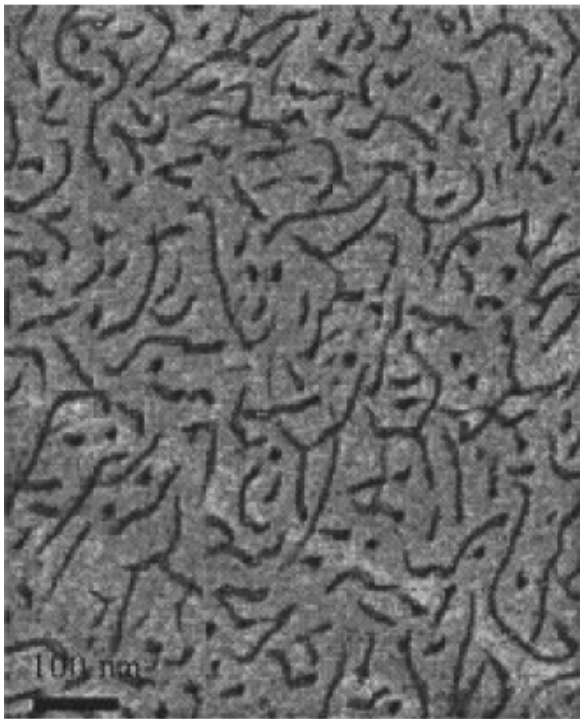

(b)

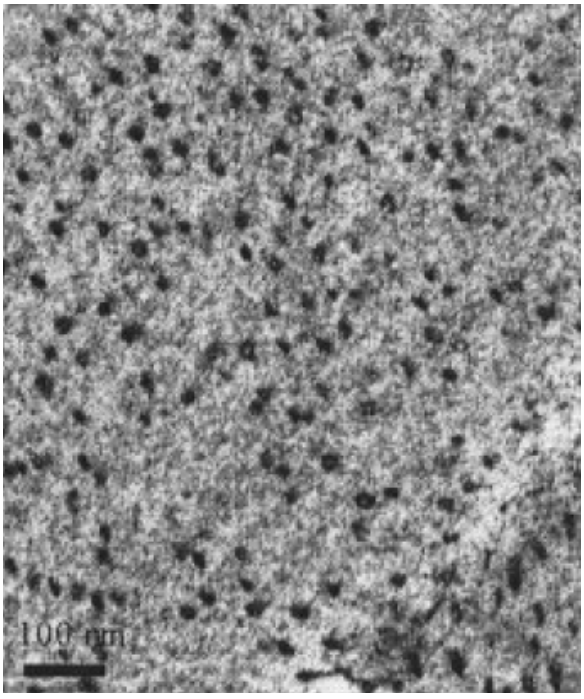

(c)

Figure 2.6. Continued.

Bates et al.[89-91, 109-112] have studied the phase behavior of neat BCPs as a function of f_A, volume fraction of the A block, and the conformational asymmetry. Several reports[42, 43, 92-103] have investigated BCP blends with a solvent (or homopolymer) selective for the A block and the critical parameters including f_A, χ_{AB}, N_{AB}, Φ_{BCP} (volume fraction of BCP in the blend), N_C/N_A (ration of the solvent or homopolymer molecular weight to the A block molecular weight), χ_{AC}, and χ_{BC}. If the ratio of N_C/N_A is larger than approximately 1, the system is prone to macroscopic phase separation.[95] At high BCP concentrations, ordered morphologies form (Figure 2.4), while in the dilute limit, disordered morphologies, such as spherical micelles, wormlike micelles and vesicles, result (Figures 2.5 and 2.6). It is interesting to note that the behavior of BCPs in monomeric epoxy resins resembles that of amphiphilic BCPs in water. The same fundamental physics, selective solvation of the miscible block by a low molecular weight solvent, governs the phase behavior.

At high BCP concentrations, ordered morphologies in cured epoxy support potential applications as solid polymer electrolytes, nanoporous thermosets, and low k dielectric materials. Meanwhile, the primary application for low BCP concentrations is toughening brittle polymers.

Lipic et al.[32, 42, 43] have studied the phase behavior of symmetric BCP and epoxy blends and evaluated the mechanical properties of spherical micelle-modified epoxies. In their reports, however, spherical micelles have not been found to be particularly effective in toughening epoxy.[32] In addition to spherical micelles, wormlike micelles and vesicles can also be created in dilute BCP blends.[92] Figure 2.5 presents how BCPs are

organized in vesicles, wormlike micelles and spherical micelles. Vesicles are closed spheres; the vesicle membrane is a bilayer formed by the self-assembly of BCP and the interior is entirely composed of the solvent or polymer matrix.[113] Vesicles have previously been observed in BCP and solvent blends,[97, 99-101, 103, 114-117] and BCP and homopolymer blends.[92, 94] Because the BCP forms only the shell, but the volume of the vesicle phase consists of both the shell and the encapsulated matrix, a small amount of BCP possibly can produce a disproportionate effect as a modifier. This unique morphology also is exploited for drug delivery application, a commonly cited goal of vesicle research.[113, 115-117] Wormlike micelles are long, thin tubes where the epoxy-philic block forms a corona that shields the epoxy-phobic cylinder interior.[92, 103] In addition, spherical micelles, which are the simplest structure, consist of a sphere core of epoxy-phobic block and a corona of mixed epoxy and epoxy-philic block.

Fracture properties of epoxies modified by BCPs with the above disordered morphologies have been measured by Wu et al.[38] They have found that the addition of BCPs to epoxy resins can improve the fracture toughness to different levels. Toughening mechanisms like voiding, debonding and crack deflection have been proposed, as schematically shown in Figure 2.7. However, no conclusive experimental evidence has been reported. Lately, a few researchers have also blended triblock copolymers in epoxy resins, as part of their efforts to improve the fracture toughness of epoxy.[36, 41, 118] Again, fundamental knowledge of the toughening mechanisms accounting for such toughening effect is still lacking.

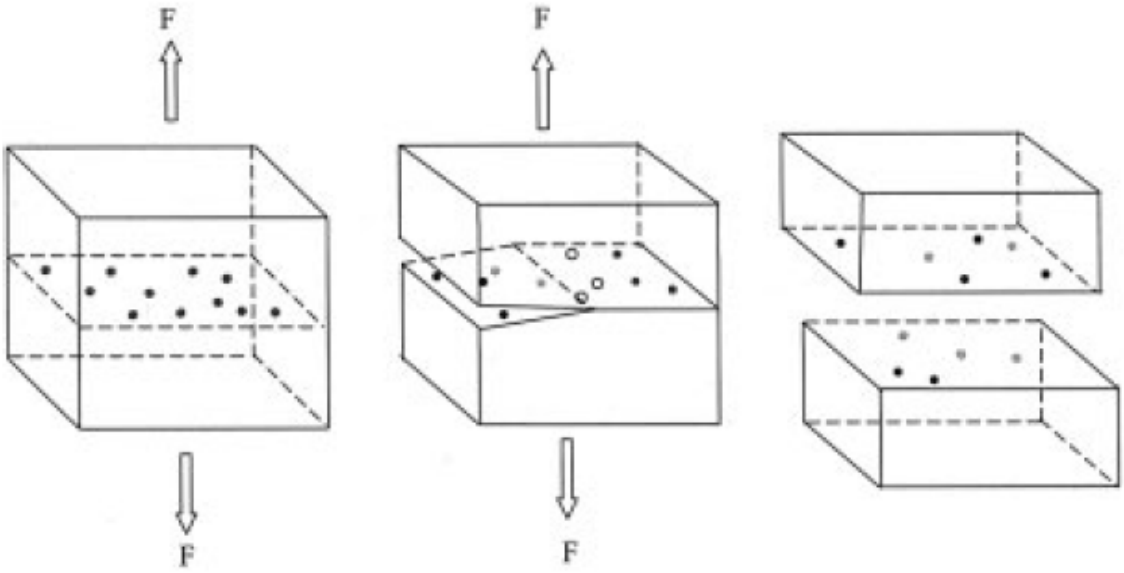

(a)

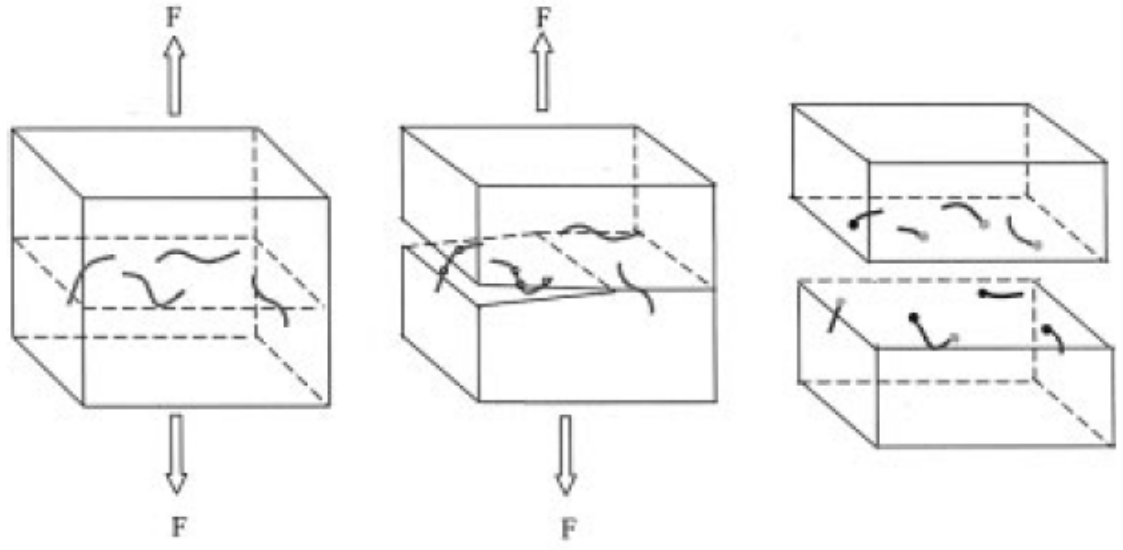

(b)

Figure 2.7. Schematics of proposed fracture process associated with the epoxies modified by (a) spherical micelles, (b) wormlike micelles, and (c) vesicles. (After Wu et al.[38]).

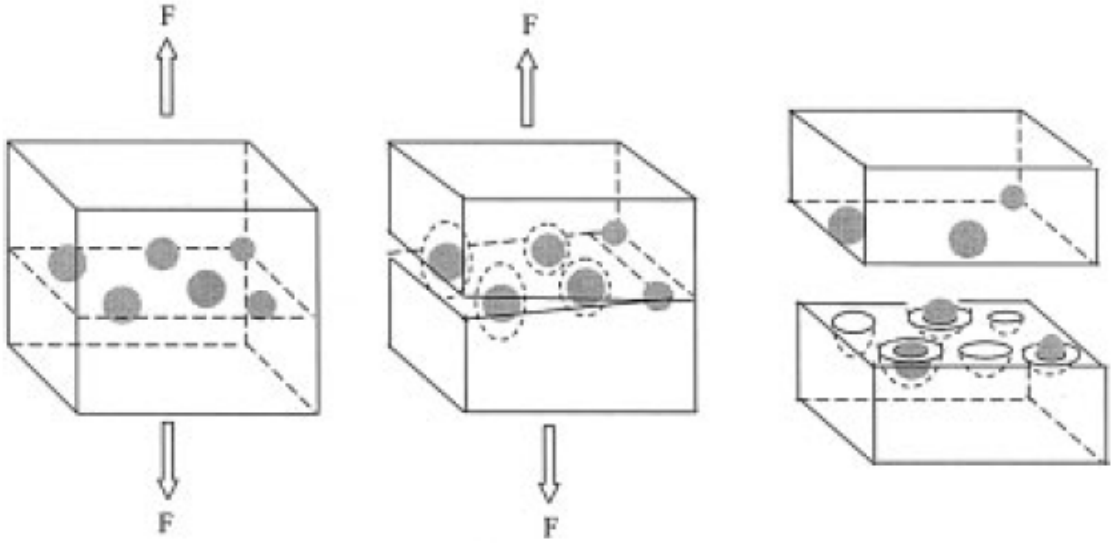

(c)

Figure 2.7. Continued.

In summary, a key objective of the current research is to investigate the toughening effects of self-assembled BCPs in epoxy resins, and unambiguously discover the toughening mechanisms involved, with direct and solid experimental evidence. By doing that, a fundamental understanding of structure-property relationship of this unique family of nano-domain modified thermosets has been gained.

CHAPTER III

TOUGHENING MECHANISMS IN EPOXIES CONTAINING NANO-SIZED BLOCK COPOLYMER MICELLES

An amphiphilic block copolymer (BCP) toughener was incorporated into a liquid epoxy resin formulation and self-assembled into well-dispersed nanometer scale spherical micelles with a size of about 15 nm. The nano-sized BCP at 5 wt% loading can significantly improve the fracture toughness of cured epoxy thermosets without reducing modulus at room temperature and with only a 5 °C drop in glass transition temperature. The toughening mechanisms were investigated and it was found that the 15 nm size BCP micelles could cavitate to induce matrix shear banding, which mainly accounts for the observed remarkable toughening effect. Other mechanisms, such as crack tip blunting, may also play a role in the toughening. A discussion of the possible reasons responsible for the observed mechanical property improvements caused by the BCP modification is given. Implications of the present finding for designing toughened polymers are also discussed.

3.1. Introduction

Untoughened epoxies are inherently brittle, which has been a major weakness of this material. Thus, epoxy toughening has become an interesting and challenging topic for several decades. Incorporation of a dispersed rubbery phase as a toughening agent is

well-know as an effective approach to improve the fracture resistance of epoxies.[3-6, 8-10, 12, 13, 17, 19, 49-74] One of the major toughening mechanisms in rubber-toughened epoxies is found to be rubber cavitation-induced matrix shear banding.[3-6, 8] Since then, many researchers have studied the effectiveness of rubber cavitation on toughening, including the importance of particle size.[6, 13, 70-74]

Recently, Bates et al. have found that amphiphilic diblock copolymers with disordered morphologies in dilute epoxy blends are effective in toughening brittle epoxy resins.[32-34, 38, 42-48] Similar effect in triblock copolymers has also been reported by others.[36, 41] However, a fundamental understanding of corresponding toughening mechanisms with conclusive experimental evidence is still lacking.

In the present study, poly(ethylene-*alt*-propylene)-*b*-poly(ethylene oxide) (PEP-PEO) diblock copolymer which self-assembles as nano-scale spherical micelles with a size of about 15 nm in diameter was chosen as a toughening agent for a commercially available epoxy resin. Mechanical properties and fracture behavior of the cured PEP-PEO-modified epoxy matrix were investigated. Unambiguous evidence of nano-cavitation of the nano-sized spherical micelles is presented. The physical significance of the present finding will also be discussed.

3.2. Experimental

3.2.1. Materials

The epoxy monomer used for this study was diglycidyl ether of bisphenol-A (DGEBA) based epoxy resin (D.E.R. 332, Dow Chemical). The crosslinker chosen for

curing the epoxy was 1,1,1-tris(4-hydroxyphenyl)ethane (THPE, Aldrich). Bisphenol-A (BPA) chain extender (PARABIS, Dow Chemical) was utilized to alter the crosslink density of the cured network in a controlled manner. Ethyltriphenylphosphonium acetate (70% in methanol, Alfa Aesar) was used as the catalyst.

The PEP-PEO amphiphilic BCP was synthesized using previously described methods by Hillmyer and Bates.[119] PEO is an epoxy-miscible block and PEP is an epoxy-immiscible block. The number-average molecular weight (M_n) of the BCP is 9100 g/mole. The weight fraction of ethylene oxide in the BCP was chosen to be 0.40.

3.2.2. Preparation of BCP-Modified Epoxy

The BCP and epoxy resin were mixed in a round-bottom flask and heated to 150 ºC. The sample was allowed to mix until the BCP was completely dissolved into the resin. The crosslinker, THPE, was then added and the mixture was heated up to 170 ºC. Once the THPE was completely dissolved, the BPA chain extender was added and the mixture was heated up to 180 ºC. When the mixture became homogeneous at 180 ºC, the round-bottom flask was connected to a vacuum line for degassing. The mixture was cooled to 130 ºC and remained under vacuum until no more bubbles were present. An amount of 10 μL of catalyst in an overall batch of 40 g was then added and the mixture was stirred for 1-2 minutes. The sample was then poured into a mold that had been preheated to 130 ºC. The mold was placed back into the oven and heated up to 200 ºC for two hours. Afterwards the cured sample was allowed to cool to room temperature in the oven.

The BCP loading in the resulting epoxy plaque was 5 wt% and the molecular weight between crosslinks (M_c) of epoxy matrix was designed to be around 1550 g/mole. The theoretical value of M_c was estimated by determining the average crosslink functionality (f_{cav}) and the average molecular weight per crosslinks (M_{pc}), assuming a balanced stoichiometry:[120]

$$f_{cav} = \frac{\sum_{f=3}^{\infty} \Phi_f}{\sum_{f=3}^{\infty} \frac{\Phi_f}{f}} \tag{3.1}$$

$$M_{pc} = \frac{M_e + \sum_{f=2}^{\infty} \frac{M_f}{f} \Phi_f}{\sum_{f=3}^{\infty} \frac{\Phi_f}{f}} \tag{3.2}$$

$$M_c = \frac{2}{f_{cav}} M_{pc} \tag{3.3}$$

where M_e is the epoxide equivalent weight of the resin, f is the functionality of the crosslinker/chain extender, M_f is the molecular weight of the fth functional crosslinker/chain extender, and Φ_f is the mole fraction of hydrogens provided by the fth functional crosslinker/chain extender. The crosslink density of the matrix was also experimentally estimated by measuring the equilibrium storage modulus in the rubbery state, according to Nielsen's equation.[121, 122]

All the specimens were dried in a vacuum oven for at least 24 hours at 80 °C prior to being characterized as described below.

3.2.3. Morphology Characterization

Transmission electron microscopy (TEM) was used to characterize the morphology of the BCP-toughened epoxy. The material was first microtomed at room temperature using an Ultracut® E microtome and a Micro Star® diamond knife. The ultrathin sections (ca. 80 nm in thickness) were collected on carbon-coated copper grids. The sections on the grids were then vapor-stained with a fresh 0.5 wt% RuO_4 aqueous solution for ten minutes at ambient temperature. The stained sample sections were examined on a JEOL 1200 EX electron microscope operated at an accelerating voltage of 100 kV. TEM micrographs were taken using a calibrated Kodak® electron microscope film.

3.2.4. Density Measurements

The density of neat epoxy and BCP-toughened epoxy samples was measured at room temperature by the displacement method in accordance with ASTM D792-91. Isopropyl alcohol, with a known density of 0.785 g/cm^3, was used for the immersion of epoxy samples. The density of epoxies was determined using the equation:

$$\rho = \frac{W_a}{W_a - W_i}\rho_i \tag{3.4}$$

where W_a is the weight of sample in air, W_i is the weight of sample in isopropyl alcohol, and ρ_i is the density of isopropyl alcohol. Thermal mechanical analysis (TMA) was performed on a Q400 instrument (TA Instruments) to calculate the sample density above T_g.

3.2.5. Mechanical Property Measurements

Dynamic mechanical analysis (DMA) was performed using an RSA III instrument (TA Instruments), ranging from -120 to 200 °C at a fixed frequency of 1 Hz and a temperature increase at 5 °C per step. A sinusoidal strain-amplitude of 0.05% was chosen for the analysis. The dynamic storage modulus (*E'*) and tan δ curves were plotted as a function of temperature. The temperature at the peak in the tan δ curve was recorded as the T_g.

Room temperature tensile tests were conducted in accordance with ASTM D638-98, using an MTS® servo-hydraulic test machine at a crosshead speed of 0.2 in/min (5.08 mm/min). Strain was measured by a calibrated MTS® extensometer (Model 632.11B-20). Young's modulus and yield stress of each sample were obtained based on at least five specimens per sample. Average values and standard deviations were reported.

Fracture toughness measurements were performed based on the linear elastic fracture mechanics (LEFM) approach. A single-edge-notch 3-point-bending (SEN-3PB) test was used to obtain the Mode-I critical stress intensity (K_{IC}) of the neat epoxy and BCP-toughened epoxy in accordance with the ASTM D5045 method. The test was performed on an MTS Insight™ machine at a testing speed of 0.02 in/min (0.508 mm/min). Care was taken to ensure that the initial crack, generated by tapping with a fresh razor blade chilled with liquid nitrogen, exhibited a thumbnail shape crack front prior to testing. At least five specimens were used to determine K_{IC} of the samples. The critical stress intensity factor was calculated using the following equation:

$$K_{IC} = \frac{P_C S}{BW^{3/2}} f(a/W) \tag{3.5}$$

where P_C is the load at crack initiation, S is the span width, B is the thickness of the specimen, f(a/W) is the hinge factor, W is the width of the specimen, and a is the initial crack length.

3.2.6. Investigation of Fracture Mechanisms

Knowledge on the sequence of fracture events is crucial in the fundamental understanding of fracture behavior of polymers. To do so, the double-notch four-point-bending (DN-4PB) test[7, 119, 123, 124] was employed to probe the detailed fracture mechanisms of the BCP-toughened epoxy.

Two nearly identical cracks were cut into the same edge of a rectangular specimen beam with dimensions of 75 mm × 12.7 mm × 3.5 mm. DN-4PB tests were conducted at room temperature on an MTS Insight™ machine at a testing speed of 0.02 in/min (0.508 mm/min). The specimen was loaded in a 4-point bending geometry with the cracks positioned on the tensile side (Figure 3.1a). The arrested subcritical crack tip damage zone from the core region of the specimen was isolated, trimmed, thin-sectioned and stained for optical microscopy (OM) and TEM observations (Figure 3.1b).

For OM investigations, thin sections of the mid-section with thickness of about 40 μm of the DN-4PB crack tip damage zone were obtained by sectioning and polishing, following the procedures described by Holik et al.[125] These thin sections were then examined using an Olympus BX60 optical microscope at both bright field and cross-polarized field modes.

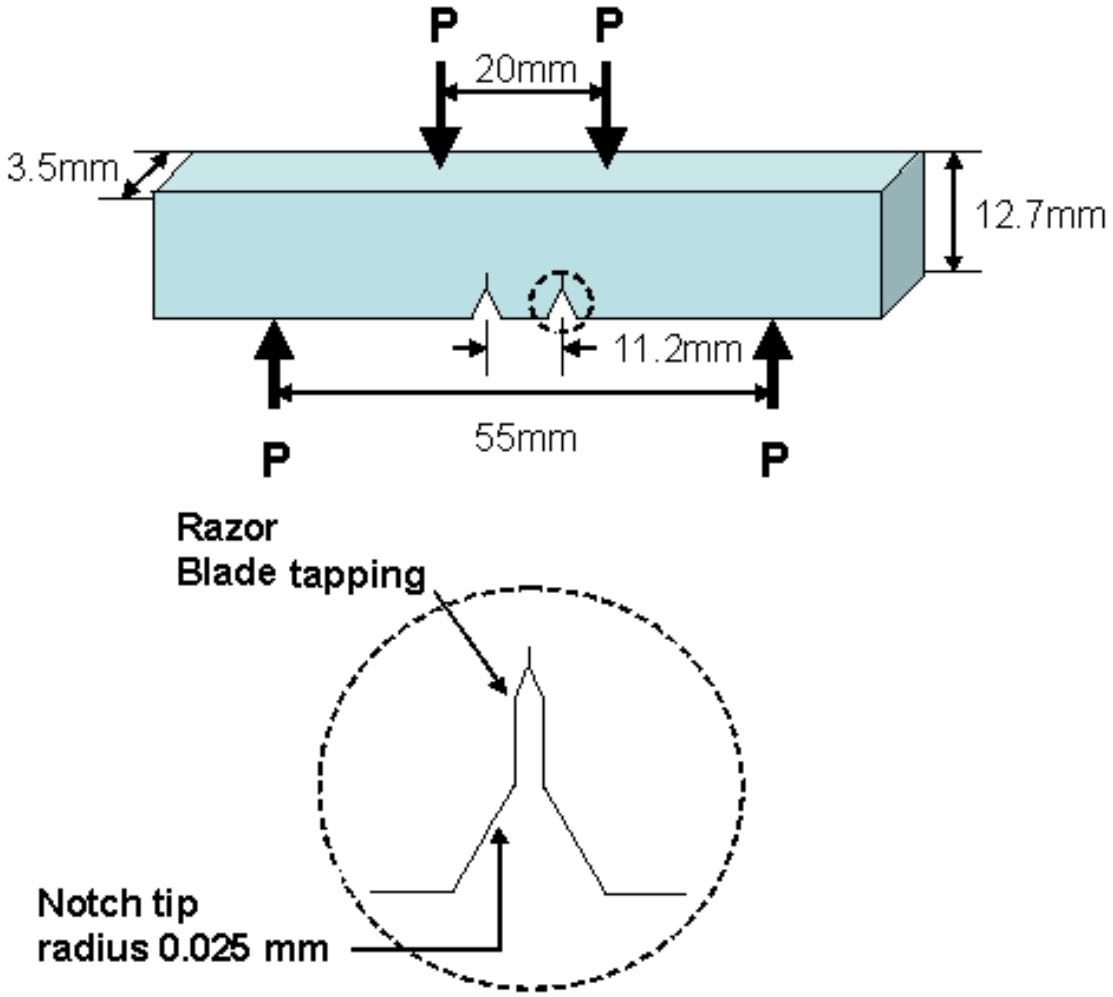

(a)

Figure 3.1. Schematics of (a) a DN-4PB specimen and (b) microscopy study on a DN-4PB specimen. The arrested subcritical crack tip damage zone from the core region was examined by OM and TEM.

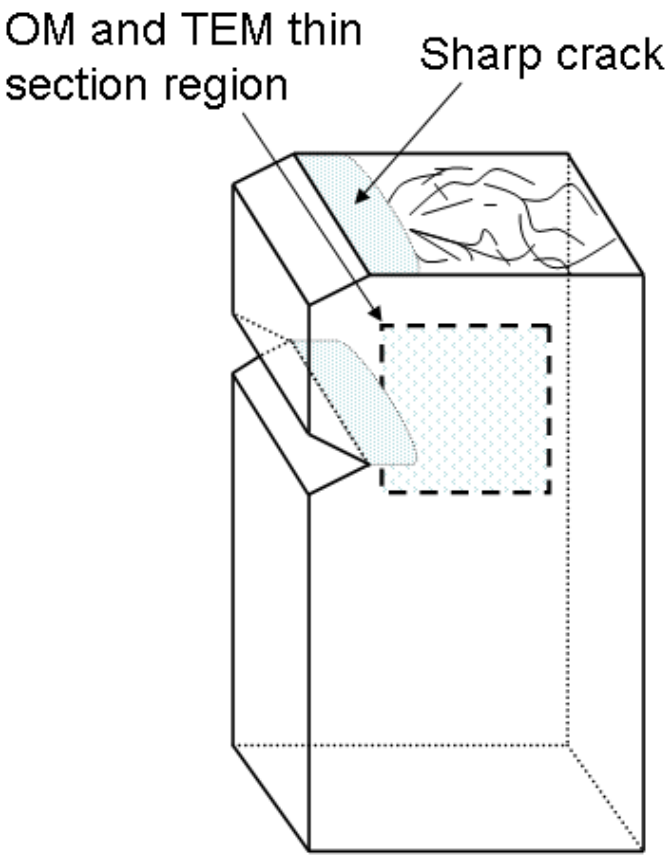

(b)

Figure 3.1. Continued.

To prepare TEM specimens, a block with the crack tip damage zone was diced off from the specimen and embedded in epoxy resin. After curing, the block was trimmed to about 0.3 mm × 0.3 mm, having a trapezoid shape at the tip. Then, the trimmed block was faced off by a diamond knife at room temperature, followed by microtoming and staining as aforementioned.

3.3. Results

3.3.1. Morphology of BCP-Toughened Epoxy

To the naked eye, the BCP-toughened epoxy appears transparent without aggregations, similar to neat epoxy. The TEM micrographs of the RuO_4-stained sample are shown in Figures 3.2a and 3.2b. The BCP phase was stained by the heavy metal and appears dark in the images while the light surroundings are epoxy matrix. The TEM micrographs show that the BCP has been self-assembled into well-defined spherical micelles and is homogeneously dispersed in the epoxy matrix. No aggregation or macro-phase separation was found and the diameter of the PEP-rich core is around 15 nm, which is found consistent with the relationship between the molecular weight and the size of BCPs.[32] An illustrative cartoon of the nano-structured morphology is presented in Figure 3.2c.

3.3.2. Dynamic Mechanical Behavior

The DMA plots are presented in Figure 3.3 and the storage modulus and T_g values are summarized in Table 3.1. A slight T_g drop of about 5 °C is observed for the BCP-toughened epoxy sample. Relative to the neat epoxy, adding BCP phase shows a slight increase in storage modulus below room temperature, and a drop at the rubbery plateau region. Interestingly, the BCP-toughened epoxy exhibits a broader T_g peak and higher tan δ values at temperatures between 0°C and the α-relaxation peak (T_g). This suggests the participation of the BCP in epoxy network formation and increased damping characteristics of the BCP-toughened epoxy. This finding signifies that the

addition of the BCP enhances the energy dissipation capacity of the epoxy matrix above 0 °C. This finding also implies that the mechanical properties of BCP-toughened epoxy can become quite rate-sensitive. The rate sensitivity issue of BCP-toughened epoxy will be addressed in Chapter V.

Table 3.1. Storage modulus, T_g and fracture toughness values of neat epoxy and BCP-toughened epoxy.

		Neat epoxy	BCP-toughened epoxy
T_g (°C)		115	110
Storage Modulus (Pa)	at low temp. (-100°C)	3.86×10^9	4.04×10^9
	at room temp. (25°C)	2.25×10^9	2.36×10^9
	at rubbery plateau	1.41×10^7	1.01×10^7
Fracture Toughness, K_{IC} (MPa-m$^{1/2}$)		0.96±0.04	2.73±0.08

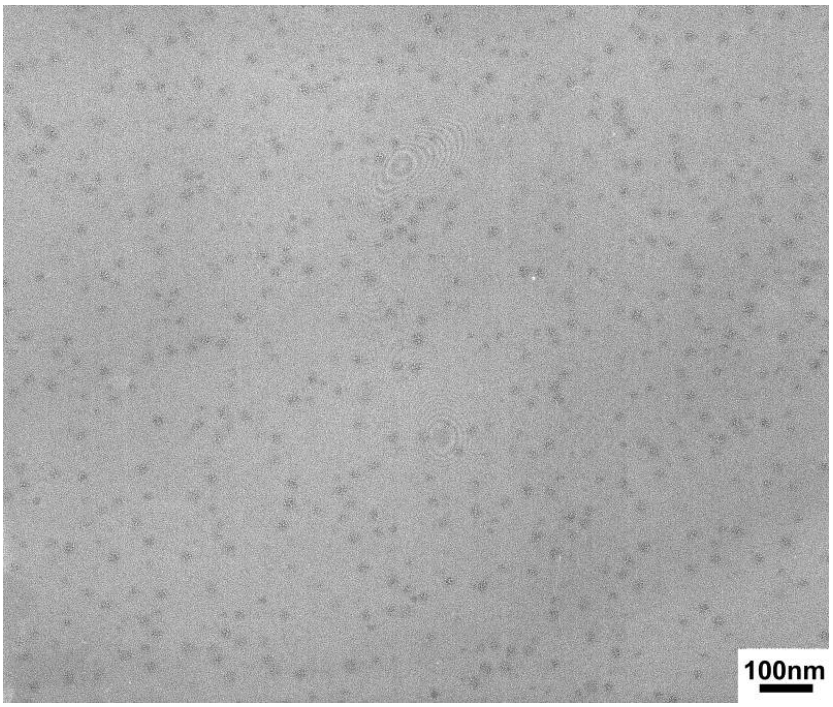

(a)

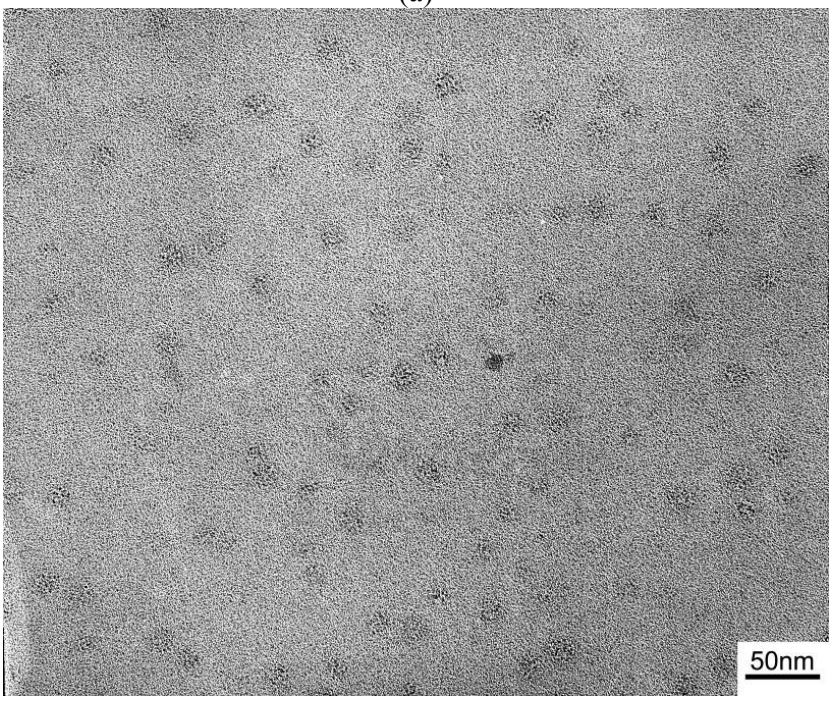

(b)

Figure 3.2. Nano-structured morphology of BCP-toughened epoxy: TEM micrographs at (a) low magnification and (b) high magnification, and a schematic illustration (c). The amphiphilic BCP consists of an epoxy-miscible PEO block and an epoxy-immiscible PEP block and forms as spherical micelles with an average diameter of 15 nm. The BCP phase was stained by RuO_4 prior to the TEM observation and shows a darker color in the micrographs.

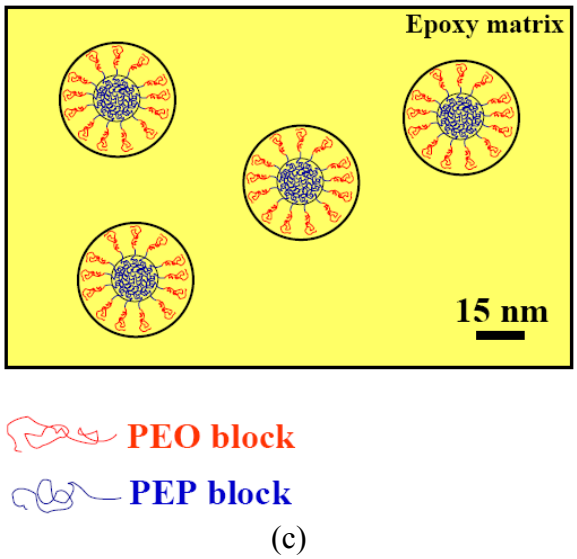

(c)

Figure 3.2. Continued.

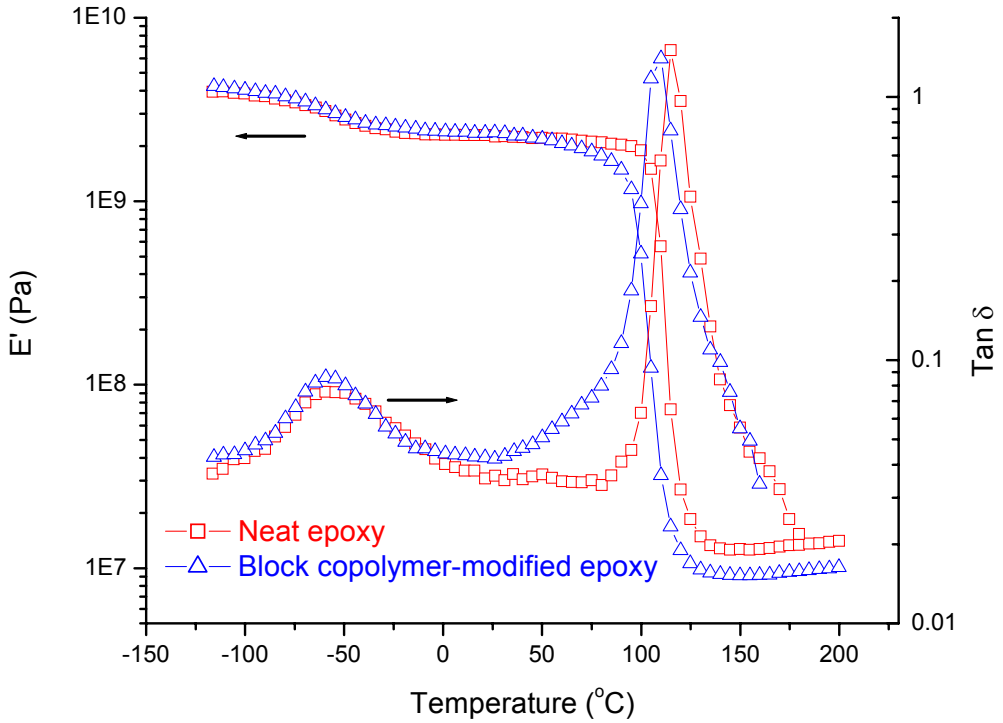

Figure 3.3. DMA plots of neat epoxy and BCP-toughened epoxy. Storage modulus (*E'*) and tan δ curves are presented. The temperature maximum peak in the tan δ curve is recorded as glass transition temperature (T_g). The storage modulus and T_g values are summarized in Table 3.1.

Additionally, the shear equilibrium storage modulus in the rubbery state (G_r) was used to determine the crosslink density of the epoxy. According to Nielsen's semi-empirical equation[121, 122], the molecular weight between crosslinks (M_c) can be estimated by the following equation:

$$\log_{10} G_r = 6.0 + \frac{293\rho}{M_c} \tag{3.6}$$

where ρ is the density of the polymer in g/cm^3, G_r in Pa, and M_c in g/mole. Since the density of the neat epoxy plaque at room temperature was measured by the displacement method as 1.20 g/cm^3, the density in the rubbery state was calculated to be 1.11 g/cm^3 (ρ), based on the coefficient of thermal expansion (CTE) information obtained from TMA. The G_r value is assumed to be related to the flexural equilibrium storage modulus, E_r, in the following manner:

$$E_r = 2G_r(1+\nu) \tag{3.7}$$

with ν being the Poisson's ratio and assumed to be 0.5 which is typical for a rubbery material. E_r obtained from the DMA measurements is 1.41×10^7 Pa, which gives an estimated M_c of about 480 g/mole. It is noted that there is a significant discrepancy between the experimentally measured M_c *via* Nielsen's equation and the expected theoretical value.

3.3.3. Tensile Behavior

The engineering stress-strain curves of neat epoxy and BCP-toughened epoxy are plotted in Figure 3.4. The Young's moduli and yield stresses are summarized in Table 3.2. It is clearly shown that addition of BCP toughener has no reduction in Young's modulus at room temperature, which is consistent with the results obtained from DMA. Meanwhile, the presence of BCP has resulted in pronounced shear yielding of the epoxy matrix, with a lower yield stress. The increase in ductility and a drop of yield stress may facilitate the formation of crack tip blunting, which will be discussed below.

Table 3.2. Young's modulus and yield stress values of neat epoxy and BCP-toughened epoxy.

	Neat epoxy	BCP-toughened epoxy
Young's Modulus (GPa)	2.59±0.06	2.58±0.05
Yield Stress (MPa)	77.7±1.1	65.8±0.4

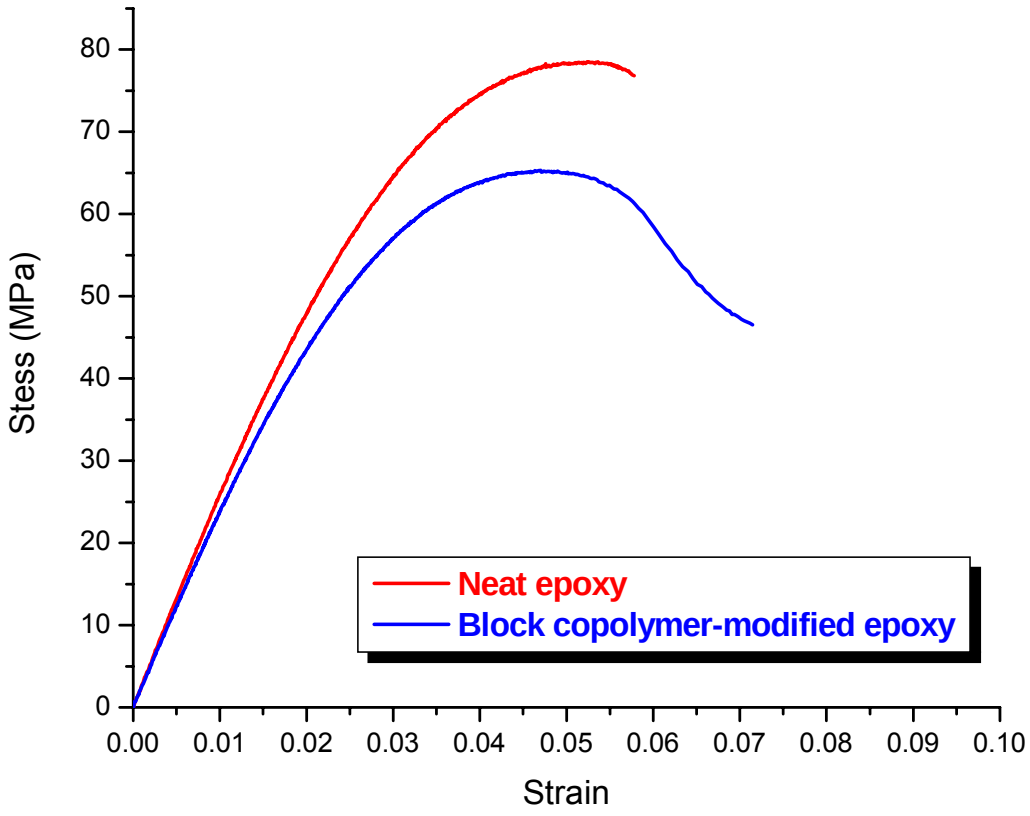

Figure 3.4. Engineering stress-strain curves of neat epoxy and BCP-toughened epoxy. The Young's modulus and yield stress values are summarized in Table 3.2.

3.3.4. Fracture Toughness Measurements

The K_{IC} values of neat epoxy and BCP-toughened epoxy are summarized in Table 3.1. A significant improvement in K_{IC} (by 180%) over neat epoxy is observed. To show evidence of stress whitening, the fracture surfaces of the samples were recorded *via* a digital camera and are shown in Figure 3.5. In contrast to the neat epoxy, the BCP-

toughened epoxy clearly shows a stress-whitening zone in front of the initial crack line. This stress-whitening phenomenon indicates the existence of some form of cavitation in the crack tip region. Cavitation can be due to debonding or internal cavitation of the BCP micelles, or both. Although unlikely, the cavitation can also be due to the presence of microcracking or crazing. To unambiguously determine the source(s) for the observed stress-whitening zone, OM and TEM observations were conducted, and are described below.

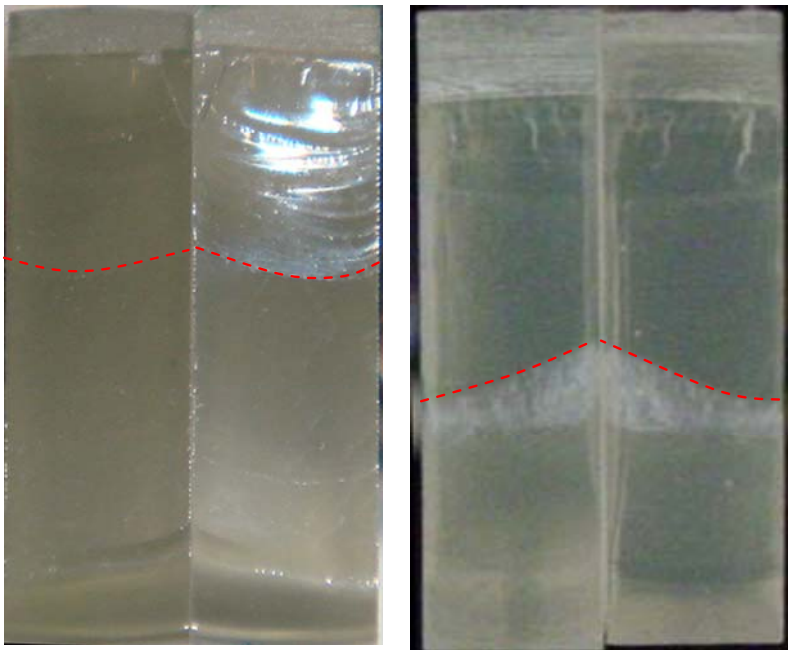

(a) (b)

Figure 3.5. Fracture surfaces of (a) neat epoxy and (b) BCP-toughened epoxy after SEN-3PB tests. A stress-whitening zone was clearly observed in front of the initial crack, as seen in (b). The red dashed lines represent the initial crack marks.

3.3.5. Toughening Mechanisms Studies

The toughening mechanisms of the BCP-toughened epoxy were investigated *via* the observation of the survived crack tip damage zone of the DN-4PB specimens using OM and TEM.

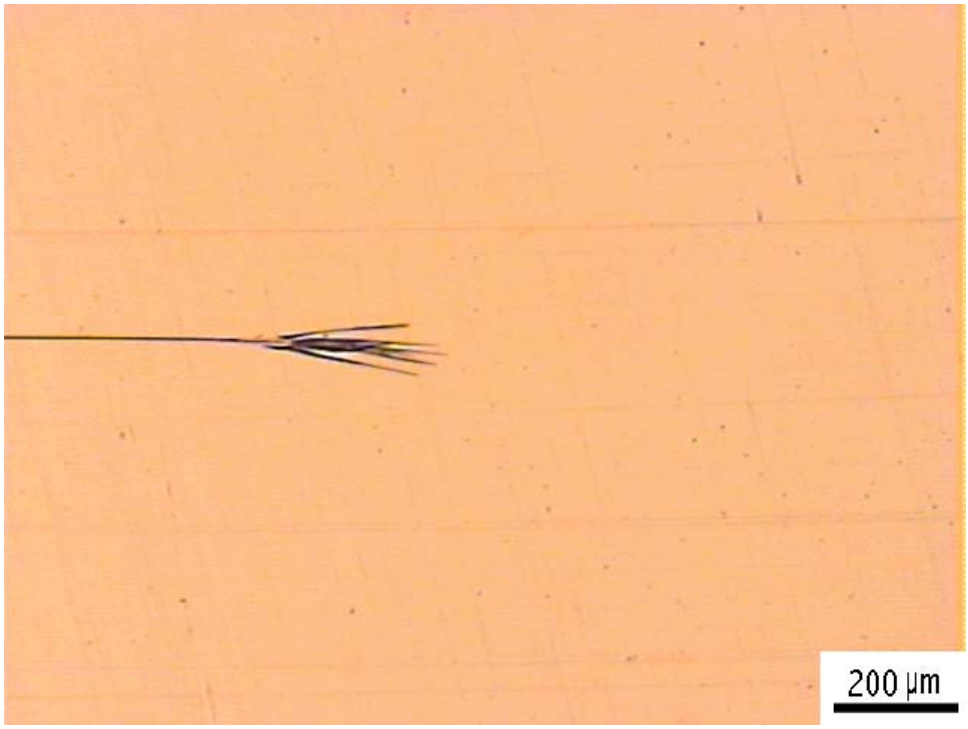

(a)

Figure 3.6. OM images of the BCP-toughened epoxy DN-4PB specimen with the subcritical crack tip damage zone at (a) bright field and (b) cross-polarized light field. The crack propagates from left to right. The images were taken at the same location.

(b)

Figure 3.6. Continued.

Microcrack-like damage in BCP-toughened epoxy can be observed by OM under bright field in the crack tip region (Figure 3.6a). This microcrack-like damage feature can be formed due to the presence of dilatation bands,[9-11, 17, 126] microcracks, or crazes. Meanwhile, a small birefringent zone is observed under the cross-polarized light (Figure 3.6b), indicating a shear banding process. Considering the significant improvement in fracture toughness, the size of the shear banding zone seems too small to account for this improvement. Thus, we surmise that other toughening mechanisms, such as crack tip

blunting,[127] may also play a role in the toughening process. This fact can be corroborated by the lower yield stress of the BCP-toughened epoxy (see Figure 3.4 and Table 3.2). A reduction of yield stress implies that it is easier to undergo plastic deformation ahead of the crack tip. A larger scale plastic deformation will lead to crack tip blunting, thereby increasing the fracture toughness of the polymer. An estimate of fracture toughness improvement due to crack tip blunting is calculated following the work of Kinloch and Williams.[127] This results in an increase of 20% in fracture toughness, which is only a small portion of the total fracture toughness increase (180%). The majority of the toughening effect therefore appears to be coming from the rubber particle cavitation induced shear banding of the matrix.

It should be noted that OM does not have sufficient resolution to show a BCP cavitation zone as in other rubber-toughened epoxy systems where the rubber particle sizes are greater than 100 nm. TEM observation is needed to conclusively identify this toughening mechanism.

The damage zone of the DN-4PB specimen was examined using TEM. In the region adjacent to the crack wake (Figure 3.7a), cavitation is clearly shown inside the elongated and orientated BCP micelles. In the region slightly above (Figure 3.7b), the elongation and orientation of the micelles are greatly reduced, but the cavitation of the BCP micelles is still observed. In contrast, in the region outside the damage zone (Figure 3.7c), neither shape change nor cavitation of the BCP micelles is observed. This has morphology similar to the uncracked specimen shown in Figure 3.2. TEM micrographs in Figures 7a and 7b clearly show that cavitation of the BCP micelles are present around

the crack tip and crack wake. Detailed observation suggests that the cavitation takes place inside the BCP phase, not at the micelle-epoxy interface. This cavitation phenomenon is consistent with the stress-whitening feature shown in Figure 3.5b. Since the BCP micelles show significant shape changes, this suggests that the epoxy around the BCP micelles have undergone equally significant amount of shear deformation. As a result, a cavitation-induced matrix shear banding process is believed to be at least partially accounted for the effective toughening of BCP-toughened epoxy. It is important to mention that the nano-cavitation phenomenon observed in the 15 nm BCP particles is the smallest rubber particle size experimentally shown to cavitate and to promote shear banding of a polymer matrix. The sequence of events in the cavitation-induced shear banding mechanism is schematically illustrated in Figure 3.8. It is also worth mentioning that, unlike other studies,[9-11, 17, 126] dilatation bands around the crack tip region found in OM were not observed by TEM even after exhaustive attempts. This may be due to the scarce or fragmented formation of dilatation bands in the crack tip region.

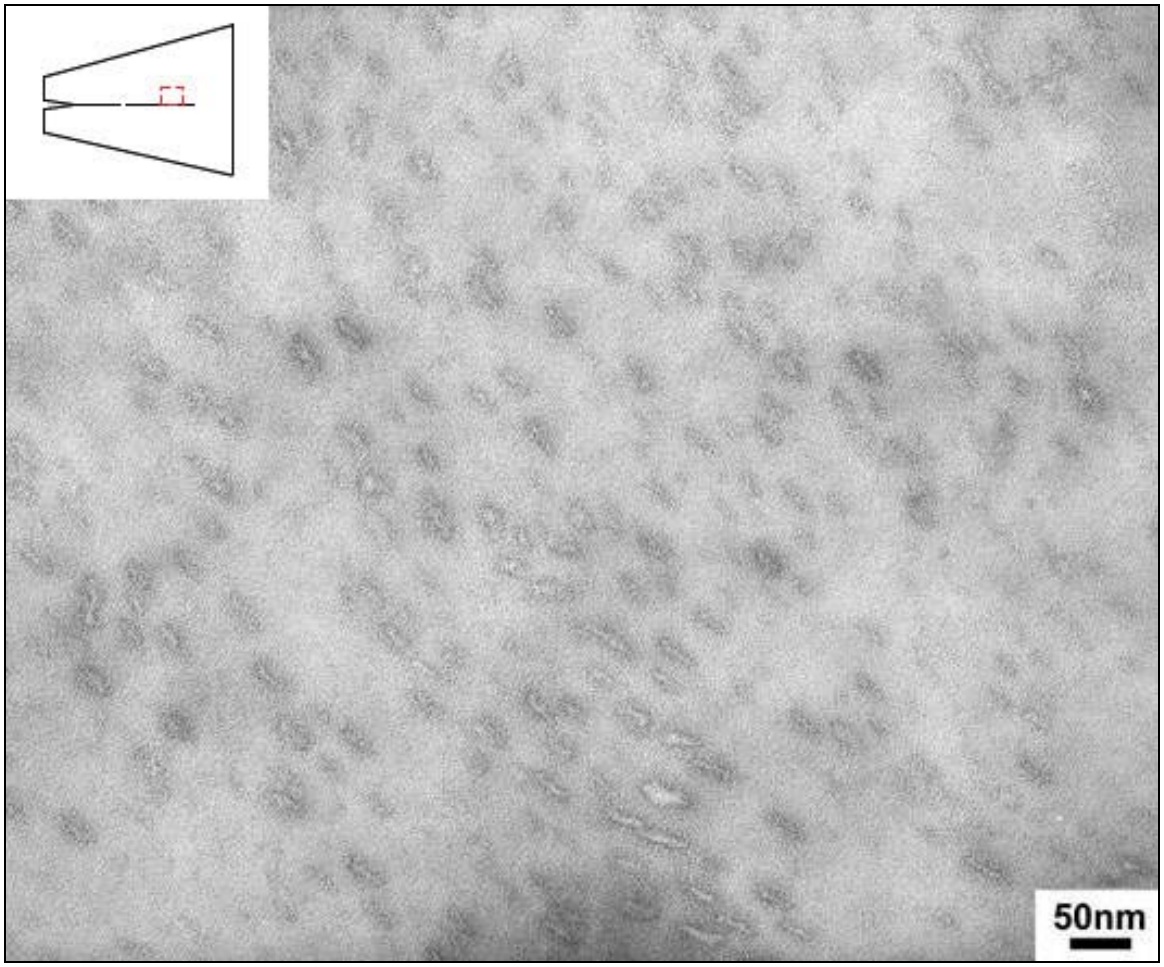

(a)

Figure 3.7. TEM micrographs of the BCP-toughened epoxy DN-4PB specimen at different locations: (a) adjacent to the crack wake, (b) some distance (in a range of 0.8-1.6 μm) from the crack wake, and (c) further away (more than 1.6 μm) from the crack wake. Insets demonstrate the spots where TEM micrographs were taken for each case. The BCP phase was stained by RuO_4 prior to the TEM observation.

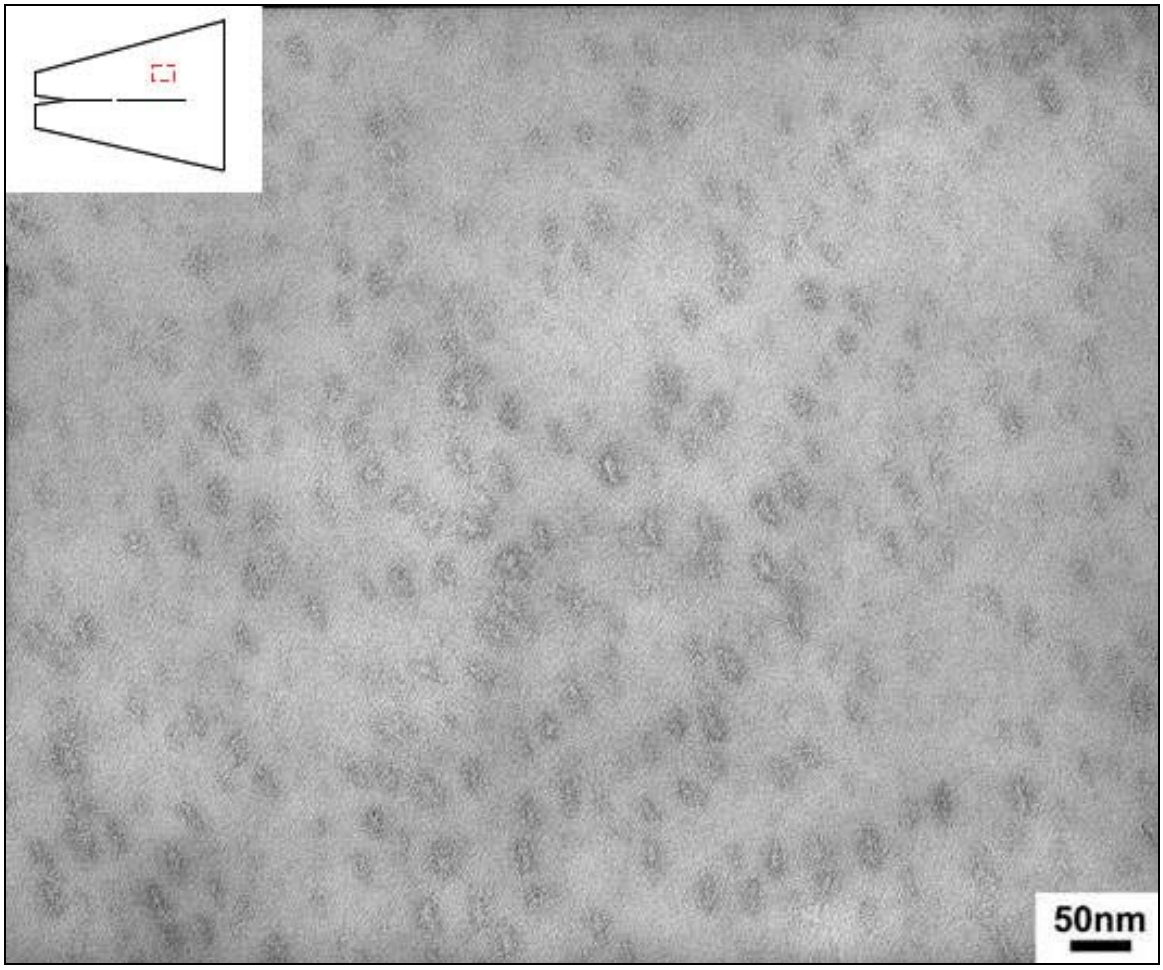

(b)

Figure 3.7. Continued.

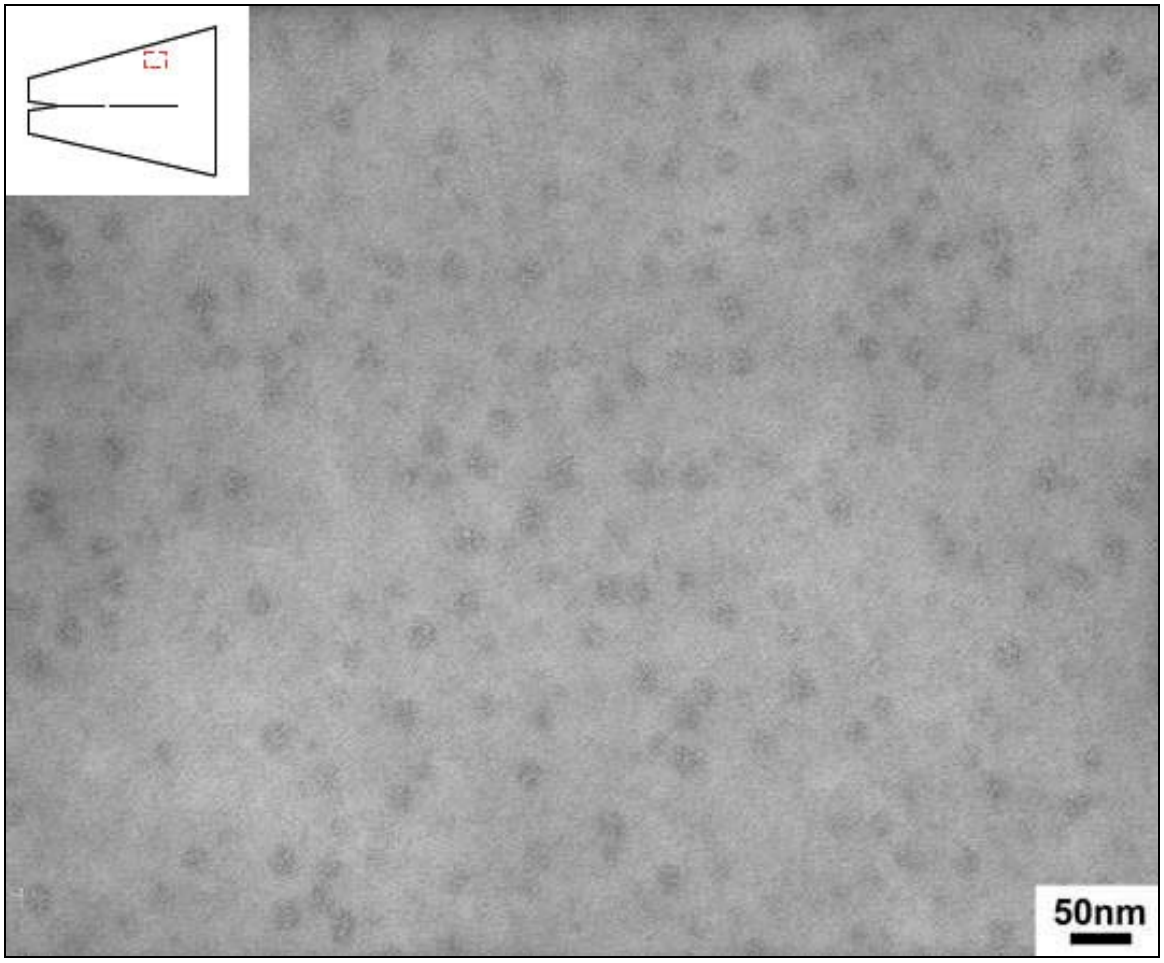

(c)

Figure 3.7. Continued.

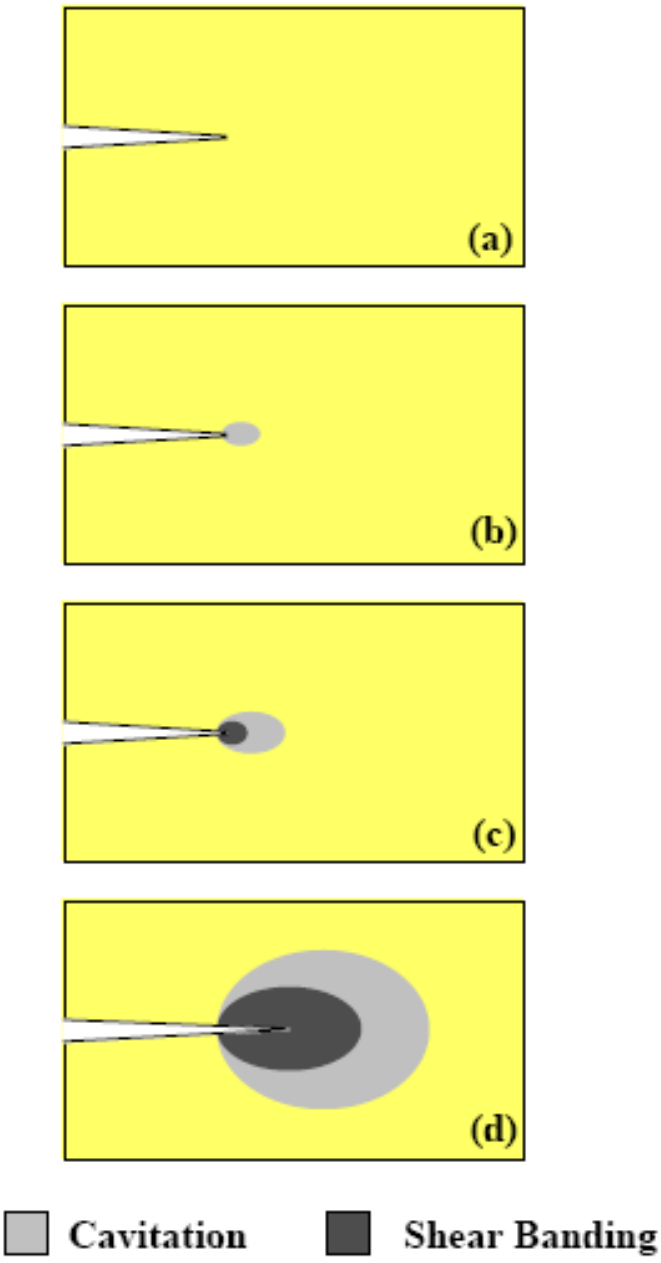

Figure 3.8. An illustration of the sequence of cavitation-induced shear banding process as one of the toughening mechanisms in BCP-toughened epoxy. (a) initiation of a starting crack; (b) formation of a BCP cavitation zone at the crack tip when the specimen is loaded; (c) expansion of the cavitation zone and initiation of a matrix shear banding zone at the crack tip when the hydrostatic stress is relieved by the cavitation; (d) crack propagates when the shear strain energy builds up to a critical value, with a damage zone surrounding the crack. The sizes of the crack, cavitation and shear banding zone are not drawn to scale.

3.4. Discussion

3.4.1. Criterion for Rubber Particle Cavitation

In 1993, Lazzeri and Bucknall[71] established a cavitation model for rubber toughening based on energy balance calculations. The assumptions for their models are summarized as follows:

(I) The largest defects within a typical rubber particle under triaxial tension are nanovoids with dimensions of the order of a few nanometers.

(II) These nanovoids will expand only if the resulting release of stored volumetric strain energy is sufficient both to increase the surface area of the void and to stretch the surrounding layers of rubber.

Assuming that the void is a sphere of radius *r* located at the center of a spherical rubber particle of radius *R*, which is well bonded to the polymer matrix, the strain energy of the rubber particle immediately before the initiation of cavitation is given by:

$$U_0 = \frac{4}{3}\pi R^3 W^* = \frac{2}{3}\pi R^3 K \Delta_{V0}^2 \tag{3.8}$$

where W^* is the stored energy density of rubber, K is bulk modulus of rubber, Δ_{V0} is volume strain within the rubber phase immediately before cavitation.

The volume fraction of the cavity is $\frac{r^3}{R^3}$ and thus the resulting volume strain within the cavitated rubber particle is $(\Delta_{V0} - \frac{r^3}{R^3})$.

The process of cavitation introduces two additional contributions to the total energy of the rubber particle: (i) a surface energy $4\pi r^2\Gamma$, where Γ is the surface tension of

rubber phase, and (ii) a shear strain energy of $\int W_S^* dV$ required to stretch the surrounding rubber to allow the cavity to expand. Therefore, the total energy of a rubber particle after cavitation is given by:

$$U = \frac{2}{3}\pi R^3 K(\Delta_{V0} - \frac{r^3}{R^3})^2 + 4\pi r^2 \Gamma + \int W_S^* dV \tag{3.9}$$

After a series of mathematical derivation and transformation, the final expression of the energy of a cavitated particle is then:

$$U = \frac{2}{3}\pi K R^3 [(\Delta_{V0} - \frac{r^3}{R^3})^2 + \frac{6\Gamma}{KR}\frac{r^2}{R^2} + \frac{3G\rho F(\lambda_f)}{K}\frac{r^3}{R^3}] \tag{3.10}$$

where G is shear modulus of rubber, ρ is density ratio of rubber before and after cavitation, and λ_f is the extension ratio of the rubber at failure in equibiaxial tension.[71]

As mentioned before, the criterion for rubber particle cavitation is that the energy released during cavitation has to be greater than the total energy required to form a cavity. Lazzeri and Bucknall plotted Equation (3.10) in terms of the reduced variables $\frac{U}{U_0}$ and $\frac{r}{R}$, where U_0 is the energy of a rubber particle immediately before cavitation (Equation 3.8), by keeping Δ_{V0} constant at 0.004 and varying R from 0.1 to 100 μm (Figure 3.9a). The calculation for the plots is based on a rubber with shear modulus G = 0.4 MPa, bulk modulus K = 2 GPa, surface tension Γ = 0.03 Nm^{-1}, ρ = 1.0 and $F(\lambda_f)$ = 1.0. Based on the plots, the authors found that only rubber particles with radii larger than 125 nm are able to cavitate under these conditions.

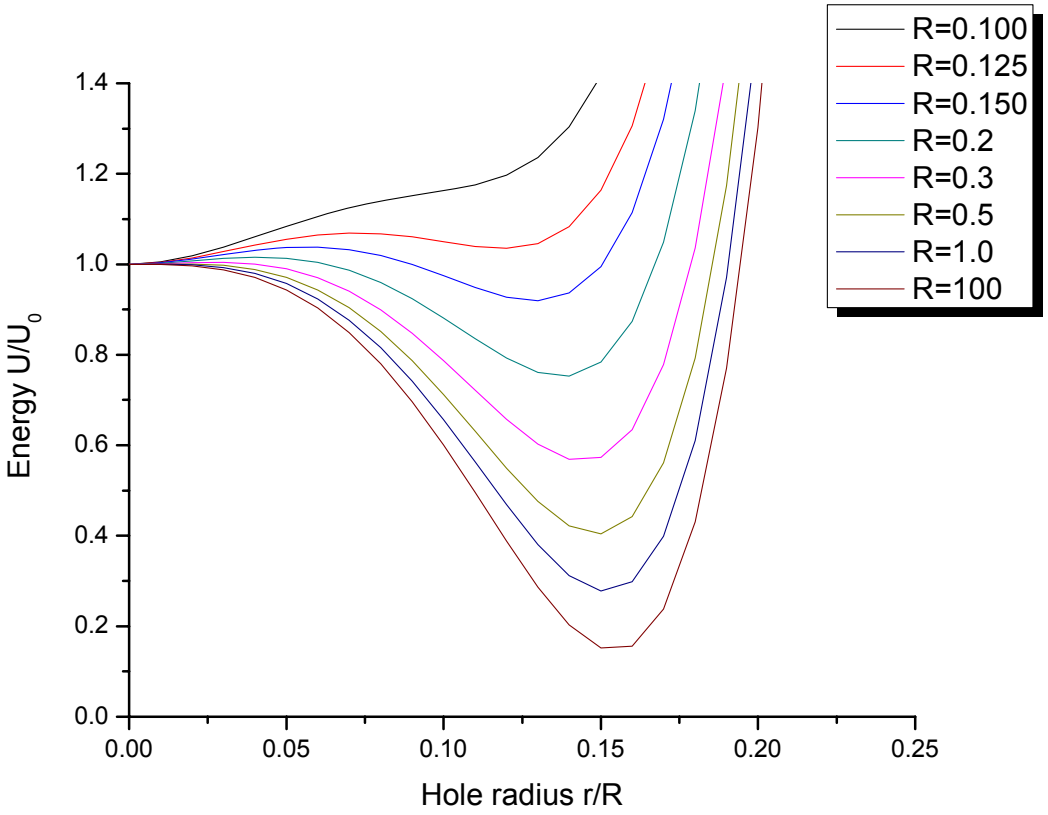

(a)

Figure 3.9. Calculated potential energy of a cavitated rubber particle as a function of the reduced radius of cavity, *r/R*, based on Lazzeri and Bucknall's energy balance model, at rubber particle volume strains of Δ_{V0} = (a) 0.004, (b) 0.03, and (c) 0.2, respectively. The curves were generated using Equation 10 with various particle radii *R* (in μm) and *G* = 0.4 MPa, *K* = 2000 MPa, Γ = 0.03 Nm^{-1}, ρ = 1.0 and $F(\lambda_f)$ = 1.0.

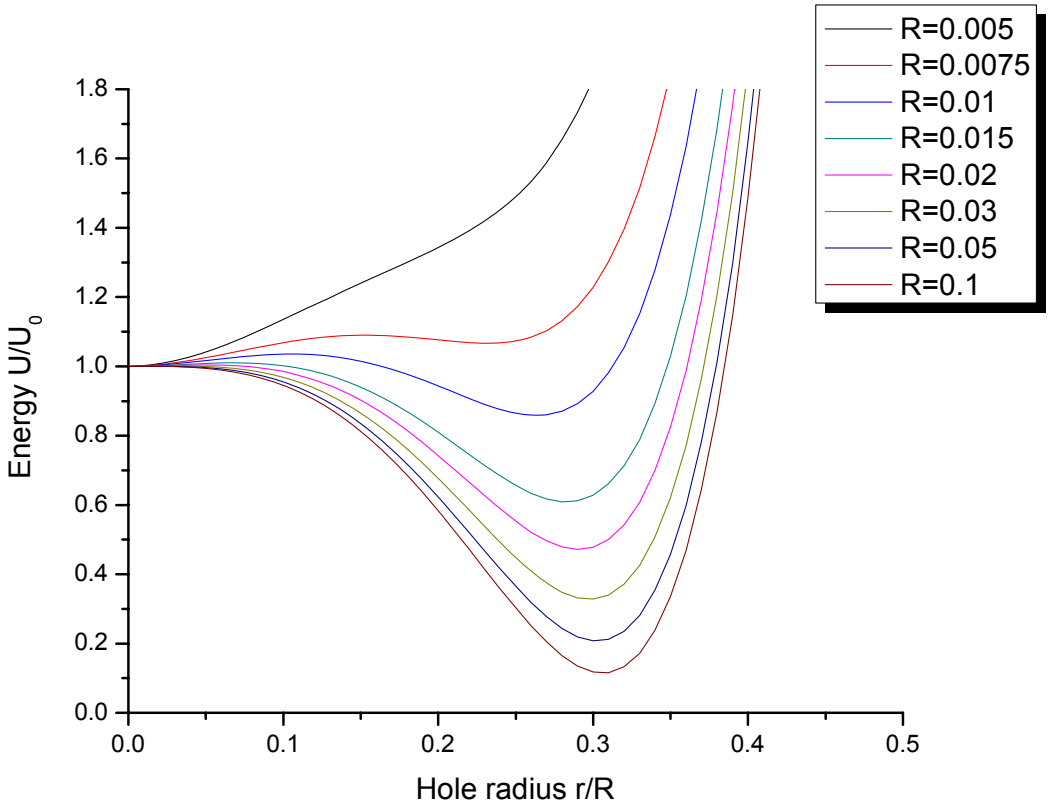

(b)

Figure 3.9. Continued.

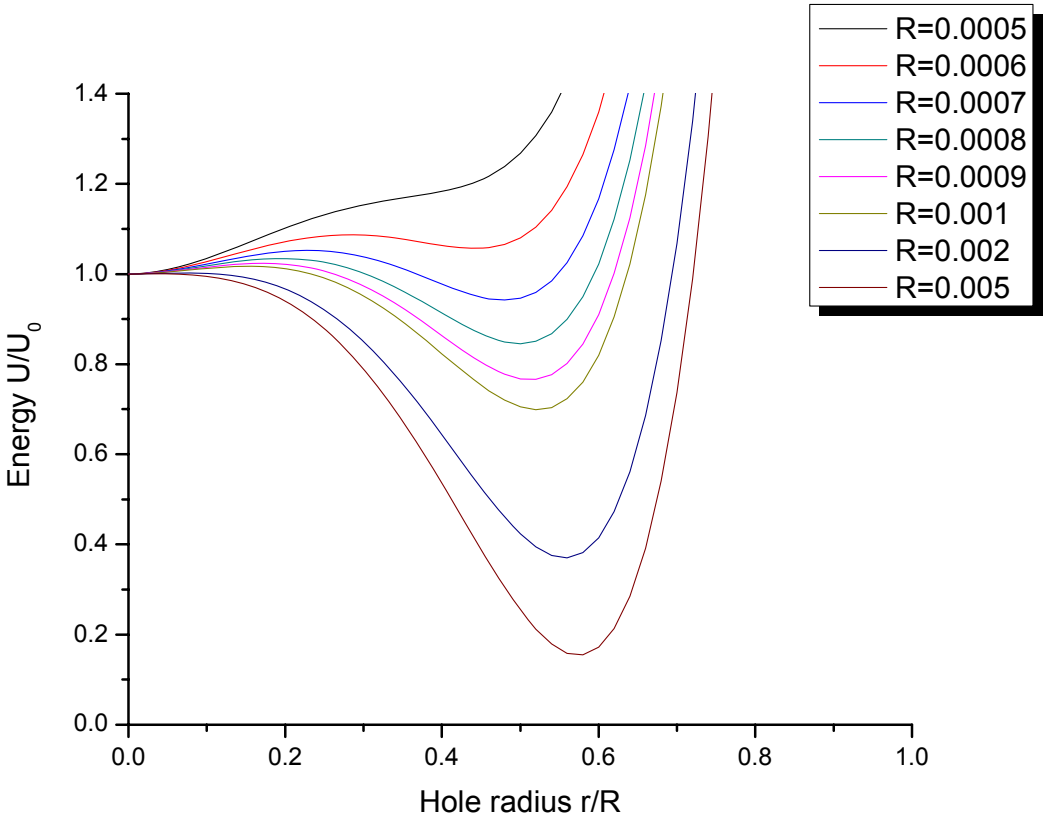

(c)

Figure 3.9. Continued.

Modifications of this energy balance model and a few other models have been proposed, yet without much difference in the prediction of particle size effect.[72, 73, 128, 129] Furthermore, a recent finite element analysis effort also confirms the ineffectiveness of small toughening particles for initiating shear banding formation.[130] Some experimental studies have supported the lower size limit of rubber particle cavitation to be about 0.2 μm, as proposed by various models.[13, 74] However, cavitation of rubber particles having 100 nm in size has been repeatedly observed in the toughening of various kinds of thermosetting matrices.[9, 10, 12, 17, 19, 55-57] In this study, clear evidence of nano-cavitation of BCP micelle particles in epoxy is shown, and the size of the particles is definitely much smaller than the sizes predicted by the energy balance model under the prescribed conditions.

3.4.2. Nano-Cavitation Phenomenon in BCP-Toughened Epoxy

It is important to note that, for a given volume strain the rubber particles experience, there exists a minimal rubber particle size for cavitation. Such a correlation was illustrated by Bucknall.[131] The $U/U_0 \sim r/R$ plots with a larger volume strain of Δ_{V0} = 0.03 are illustrated in Figure 3.9b. Under this condition, the lower limit of particle diameter for cavitation is downshifted to 15 nm. This suggests that, based on the above theory, a volume strain of at least 0.03 is experienced by the BCP for cavitation to occur. Experimental observation of the residual volume strain around the cavitated BCP based on the size change of the particles shown in Figure 3.7 is found to be greater than 0.03. Thus, it is possible that the high volume strain the epoxy matrix and BCP experience

induces the 15 nm BCP particles to cavitate. If plotting the $U/U_0 \sim r/R$ curves with a even larger volume strain of $\Delta_{V0} = 0.2$, the lower size limit of rubber particles for cavitation will be further downshifted to 1.2 nm, as shown in Figure 3.9c. However, the question as to why experimental observations made by others did not show optimal toughening effect for sizes below 0.2 μm[13, 74, 130] remain unanswered.

Another consideration in explaining nano-cavitation is the pre-existence of transient voids in BCP. The model proposed by Lazzeri and Bucknall assumes pre-existence of nanovoids with dimensions on the order of a few nanometers in rubber particles and the cavitation is a process of nanovoid expansion. However, their criteria were based on the energy conservation between the initial state (non-cavitated rubber particles) and the final state (cavitated rubber particles) without consideration of the true onset of the cavitation event. This is because of the difficulty associated with calculation of the energy or stress states at such a small scale, either from a molecular point of view or from a mechanics point of view. The consideration at such a small scale does not need to be included when applying Lazzeri and Bucknall's model in large rubber particle size cases (≥ 100 nm). In smaller rubber particle cases, however, the model may need refinement.

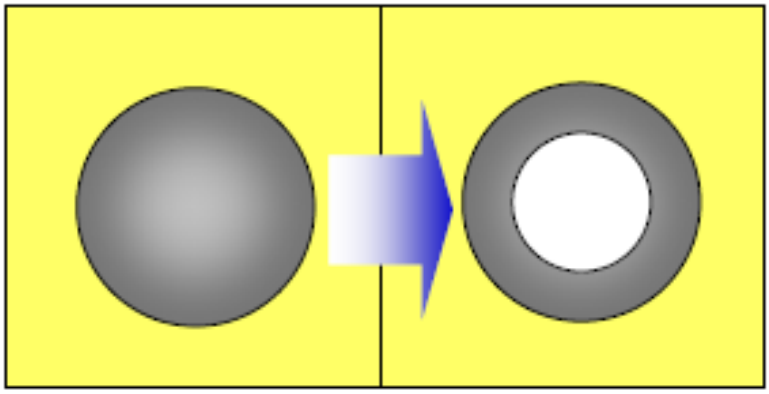

(a)

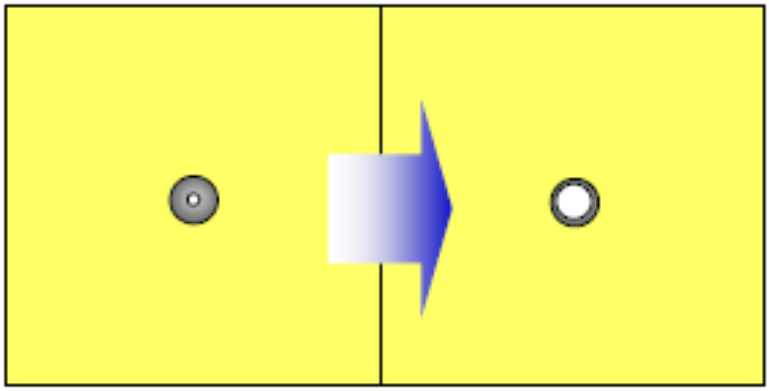

(b)

Figure 3.10. Schematic illustration of the cavitation processes based on (a) Lazzeri and Bucknall's model[71] and (b) the present work. Lazzeri and Bucknall neglected the energy contribution from the pre-existence of transient nanovoids within rubber particles, while that part has to be considered when dealing with nanometer-sized particles.

The pre-existing cavities are believed to be the transient nanovoids in the rubber phase, in the form of free volume, with the size ranging from a few Å to a few nanometers.[132-135] The size of the pre-existing voids is similar to the size of the BCP (around 15 nm) utilized in the present study. Therefore, to construct an energy balance

criterion for the system with such small rubber domains, the contribution from the pre-existence of nanovoids has to be taken into account for the energy calculation. In other words, the difference between the case Lazzeri and Bucknall[71] based their model on and the cavitation phenomenon observed in this study may lie in the consideration of the cavitation initiation from the pre-existing 'holes'. An illustrative comparison of the two different scenarios is shown in Figure 3.10.

Another important factor that should be considered is the distinction between the void expansion process in an ideal rubber particle and in a BCP micelle particle. An ideal rubber can be regarded as randomly coiled long flexible molecules with physical entanglements and/or chemical crosslinks (if vulcanized).[136, 137] The stretching of a rubber particle involves either the stretching of polymer network or disentanglement of molecules, or both. In the case of an ideal rubber, only the stretching of the polymer network is present and can be considered as elastic deformation, which stores potential energy in the system. In order to make cavitation of an ideal rubber a thermodynamically favorable process, breakage of covalent bonds will eventually occur, which requires a large amount of energy. On the other hand, in the case of self-assembled BCP, the molecules are generally well organized into micelle structure (see the schematic structure in Figure 3.2c). Thus, the expansion of micelle particles is simply a separation of adjacent molecules, which only involves destruction of secondary bonds like van der Waals forces or hydrogen bonds. Besides, the more the expansion of the micelle particles, the weaker the attraction between the molecules becomes, making cavitation more favorable. Comparing the above two scenarios, it is easy to understand that the

strain energy required for cavitation in a BCP micelle particle should be much less than that for an ideal rubber particle case. For clarity, the difference between the two expansion scenarios is sketched in Figure 3.11.

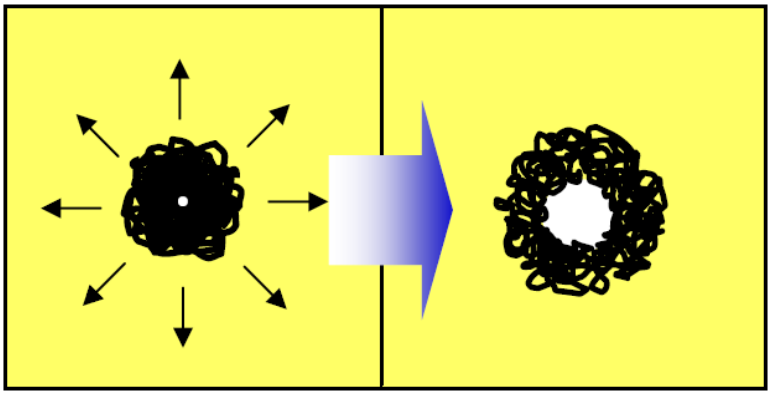

(a)

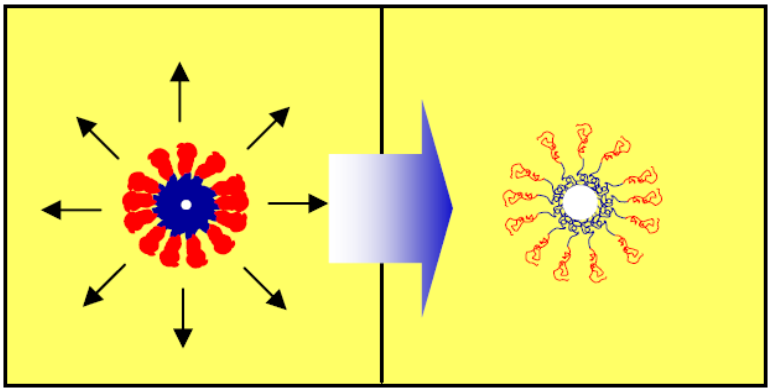

(b)

Figure 3.11. Schematic illustration of the two different expansion processes in (a) an ideal rubber particle and (b) a BCP micelle particle. The size expansion of the voids and the particles are not drawn to scale.

The actual cavitation process in such a small scale is likely to be far more complicated. In-depth efforts are still needed for physical understanding of the nano-cavitation phenomenon. The matrix is also believed to play an important role in the cavitation process and its resulting toughening effect. This fact is indicated by the significant differences in their DMA tan δ curves (Figure 3.3) and a strong strain rate dependency of fracture toughness of this BCP-toughened epoxy system. This issue will be discussed in Chapter V.

3.4.3. Other Toughening Mechanisms

Although it is evident that BCP cavitation and epoxy matrix shear banding are the two important mechanisms responsible for the observed toughening effect, crack tip blunting and the formation of dilatation bands around the crack tip region may also contribute to the toughening. It appears that rubber cavitation and shear banding of the matrix are the main causes for the observed significant improvement in fracture toughness. The contribution from crack tip blunting and the scarce dilatation bands found in OM will contribute to the toughening but to a lesser degree.

3.4.4. Implication of the Present Findings

The present and previous findings[18] suggest that it is feasible to simultaneously increase fracture toughness while maintaining the Young's modulus and T_g of epoxies. Generally speaking, T_g appears to be affected by larger scale main-chain motions, such as molecular motions involving the scales of distance between crosslinks and multi-

monomer length scale.[17, 138, 139] Ductility and toughenability involves smaller scale cooperative molecular motions, which can still be several monomer units long.[138, 139] The increase in *intra*-chain cooperative motions will favor the formation of dynamic "free volumes", which facilitate the material to relax the imposed stresses. In the case of modulus, it seems to be influenced more by backbone rigidity, chain rotation, and localized small-scale molecular motions. Some researchers have also correlated the macroscopic mechanical properties to the *inter*-chain packing.[140] The size scale that will influence the above properties strongly depends on the type of polymer matrices involved. Also, the sub-T_g or higher-order transitions are considered to be related to mechanical properties and fracture behaviors.[139, 141]

It should be noted that the holes present due to density fluctuation inside a polymer matrix are in a range of 2.5-5.0 Å in size, as measured by small angle X-ray scattering[142, 143] and positron annihilation lifetime spectroscopy.[143, 144] Meanwhile, the typical radius of gyration of a polymer chain is around 30 nm. In the case of networked epoxy systems, the increase in the rigidity of epoxy monomers will normally result in larger holes because rigid polymer chains are more difficult to achieve a dense packing than the flexible ones. Variations in crosslink density, however, have not been found to lead to a systematic change in the hole sizes, although they should influence the chain packing.[144]

The above literature findings strongly suggest that the molecular size scales that will influence the modulus, ductility, and T_g properties range from a few Å to tens of nanometers. The domain size of the PEP-rich phase for the present study is about 15 nm.

Assuming that the BCP forms a morphology with a PEP core and PEO tails extending freely into epoxy matrix, the PEO-epoxy intermixing phase that resides at the interphase between neat epoxy and PEP-rich phase is at least 7-8 nm. The corresponding effective volume fraction of BCP, including PEP core and PEO-epoxy interphase, is estimated to be at least 0.30.[32] If the average surface-to-surface interparticle distance (i.e. matrix ligament thickness) is around 30 nm based on TEM image analysis, the PEO-epoxy interphase where epoxy and PEO intermix is expected to have a great influence on the matrix physical and mechanical properties.

According to the DMA finding shown in Figure 3.3, the PEO-epoxy interphase has greatly altered the dynamic mechanical characteristics of the epoxy matrix. The presence of the PEO-epoxy molecular intermixing layer appears to be able to shield epoxy from lowering its modulus due to the presence of PEP-rich rubber phase at room temperature. However, as the temperature rises above 50 °C, the modulus of the BCP-toughened epoxy will drop significantly below that of the neat epoxy matrix. The tan δ values increase sharply as temperature rises above room temperature, which implies that the rate sensitivity on the mechanical properties of BCP-toughened epoxy is likely to be high. The above evidence strongly suggests that the epoxy network and its molecular motions are greatly altered by the presence of PEO-rich phase in epoxy. Consequently, the modulus, T_g, ductility, and fracture toughness of epoxy are all altered, irrespective of the presence of the PEP-rich phase. It should be noted that it is unclear if continuum mechanics still applies for the BCP-toughened epoxy system at the 15 nm length scale. If not, totally different interpretation on the present findings may be warranted.

Although this research focuses on polymer toughening at nano-scale, many other factors, such as crosslink density, monomer rigidity, concentration of toughener phase, size, and geometry of toughening agent, still need to be addressed before one can definitely understand the structure-property relationships in nano-sized rubber-toughened polymers.

3.5. Summary

A PEP-PEO diblock copolymer at 5 wt% loading was utilized to toughen bisphenol-A type of epoxy. The BCP self-assembled into ca. 15 nm spherical micelles that were well dispersed in the matrix. Mechanical characterization indicates that the PEP-PEO diblock copolymer can greatly improve the fracture toughness of epoxy without compromising its modulus. The DN-4PB test and TEM observation suggest that the major toughening mechanisms in BCP-toughened epoxy include copolymer micelle cavitation followed by matrix shear banding. The fundamental cause(s) for such a small-scale cavitation process is yet to be determined. The likely contributing factors for the observed nano-scale cavitation phenomenon may include the unique BCP micelle structural characteristics and a possible influence of the surrounding epoxy network, which is significantly modified by the PEO block.

CHAPTER IV

CROSSLINK DENSITY EFFECT ON FRACTURE BEHAVIOR OF EPOXIES CONTAINING NANO-SIZED BLOCK COPOLYMER MICELLES

Model diglycidyl ether of bisphenol-A (DGEBA) based epoxy resins containing well-dispersed 15 nm block copolymer (BCP) nanoparticles were prepared to study the effect of matrix crosslink density on their fracture behavior. The crosslink density of the model epoxies was varied *via* the controlled epoxy thermoset technology and estimated experimentally. As expected, it was found that the fracture toughness of the BCP-toughened epoxy is strongly influenced by the crosslink density of the epoxy matrix, with higher toughenability for lower crosslink density epoxies. Key operative toughening mechanisms of the above model BCP-toughened epoxies were found to be nanoparticle cavitation-induced matrix shear banding for the low crosslink density epoxies. The toughening effect from BCP nanoparticles was also compared with core-shell rubber (CSR)-toughened epoxies having different levels of crosslink density. The usefulness of the present findings for designing toughened thermosetting materials with desirable properties is discussed.

4.1. Introduction

Rubber modification has been reported as an effective approach for toughening brittle epoxy thermosets since the beginning of the 1970s.[53, 75] Since then, significant

work has been done to gain a better understanding of the structure-property relationship between the polymer matrix and the toughening agents for designing epoxy thermoset systems with desired properties.[3, 4, 6-10, 12, 21, 23-25, 31, 76-79] Self-assembled amphiphilic BCP are a new type of toughening agent that has been shown to greatly improve toughness without sacrificing other mechanical properties. In Chapter III, we identified the toughening mechanisms of a BCP-modfied controlled epoxy thermoset (CET) system at a specific crosslink density. The major toughening mechanisms are BCP particle cavitation and subsequent matrix shear banding, which are analogous to those found in other rubber-toughened systems. But the BCP appears to be more effective than other conventional rubber particles, probably due to its much smaller sizes and unique morphology. In this chapter, we report the fracture behavior of BCP-toughened epoxy with variation in crosslink densities.

Although rubber modification has been recognized as an effective toughening approach, not all epoxy resins can be toughened to significant extents. Toughenability has been found to be related to thermoset crosslink density,[5, 17, 145-151] It is known that the crosslink density of a cured thermoset generally dictates its intrinsic ductility, simply because ductile deformation requires large-scale cooperative conformational arrangements of polymer backbones. Because matrix shear banding has been identified as the major energy dissipation process in rubber toughened epoxies,[3, 4, 6, 8] it is not difficult to understand that modifying the matrix ductility can change its toughenability. The function of rubber particle cavitation is to relieve the triaxial stress at the crack tip

and consequently to facilitate matrix shear banding. Thus, the thermoset matrix ductility plays an important role in enhancing fracture toughness of rubber-modified thermosets.

The present study is part of a larger effort to understand the fundamentals of structure-property relationships in a model epoxy system containing poly(ethylene-*alt*-propylene)-*b*-poly(ethylene oxide) (PEP-PEO) BCP nanoparticles. The toughening mechanisms of this modified epoxy system have been discussed in Chapter III. In this chapter, attention will be placed on determining whether or not the BCP-modified epoxy thermosets with variation in crosslink densities will exhibit a similar toughening effect on fracture behavior as what has been observed in other rubber toughened systems. The implication of the present findings for designing high performance thermosetting resins is discussed in detail.

4.2. Experimental

4.2.1. Materials

The epoxy chemistry used for this study consisted of three components: DGEBA-based epoxy monomer (D.E.R. 332, Dow Chemical), bisphenol-A (BPA) chain extender (PARABIS, Dow Chemical), and 1,1,1-tris(4-hydroxyphenyl)ethane crosslinker (THPE, Aldrich). The chemical structures of these reactants are given in Table 4.1.

Table 4.1. Chemical structures of epoxy resin, chain extender, crosslinker and block copolymer used in this investigation.

Product	Chemical Structure
DGEBA epoxy resin	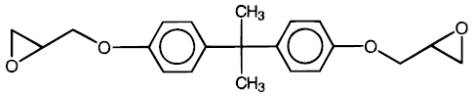
BPA chain extender	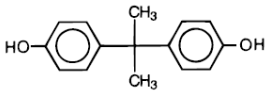
THPE crosslinker	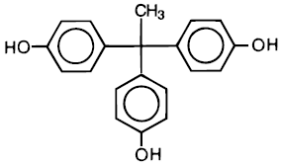
PEP-PEO block copolymer	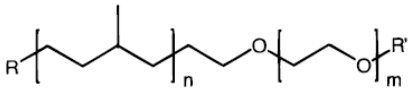 R = *s*-butyl or *t*-butyl R' = H or CH_3

A scheme of the chain extension and crosslinking reactions is illustrated in Figure 4.1. The ratio of epoxy monomer and chain extender was altered to vary the crosslink density. The theoretical value of the molecular weight between crosslinks (M_c)

was estimated by determining the average crosslink functionality (f_{cav}) and the average molecular weight per crosslinks (M_{pc}), assuming a balanced stoichiometry (see Chapter III).

It is noted that ethyltriphenylphosphonium acetate (70% in methanol, Alfa Aesar) was utilized as a catalyst to promote reactions between primary epoxide groups in the epoxy resin and phenolic functionalities in the chain extender and the crosslinker. This largely reduced the chances of branching reactions with secondary hydroxyl groups and lead to a more uniform and controlled epoxy network.

As a toughing agent, the PEP-PEO amphiphilic BCP was synthesized using a multi-step polymerization method previously described by Hillmyer and Bates.[119] PEO is an epoxy-miscible block and PEP an epoxy-immiscible block, which forms a rubber domain with a size of about 15 nm. The number-average molecular weight (M_n) of the BCP is 9100 g/mol and the weight fraction of ethylene oxide in the BCP is 0.40. The chemical structure of PEP-PEO is also shown in Table 4.1.

4.2.2. Preparation of BCP-Modified Epoxy Resin

The procedure for sample preparation has been reported in detail earlier, so it is only briefly described here. The BCP was mixed and completely dissolved in the epoxy resin at around 150 ºC. Then, the chain extender and crosslinker were added into the mixture and dissolved. After degassing, the catalyst was added and the mixture was cured in a pre-heated mold for 2 h at 200 ºC.

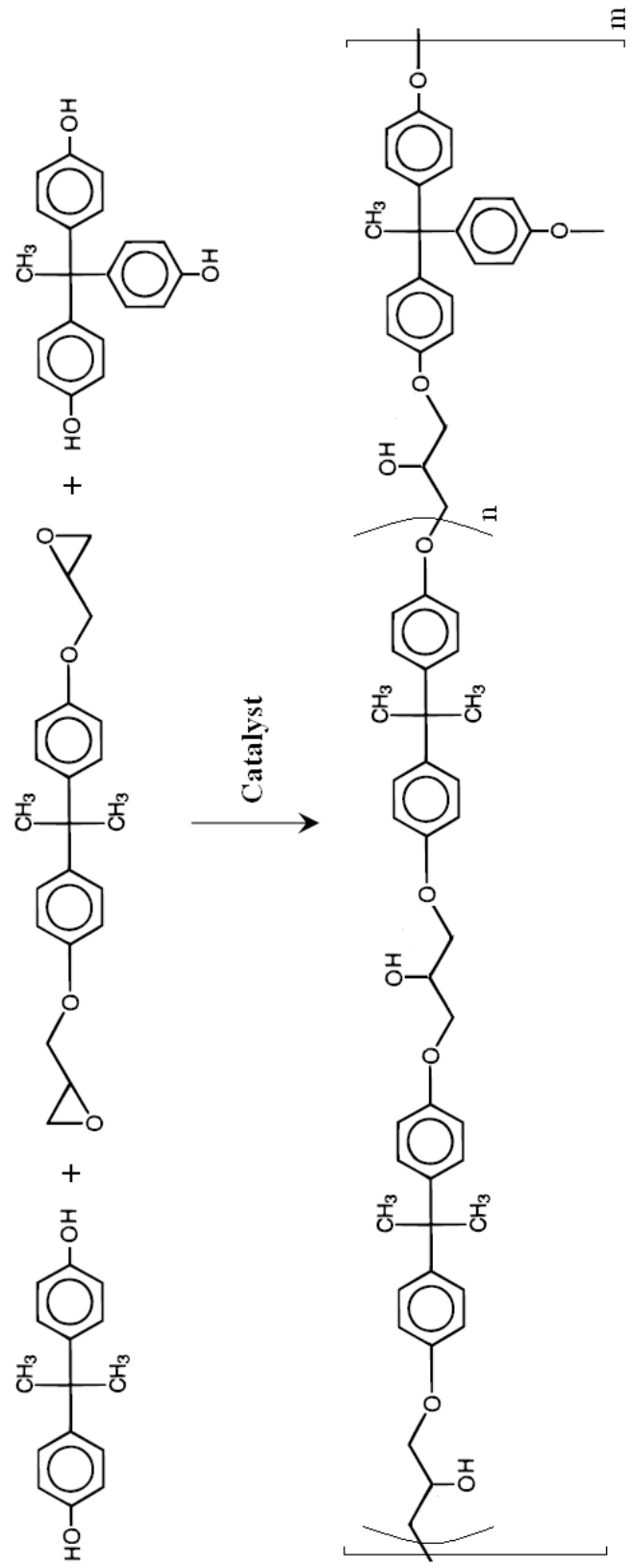

Fig. 4.1. Scheme of chain extension and crosslinking reactions in the present epoxy curing process.

The BCP concentration in all final epoxy products was 5 wt%. Three crosslink densities of epoxy matrix were designed with theoretical M_c being 900, 1550 and 2870 g/mol, respectively. For convenience, the neat and modified epoxy samples with different M_c are designated as CET900, CET1550, CET2870, CET900/BCP, CET1550/BCP, and CET2870/BCP.

All the specimens were dried for at least 24 h in a vacuum oven set at 80 °C prior to characterizations.

4.2.3. Density Measurement

The densities of all the samples were measured by the displacement method at room temperature following the ASTM D792-91 standard. Isopropyl alcohol, which has a known density of 0.785 g/cm^3, was used for immersion of the samples. To calculate the density at elevated temperatures, thermal mechanical analysis (TMA) was performed on a Q400 instrument (TA Instruments) to obtain the coefficient of thermal expansion (CTE) and to measure the dimensional change as the temperature increased.

4.2.4. Dynamic Mechanical Analysis (DMA)

DMA was performed using an RSA III instrument (TA Instruments) at temperatures ranging from -120 to 200 °C with a 5 °C per step increase. The tests were performed at a fixed frequency of 1 Hz. A sinusoidal strain-amplitude of 0.05% was chosen for the analysis. The dynamic storage modulus (E') and tan δ curves were plotted as a function of temperature. The temperature at the maximum in the tan δ curve was

recorded as the T_g. The E' at 60 °C above T_g was chosen as the rubbery plateau modulus, E_r, for each system.

4.2.5. Fracture Toughness Measurement

To obtain the Mode-I critical stress intensity (K_{IC}) of the neat and modified epoxy samples, a single-edge-notch three-point-bending (SEN-3PB) test was performed using the linear elastic fracture mechanics (LEFM) approach in accordance with the ASTM D5045 standard. The dimensions of test specimens are 75 × 12.7 × 3.5 mm^3. A sharp pre-crack was generated in each sample by tapping with a fresh razor blade chilled with liquid N_2 and care was taken to make sure that the pre-crack exhibited a thumbnail-like shape crack front. The tests were done at room temperature on an MTS Insight machine. The testing crosshead speed was chosen as 0.508 mm/min. Average values and standard deviations of the K_{IC} were calculated on the basis of at least five specimens per sample.

4.2.6. Toughening Mechanisms Investigation

The double-notch four-point-bending (DN-4PB) technique was utilized to investigate the detailed toughening mechanisms of BCP-modified epoxy resins with various crosslink densities. The DN-4PB technique has been shown to be effective in probing micromechanical deformation mechanisms.[7-12, 17, 21, 24, 152] A detailed description of this technique can be found in Chapter III. The tests were conducted at a crosshead speed of 0.508 mm/min and at room temperature, on an MTS Insight machine. Thin

sections with a thickness of ca. 40 μm from the core region of the DN-4PB subcritical crack tip damage zone were obtained by sectioning and polishing, following the procedures described by Holik et al.[125] Optical microscopy (OM) images were then taken under both bright field and cross-polarized field modes using an Olympus BX60 optical microscope. For transmission electron microscopy (TEM) observation, a block containing a subcritical crack tip damage zone was isolated from the specimen and embedded in an Epo-Fix embedding resin (Electron Microscopy Sciences). A detailed procedure for the preparation and staining of the samples can be found earlier. TEM micrographs were taken from the stained sections using a JEOL 1200 EX electron microscope operated at an accelerating voltage of 100 kV.

4.3. Results and Discussion

Previous TEM work revealed that the BCP self-assembles into well-defined and well-dispersed spherical micelles with an average diameter of ca. 15 nm in CET1550/BCP. Because CET900/BCP and CET2870/BCP exhibit similar morphologies as CET1550/BCP, they are not shown here.

4.3.1. Dynamic Mechanical Behavior

The DMA spectra of all the samples are compared in Figure 4.2 and the *E*' and T_g values are listed in Table 4.2.

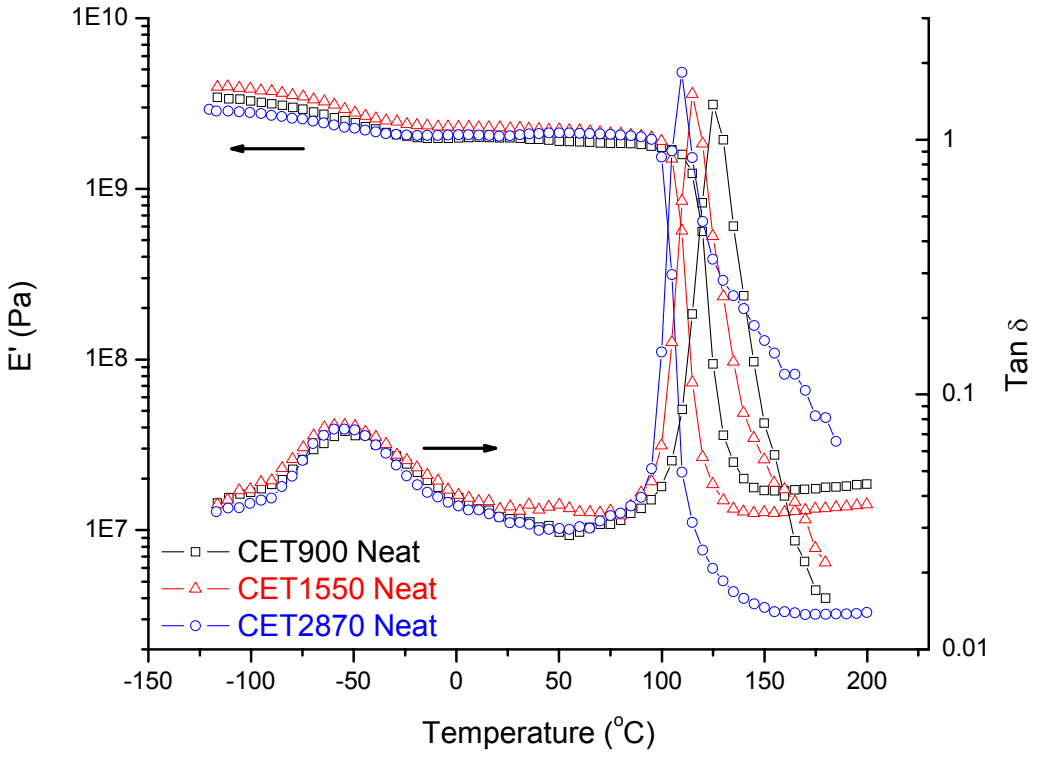

(a)

Figure 4.2. DMA spectra of (a) neat epoxies and (b) BCP-modified epoxies with different crosslink densities. The storage modulus (E') and glass transition temperature (T_g) values are summarized in Table 4.2.

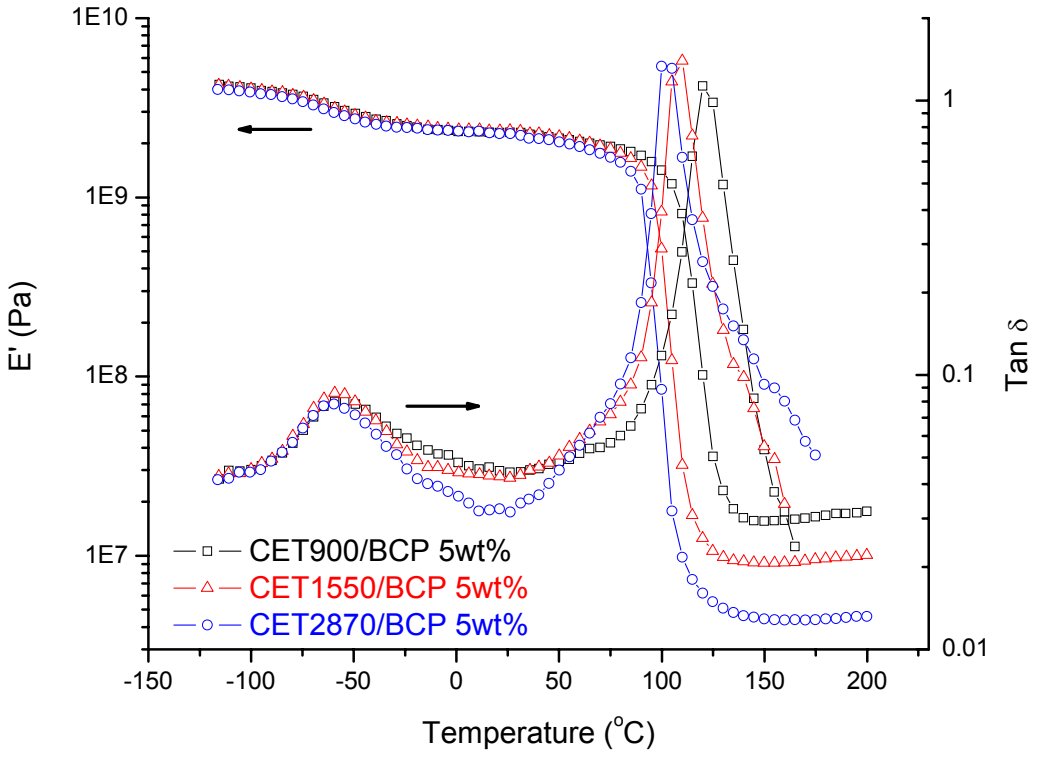

(b)

Figure 4.2. Continued.

Table 4.2. Storage modulus (E'), glass transition temperature (T_g) and fracture toughness (K_{IC}) of the samples.

Sample	E' (Pa)			T_g (°C)	K_{IC} (MPa·m$^{1/2}$)
	At low temp.	At room temp.	At rubbery plateau		
CET900	3.27×10^9	1.99×10^9	1.79×10^7	125	0.82±0.05
CET1550	3.86×10^9	2.25×10^9	1.33×10^7	115	0.96±0.04
CET2870	2.80×10^9	2.04×10^9	3.20×10^6	110	0.94±0.03
CET900/BCP	4.07×10^9	2.31×10^9	1.68×10^7	120	1.95±0.03
CET1550/BCP	4.04×10^9	2.36×10^9	9.38×10^6	110	2.73±0.08
CET2870/BCP	3.87×10^9	2.27×10^9	4.38×10^6	100	3.02±0.17

For the neat epoxies (Figure 4.2a), as expected, T_g decreased with decreasing crosslink density, because T_g is prone to be affected by larger-scale molecular motions, which are directly related to the molecular weight between crosslinks for a thermoset system. However, by comparing the heights of the tan δ curves between the α-relaxation peak (T_g) and the β-relaxation peak, it shows that the higher M_c epoxy exhibits slightly lower damping characteristics. Following this logic, the higher crosslink density epoxy

should be more capable of dissipating fracture energy (tougher), which was found not to be the case (see Section 4.3.3). This observation further implies that the toughenability of epoxies cannot be simply correlated with the magnitude of tan δ curve from DMA alone. The physical nature responsible for the observed damping phenomenon is much more important for the correlation with toughenability. To be noted, the above finding has also been found in a core-shell rubber (CSR)-modified epoxy system.[17]

As will be discussed in detail in the next section, the rubbery plateau modulus is inversely related to the M_c. But it is much more complex for storage moduli at low and ambient temperatures. The CET1550 has a higher E' than those of CET900 and CET2870. It is known that modulus is influenced more by the localized small-scale molecular motions, backbone rigidity, or chain rotation. Therefore, with the addition of more chain extender between crosslinks, there is likely to be a competition between a decrease in crosslink density and an increase in backbone rigidity, because the BPA chain is more rigid than the diglycidyl ether segment in the epoxy monomer.

For BCP-toughened epoxies (see Figure 4.2b), the general crosslink density effects on storage modulus, T_g and damping curve are analogous to those of their neat epoxy counterparts. It is worth mentioning that there is a consistent increase in room temperature storage modulus for all BCP-containing epoxy samples relative to their neat controls. This finding indicates that the modulus of the epoxy is not compromised with the incorporation of BCP toughening agent.

4.3.2. Determination of Crosslink Density

As stated earlier, the theoretical value of M_c was calculated from the stoichiometry of epoxy resin, chain extender and crosslinker. The crosslink density of each sample was also experimentally estimated by measuring the equilibrium storage modulus in the rubbery state, according to the equation from the theory of rubber elasticity[153]:

$$M_c = \frac{\rho RT}{G_r} \tag{4.1}$$

where ρ (in g/m^3) is the density of the polymer, G_r (in Pa) the shear equilibrium storage modulus in the rubbery state, M_c in g/mol and R and T are the real gas constant (8.314 J·K^{-1}·mol^{-1}) and temperature (in Kelvin), respectively. The density of each sample at room temperature was first measured by the displacement method. The density in the rubbery state was calculated on the basis of the dimensional change from the CTE information obtained from TMA (the density data are given in Table 4.3). The G_r value is assumed to be related to the flexural equilibrium storage modulus, E_r, in the following manner:

$$E_r = 2G_r(1+\nu) \tag{4.2}$$

where ν is the Poisson's ratio and assumed to be 0.5 which is typical for a rubbery material. E_r was obtained from DMA at rubber plateau region (see Table 4.2).

For convenience, the theoretically and experimentally determined M_c values of all the samples in this study are listed in Table 4.3. As expected, there is a discrepancy between the experimentally determined M_c and the expected theoretical value of M_c, but

the correlation between the experimental and theoretical M_c values follows a linear trend except for the neat CET2870 sample (Figure 4.3a). We also tried to estimate M_c using the empirical equation derived by Nielsen[154] and Timm et al.[155]:

$$\log_{10} G_r = 6.0 + \frac{293\rho}{M_c} \tag{4.3}$$

where ρ is in g/cm^3, G_r in Pa and M_c in g/mol. But the discrepancy in this scenario was much bigger than using the previous Equation (4.1) and the linear correlation was not observed (Figure 4.3b). Apparently the rubber elasticity theory fits better for the system in the current study and is therefore chosen to calculate the experimental M_c for crosslink density effect investigation.

It is noted that the cured epoxy network is far more complex than that of an ideal rubber. The estimated M_c values here are only meant to provide a semi-quantitative assessment of the crosslink density of the epoxy network investigated. To make the comparison meaningful, all the M_c values reported in this study, including those obtained from literature, were calculated using Equation (4.1).

It is interesting to note that the presence of the BCP seems to lower the crosslink density of the epoxy matrix for CET900 and CET1550 systems. There is no evidence of any chemical reaction between the BCP and epoxy components. It is believed that the major interaction between the two phases is through hydrogen bonding between the –OH groups generated during the cure reaction and the ether oxygen in the PEO backbone. The presence of the BCP phase, especially the epoxy-philic PEO block may somehow hinder the crosslinking process. This is possibly the explanation for the observed

increase in M_c with the addition of BCP. The BCP effect on crosslink density may partially account for the altered matrix toughenability and the high strain rate sensitivity as well. This effect was not observed for the lightly crosslinked CET2870 system.

Table 4.3. Density and molecular weight between crosslinks (M_c) of the model epoxy systems.

Sample	Density at room temp. (g/cm^3)	Density at rubbery plateau (g/cm^3)	Theoretically estimated M_c (g/mol)	Experimentally estimated M_c (g/mol)
CET900	1.212	1.127	900	320
CET1550	1.200	1.127	1550	950
CET2870	1.204	1.133	2870	3890
CET900/BCP	1.204	1.117	-	750
CET1550/BCP	1.200	1.127	-	1320
CET2870/BCP	1.201	1.117	-	2760

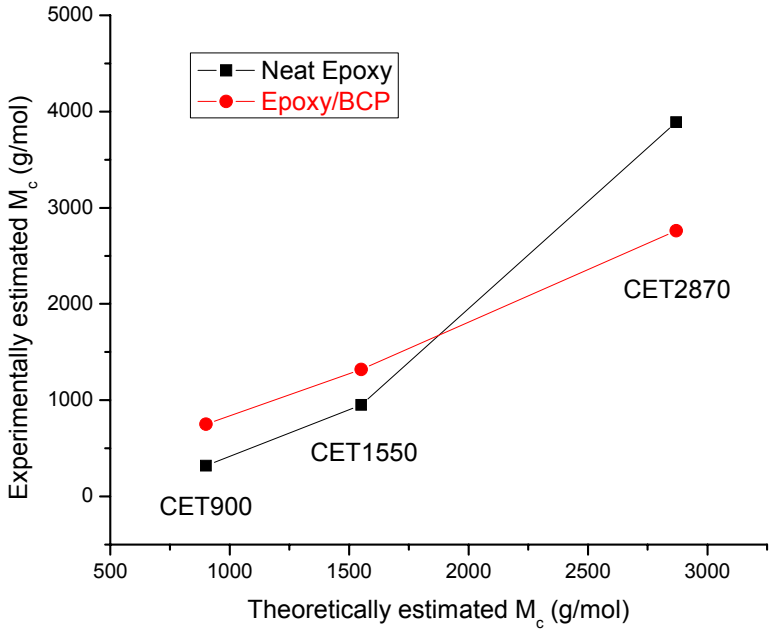

(a)

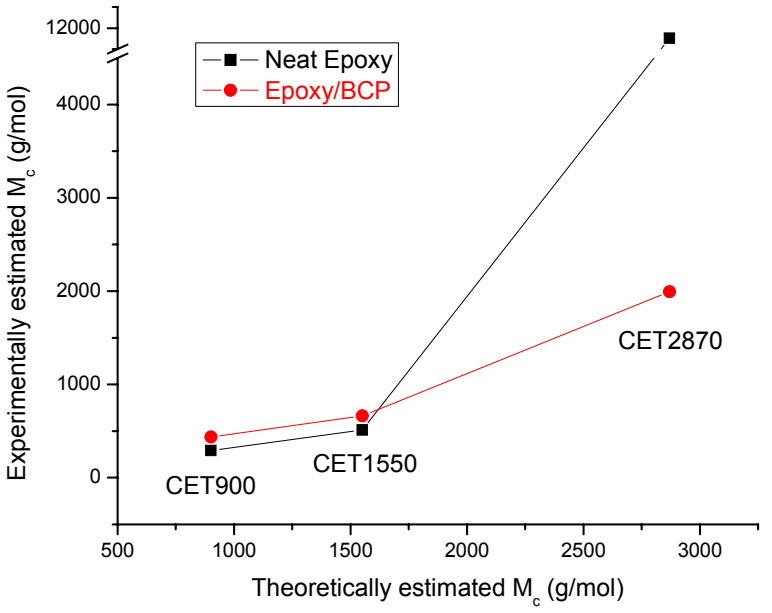

(b)

Figure 4.3. Correlations of theoretical M_c and experimental M_c estimated using (a) rubber elasticity equation and (b) Nielsen and Timm's equation, for the neat and modified epoxies in this study.

4.3.3. Fracture Toughness Measurement

The fracture toughness values of the neat epoxies and the BCP-modified epoxies with various M_c are summarized in Table 4.2. It is evident that the addition of the BCP with an overall concentration of only 5 wt% can significantly improve the fracture toughness at all crosslink densities. As expected, the fracture toughness of the BCP-modified epoxies is strongly dependent on the matrix crosslink density. The higher the epoxy M_c, the higher the K_{IC} value becomes. Such a crosslink density effect is not found in the neat system. The matrix M_c does not seem to have much influence on the fracture toughness of the neat epoxies. By comparing the relative K_{IC} improvement in each M_c case, it is not difficult to find that the lower crosslink density epoxy has a higher capability of being toughened through the incorporation of BCP toughening agent, i.e., a higher toughenability.

In addition, the above crosslink density-toughenability correlation has been compared with that in a 5 wt% CSR-modified epoxy system,[17] as shown in Figure 4.4. The comparison of toughening effect between the two rubber tougheners suggests that the BCP phase is at least as effective as CSR in toughening epoxies of various crosslink densities. In addition, there appears to be a critical M_c value for the rubber-modified systems beyond which the further enhancement in fracture toughness will diminish. The above phenomenon may be due to the fact that the high M_c rubber-toughened epoxy is too tough for the LEFM approach to become valid. The *J*-integral approach has to be undertaken to account for the high toughening effect of the high M_c epoxy resins.

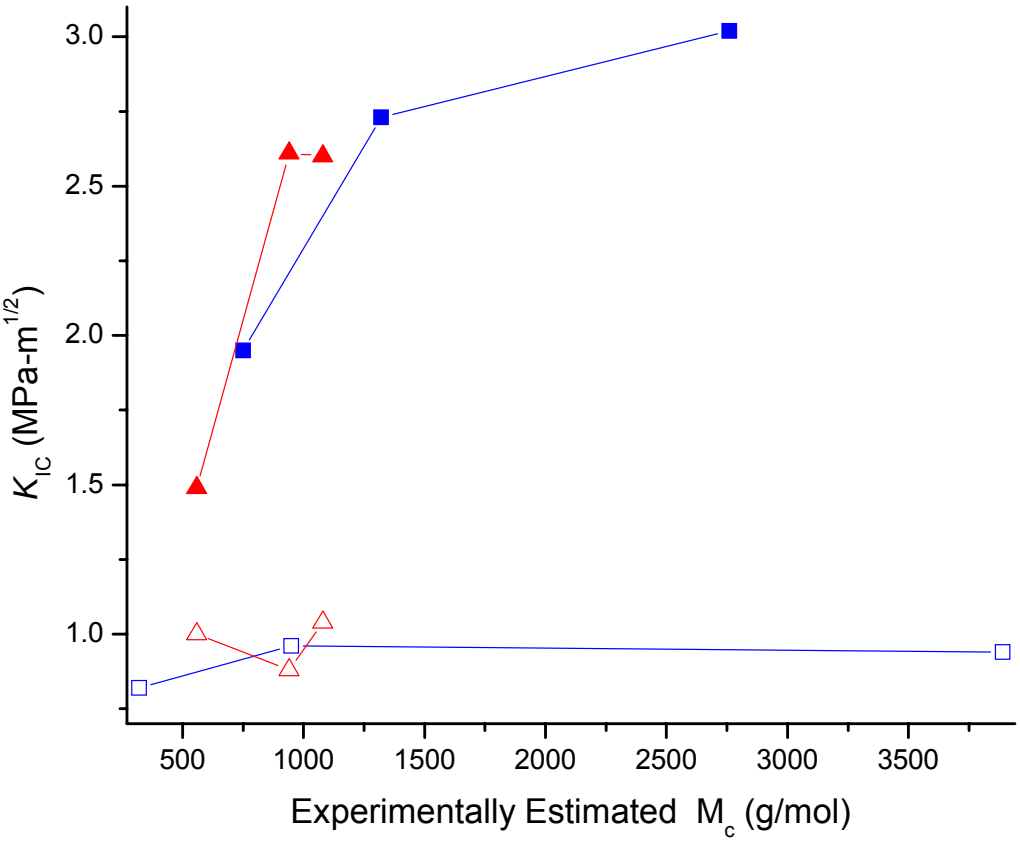

Figure 4.4. Fracture toughness, K_{IC}, plotted against the matrix M_c for two sets of neat and modified epoxy resins: the ones in the present work (□ unmodified and ■ 5 wt% BCP-modified) and in the work done by Sue et al.[17] (△ unmodified and ▲ 5 wt% CSR-modified). The experimental estimated M_c data of the CSR system were reprocessed using Equation (4.1) from the rubber elasticity theory.

4.3.4. Crosslink Density Effect on Toughening Mechanisms

As aforementioned, it is imperative to investigate the physical nature and micromechanical mechanisms of the toughening process for a fundamental understanding of crosslink density effect. With the aid of the DN-4PN technique, the key toughening mechanism in these modified epoxies has been found to be BCP nanoparticle cavitation-induced matrix shear banding. This study focuses on the difference in major toughening effects from the influence of the matrix crosslink density.

Figure 4.5 presents the OM images of the subcritical crack tip damage zones in the modified epoxies after the DN-4PB test under both bright field and cross-polars. It is clear from the bright field images that, the lower the crosslink density, the larger the damage zone size that is formed in front of the crack tip. In the images taken under cross-polarized light, a birefringent zone is observed in the middle of the crack tip damage zone, indicating a shear banding process. It is also found that the size and the intensity of the shear banding zone increase with decreasing crosslink density.

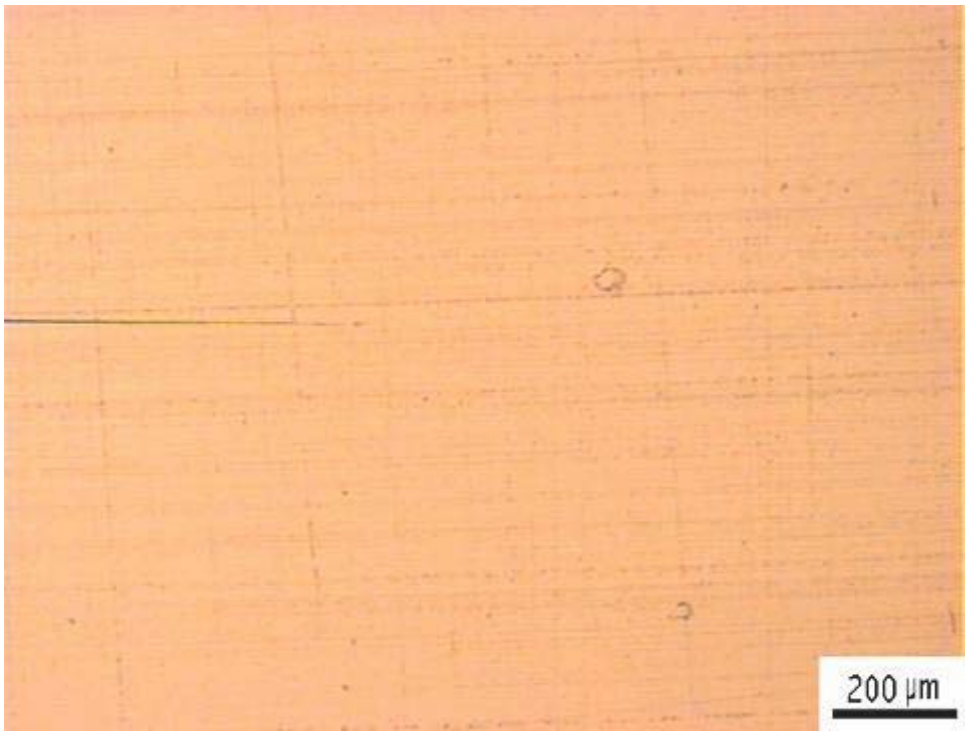

(a)

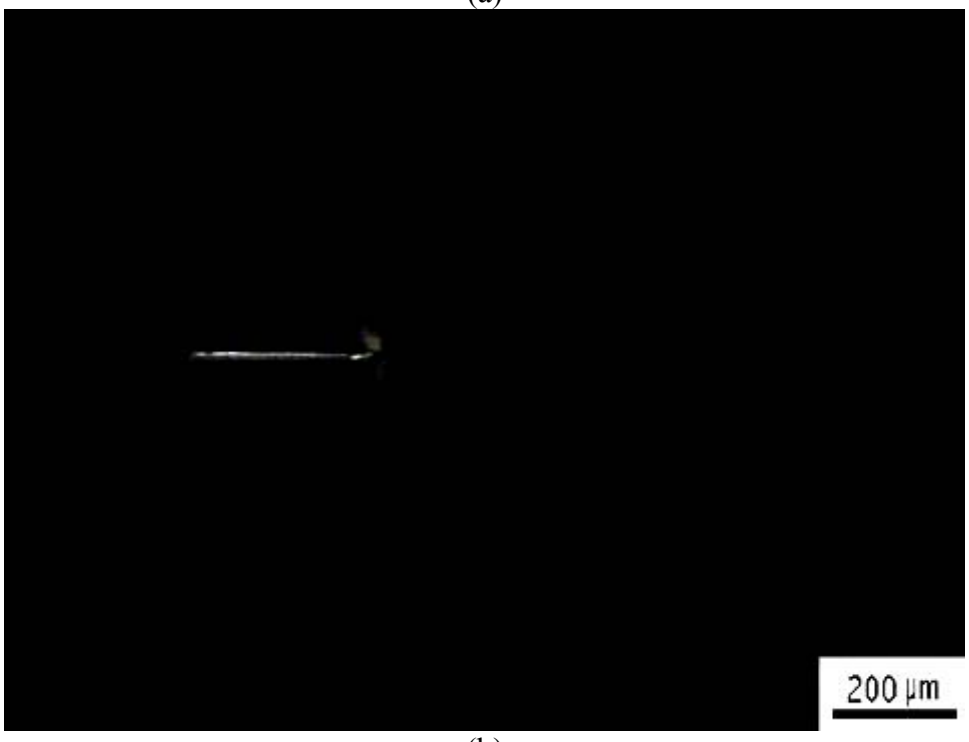

(b)

Figure 4.5. OM images of subcritical crack tip regions in CET900/BCP (a,b), CET1550/BCP (c,d) and CET2870/BCP (e,f), respectively. All the cracks propagate from left to right. The images were taken under both bright (a,c,e) and cross-polarized (b,d,f) fields at same location for each example.

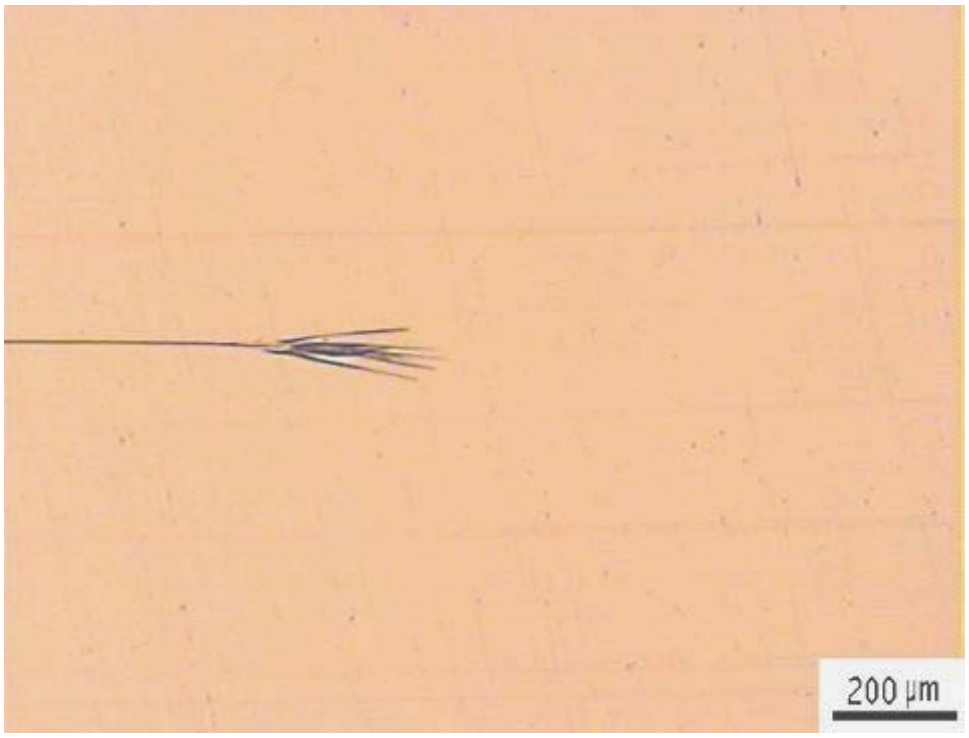

(c)

(d)

Figure 4.5. Continued.

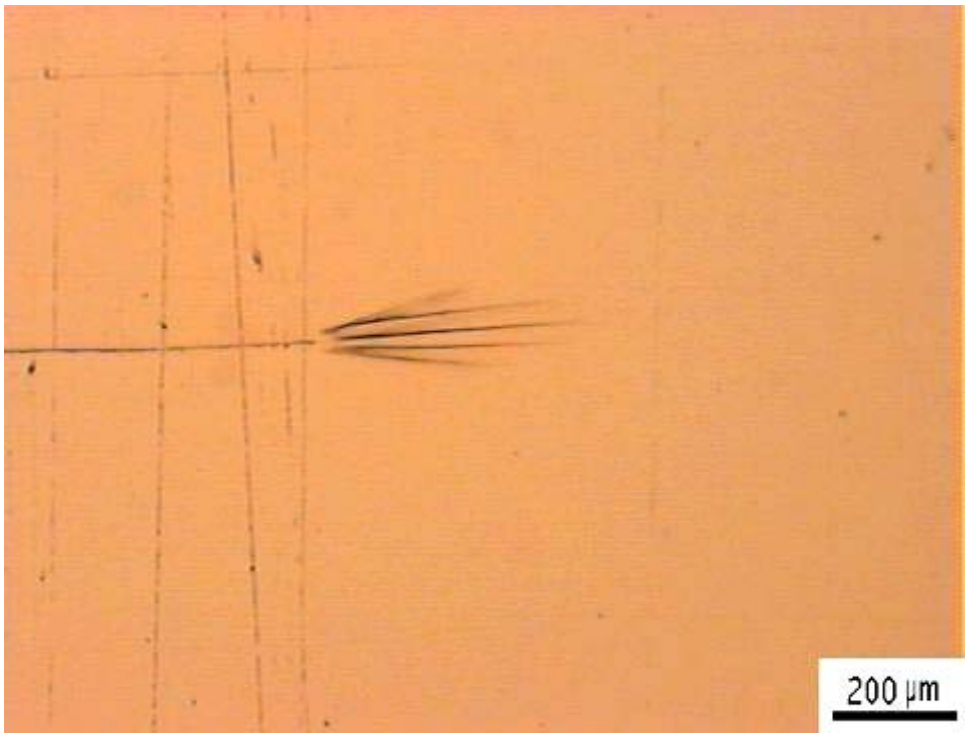

(e)

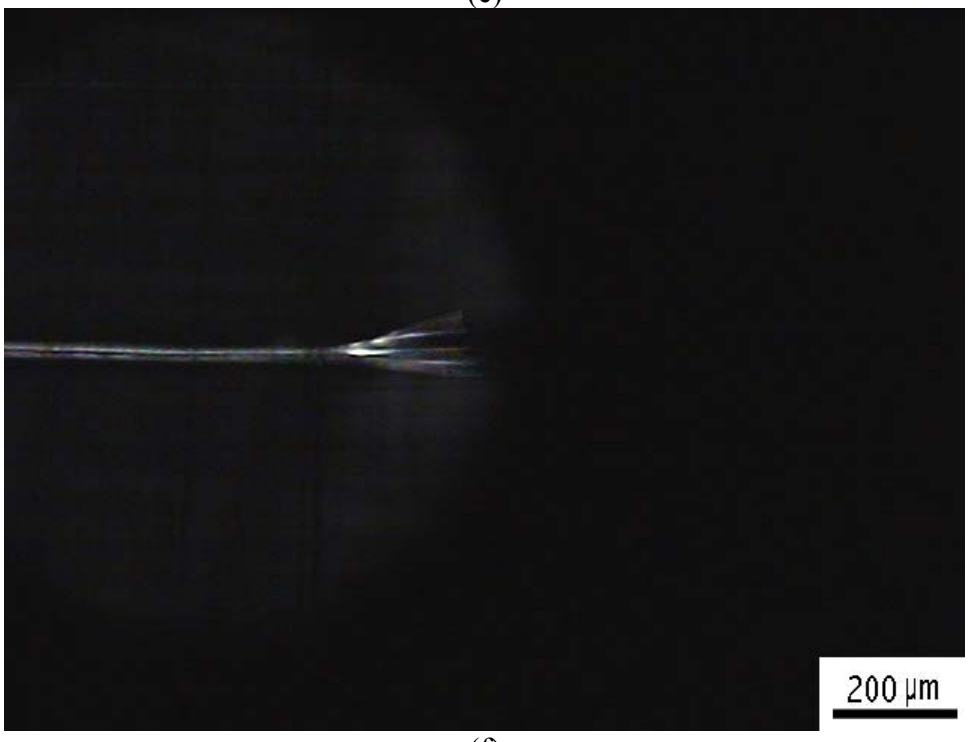

(f)

Figure 4.5. Continued.

To understand the details of the micromechanical deformation process upon fracture, TEM was performed to examine the specific location in the vicinity of the subcritical crack tips in the BCP-modified epoxies after DN-4PB (Figure 4.6). In the case of CET900/BCP, some cavitated nanoparticles have been found to remain spherical in shape, even in the regions immediately beneath the crack path. As for CET1550/BCP, the cavitation phenomenon becomes more uniform, and some form of stretching and orientation of the BCP nanoparticles has been found, which indicates the shear plastic deformation of the matrix around those particles. The micromechanical mechanisms found in the case of CET2870/BCP are similar to CET1550/BCP, but the degree of particle deformation is more pronounced. As indicated in the TEM micrograph, cavitated BCP particles adjacent to the crack seem to have undergone severe stretching.

All the information obtained from OM and TEM observations is consistent with the fracture toughness results. It is evident that the particle cavitation and matrix shear banding mechanisms are highly suppressed for high crosslink density epoxies. The higher the M_c the more flexible the network architecture becomes. This means it is more likely that the material can undergo plastic deformation and dissipate more fracture energy through intermolecular motions. On the contrary, in the low M_c cases, the capability of localized plastic deformation is highly restricted by less mobility chains with a high concentration of crosslinking sites in the network.

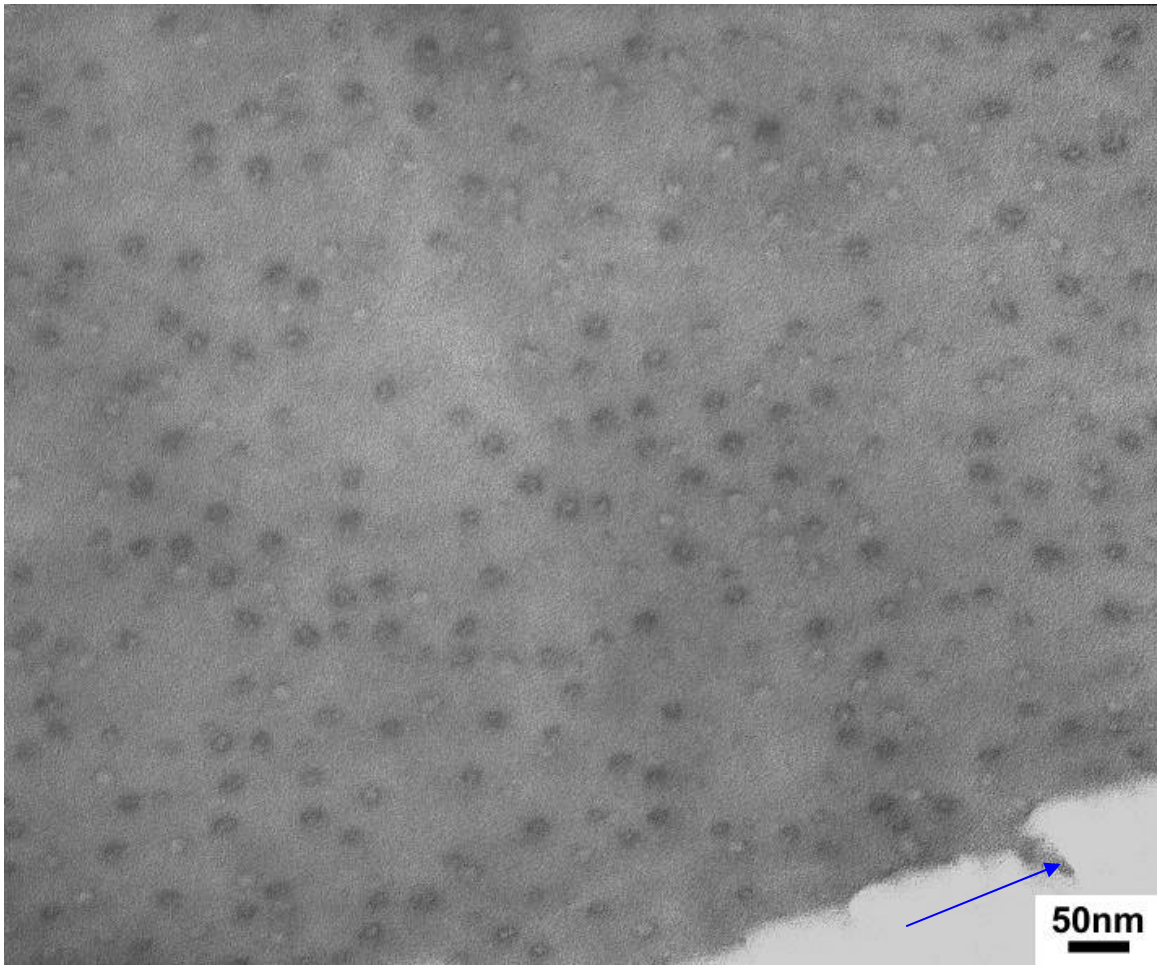

(a)

Figure 4.6. TEM micrographs taken in the vicinity of subcritical crack tips in (a) CET900/BCP, (b) CET1550/BCP and (c) CET2870/BCP, respectively. The specimen thin-sections were stained using 0.5% RuO_4 aqueous solution prior to TEM imaging. The crack propagating directions are indicated in the images. In the CET2870/BCP image, the arrows point to the BCP nanoparticles that are severely stretched.

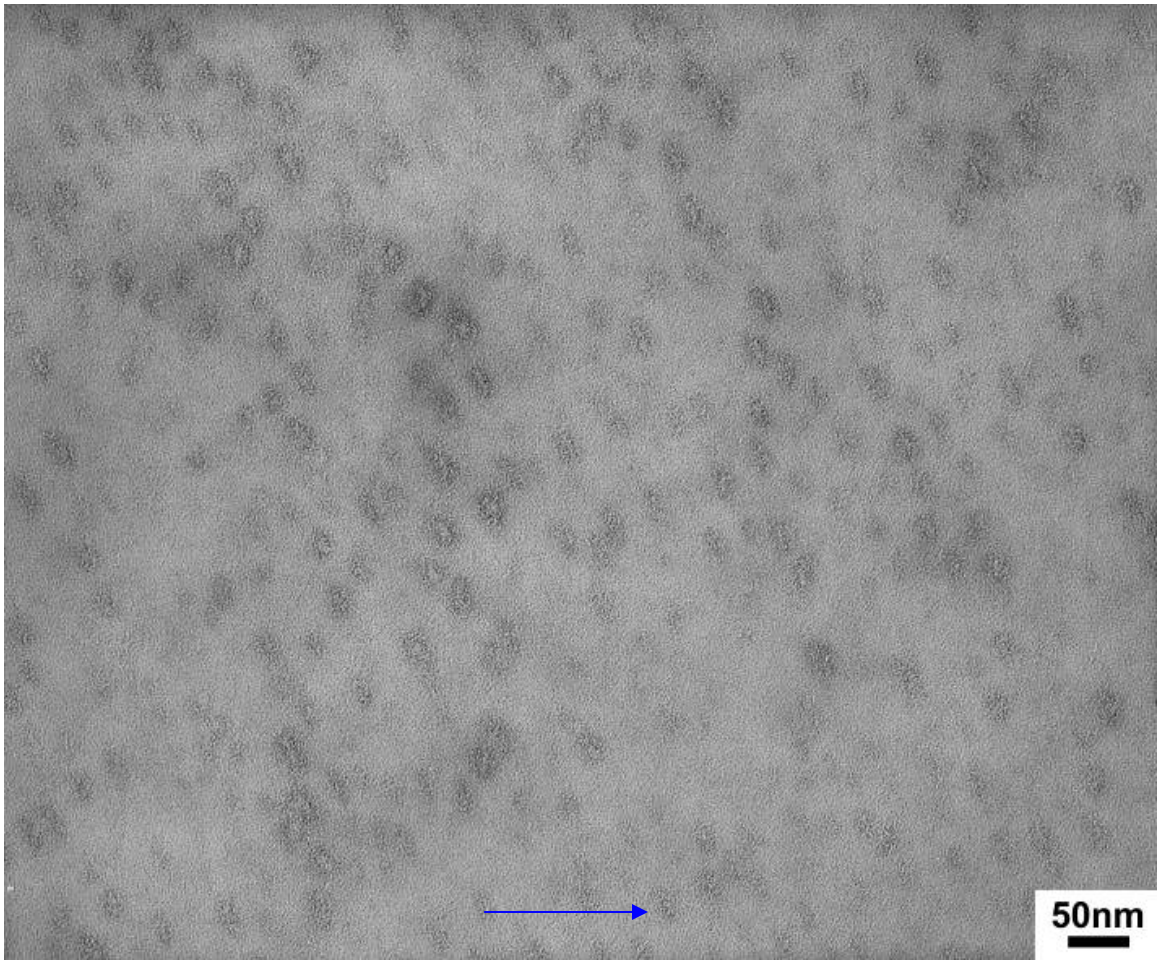

(b)

Figure 4.6. Continued.

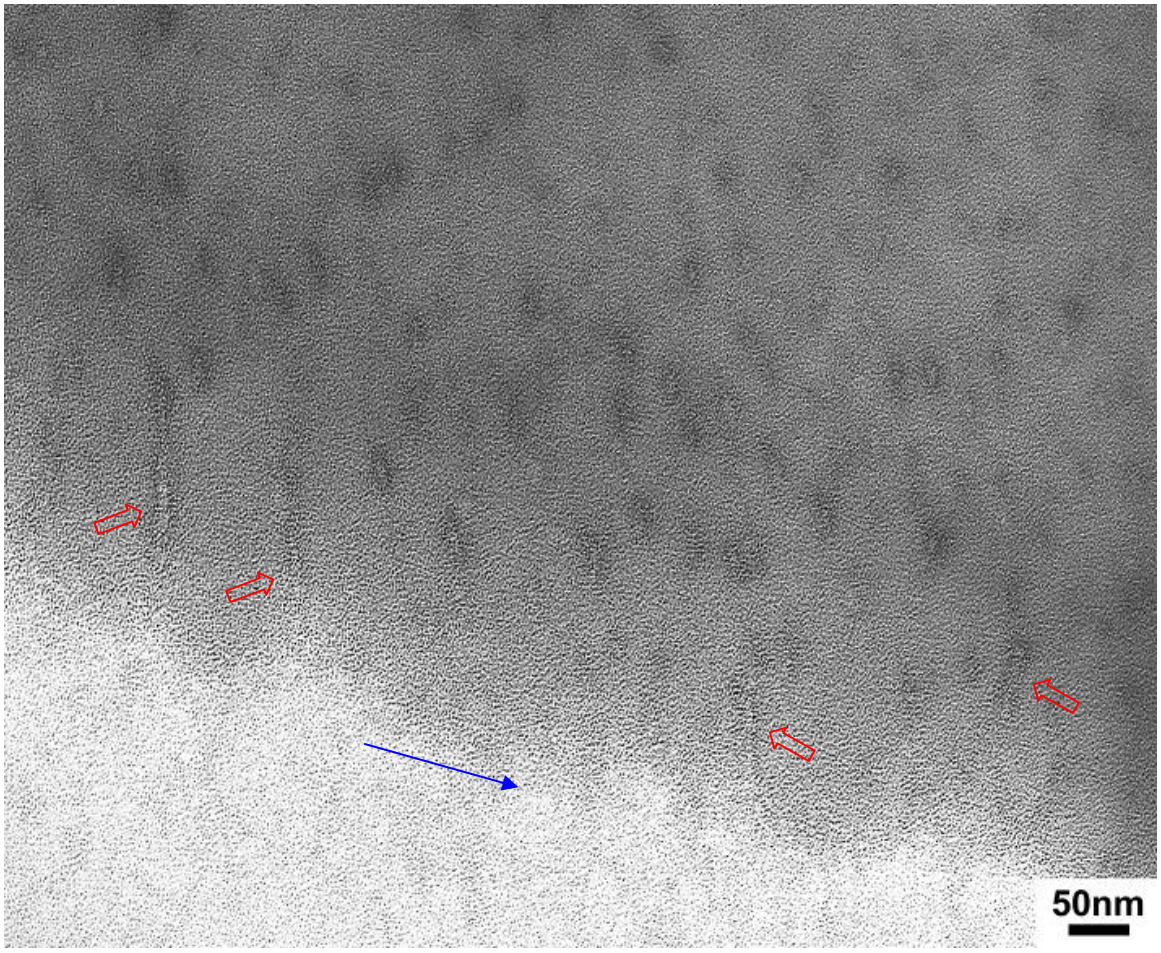

(c)

Figure 4.6. Continued.

It is known that normally epoxy itself is extremely difficult to have shear deformation under high triaxial stress state (plane-strain condition), e.g., at the crack tip. Thus, the effect on the energy dissipation process above M_c has to be with the presence of rubbery particles, because cavitation of those particles can relieve the local triaxial stress and alter the stress state to plane-stress condition. That is also why the crosslink density effect seems to be a nonfactor in neat thermosetting systems. On the other hand, a sufficiently high ductility matrix is considered a fundamental requirement for a thermosetting material to be toughenable by the incorporation of rubbery phase.

It is worth mentioning that the correlation between crosslink density and toughenability may not necessarily hold true when the nature of epoxy backbone molecular rigidity or the applied stress state is altered. Sue et al. have found a totally opposite M_c-toughenability relationship in two toughened epoxy resins with different side groups on the epoxy monomers.[17] The toughenability of an epoxy resin has also been altered by Kishi et al. by changing the stress state[150] or the shear ductility through the incorporation of ductile thermoplastic resins.[149]

4.3.5. Implications of the Present Work

The family of BCP-modified epoxies in this research has shown its versatility to meet specific engineering requirements for T_g, modulus, and ductility/toughenability. This argument is based upon the fact that these material properties can be influenced in different scales. T_g appears to be affected by large-scale main-chain motions, such as molecular motions involving multi-monomer length scales or distance between

crosslinks. Ductility or toughenability, is affected by smaller-scale intrachain corporative motions and molecular mobility. On the other hand, modulus seems to be influenced more by monomer rigidity, chain rotation, and localized small-scale molecular motions. It is very possible to design a material with a desirable combination of T_g, modulus and toughness characteristics if one can decouple the size scales influencing different properties.

Generally speaking, in rubber-toughened polymeric systems, the properties of the elastomeric phase, such as cavitational strength, particle size, concentration, etc., are critical for the resulting toughening effect. Also, the nature of the matrix definitely plays an important role in determining whether or not toughening mechanisms can operate effectively. The crosslink density in thermosetting materials is one example. Although a crosslink density-toughenability relationship has been clearly revealed with experimental evidence in this study, the questions as to how the epoxy network develops during curing and how that process can be influenced by the presence of a heterogeneous inclusion, still remain unanswered. There is also no direct technique that can definitively probe the inhomogeneity, unreacted functionality, or other defects in a thermosetting resin. More efforts are still needed to achieve a complete understanding of structure-property relationship of engineered thermosets at the molecular level.

4.4. Summary

The fracture characteristics of PEP-PEO BCP-modified epoxies were carefully studied with variations in matrix crosslink density. As expected, the findings suggest that

the toughenability of the epoxy resin has a strong dependence on its M_c. The lower the crosslink density is, the more capable the host resin can be toughened by the incorporation of the elastomeric phase. The nano-sized BCP particles appear to be at least as effective as CSR in toughening epoxies at various levels of crosslink densities. It is possible to develop a high performance thermosetting material with combined desirable T_g, modulus and toughenability. Additional work is still needed for understanding the physical nature of network formation and its interactions with BCP particles at nanometer scale, especially at their interphase.

CHAPTER V

STRAIN RATE EFFECT ON MECHANICAL PROPERTIES OF EPOXIES CONTAINING NANO-SIZED BLOCK COPOLYMER MICELLES

A bisphenol A-based epoxy was modified with an amphiphilic poly(ethylene-*alt*-propylene)-*b*-poly(ethylene oxide) (PEP-PEO) block copolymer (BCP) as a toughening agent. PEP-PEO molecules self-assemble into nano-sized spherical micelles in epoxy and give rise to a significant improvement in fracture resistance. The fracture and tensile behavior of the PEP-PEO-modified epoxy were investigated at loading rates ranging from 0.51 to 508 mm/min. The toughened epoxy exhibits mechanical properties that are significantly more rate dependent than the neat epoxy material. As expected, a higher test rate leads to a more brittle behavior of the material and a lower fracture toughness value. The implications of the current findings on nano-sized rubber toughening of epoxy are discussed in detail.

5.1. Introduction

Significant attention has been drawn onto improving the fracture toughness of brittle epoxy thermosets. Those toughening techniques include the modification with micrometer-sized liquid rubbers,[3-8] core-shell rubber (CSR) particles,[9-18] and thermoplastic particles.[21-31] The addition of rubbery toughening agents normally leads to an impressive toughening effect, but may also cause severe deterioration in glass

transition temperature (T_g), modulus, strength, and other desirable properties. The introduction of thermoplastic particles will typically give a moderate toughening effect and cannot produce satisfactory results for low temperature or high rate test conditions. Consequently, there is a significant demand to develop alternative toughening techniques to substantially increase the fracture resistance of brittle epoxies without compromising other desired physical and mechanical properties.

Recently, a new epoxy toughening approach using self-assembling amphiphilic BCP has drawn significant attention.[32-41] Incorporation of a small amount of dispersed, microphase separated, BCP can produce improvements in fracture toughness without compromising the T_g and Young's modulus of the cured neat epoxy. The three primary shapes that have been studied include spherical micelles, wormlike micelles, and vesicles.[33, 34, 38, 47] Despite recent publications that have shown a significant fracture toughness increase by the addition of BCP, only a few of them have discussed in detail the corresponding toughening mechanisms,[38, 41] but no definitive conclusions have been drawn.

Most recently, an epoxy system containing poly(ethylene-*alt*-propylene)-*b*-poly(ethylene oxide) (PEP-PEO) amphiphilic BCP, which self-assembled into well-defined 15 nm spherical micelles, was investigated. With only 5 wt% loading of the BCP phase, a significant improvement in fracture toughness was reported (see Chapter III). Detailed mechanistic investigations with direct microscopy observations revealed that the dominant toughening mechanism is BCP micelle particle cavitation-induced matrix shear banding. Furthermore, in contrast to a typical rubber-toughened epoxy, no drop in

T_g or modulus were detected. The above findings suggested that the PEP-PEO was well suited as a toughening agent for the epoxy investigated. However, upon the addition of PEP-PEO, there existed a pronounced viscoelastic damping behavior above room temperature in the cured epoxy, suggesting that its mechanical properties might be more strain rate dependent compared to the neat epoxy counterpart. A study on the strain rate dependence of BCP-toughened epoxy is therefore warranted.

Strain rate dependence on mechanical properties of polymers has been widely reported for homopolymers,[156-158] blends,[159] composites,[160-163] toughened plastics,[10, 76, 81, 164, 165] etc. Due to the viscoelastic nature of polymers, a lower strain rate usually leads to higher fracture toughness. A possible reason for the strain rate sensitivity is an increased available time for molecular mobility, thus dissipating the applied mechanical energy more effectively.[165] In this chapter, emphasis is placed on investigating the strain rate dependence of the same PEP-PEO-modified epoxy system discussed earlier. Fracture and tensile behavior, therefore, were examined at different test rates. The effects of test rate on toughening and its corresponding toughening mechanisms were carefully studied and implications of the current findings discussed.

5.2. Experimental

5.2.1. Materials

A diglycidyl ether of bisphenol A (DGEBA) epoxy resin (D.E.R. 332, Dow Chemical) was used. The crosslinker of choice was 1,1,1-tris(4-hydroxyphenyl)ethane (THPE, Aldrich). Bisphenol A (BPA) chain extender (PARABIS, Dow Chemical) was

used to control the crosslink density of the epoxy network. Ethyltriphenylphosphonium acetate (70% in methanol, Alfa Aesar) was added as a catalyst.

The PEP-PEO amphiphilic BCP was synthesized using a multi-step polymerization method previously described by Hillmyer and Bates.[119] Herein, PEO is an epoxy-philic block and PEP is an epoxy-phobic block. The weight fraction of ethylene oxide in the BCP is 0.40. The number-average molecular weight (M_n) of the BCP is 9100 g/mol.

5.2.2. Preparation of BCP-Modified Epoxy

The detailed procedure for sample preparation can be found in Chapter III. Only the key steps are described here for convenience. The BCP was mixed and completely dissolved in the epoxy resin at 150 ºC. Next, the crosslinker and chain extender were added into the mixture and dissolved. After degassing, the catalyst was added and the mixture was cured at 200 ºC for 2 h.

The overall BCP concentration in the resulting epoxy plaque was 5 wt% and the molecular weight between crosslinks (M_c) of the epoxy matrix was designed to be around 1550 g/mol. All the specimens were dried in a vacuum oven at 80 °C for at least 24 h prior to characterizations.

5.2.3. Dynamic Mechanical Analysis (DMA)

DMA was performed using an RSA III instrument (TA Instruments) at a fixed frequency of 1 Hz. The test temperature was increased from -10 to 105 °C at 5 °C per

step. A sinusoidal strain-amplitude of 0.05% was chosen for the analysis. The damping of the tested material can be expressed as tan δ which is related by:

$$\tan\delta = \frac{E''}{E'} \tag{5.1}$$

where *E*' is the storage modulus and *E*" is the loss modulus. The tan δ curves of both neat epoxy and BCP-toughened epoxy were plotted as a function of temperature.

5.2.4. Transmission Electron Microscopy (TEM)

TEM was used to characterize the morphology and fracture mechanisms of BCP-toughened epoxy. The material was thin-sectioned using room temperature microtomy. The ultrathin sections (ca. 80 nm in thickness) were collected on carbon-coated copper grids and then vapor-stained with a fresh 0.5 wt % RuO_4 aqueous solution (Electron Microscopy Sciences) for 10 min at 25 °C. The RuO_4-stained ultrathin sections were examined on a JEOL 1200 EX electron microscope operated at a 100 kV accelerating voltage. TEM micrographs were taken using calibrated Kodak electron microscope films.

5.2.5. Fracture Toughness Measurements

The linear elastic fracture mechanics (LEFM) approach was employed for fracture toughness measurements. A single-edge-notch 3-point-bending (SEN-3PB) test was performed to obtain the Mode-I critical stress intensity (K_{IC}) of the neat epoxy and BCP-toughened epoxy in accordance with ASTM D5045 on an MTS Insight machine. Three different test speeds were used: 0.51, 15.24 and 508 mm/min. A sharp crack was

generated on a 75 × 12.7 × 3.5 mm^3 specimen by inserting and tapping with a liquid N_2-chilled fresh razor blade. Special care was taken to ensure that the initial crack exhibited a thumbnail shape crack front prior to tests. At least five specimens were used to determine the K_{IC} for each sample.

5.2.6. Scanning Electron Microscopy (SEM)

Fracture surfaces were examined using a FEI Quanta 600 Field Emission-SEM (FE-SEM). Prior to imaging, the samples were sputter-coated with a thin layer (ca. 4 nm) of Pt/Pd (80/20). The microscope was operated at an accelerating voltage of 5 kV and a working distance of 10 mm.

5.2.7. Double-Notch Four-Point-Bending (DN-4PB) Test

In order to gain a fundamental understanding of the toughening mechanisms, the DN-4PB test[7, 119, 123, 124] was employed to probe the detailed micromechanical deformation of BCP-toughened epoxy upon fracture. Elaborated descriptions and schematics of the DN-4PB technique can be found in Chapter III.

DN-4PB tests were conducted at room temperature on an MTS Insight machine. Again, three different test speeds were utilized: 0.51, 15.24 and 508 mm/min. The specimen was loaded in a 4-point bending geometry with the cracks positioned on the tensile side. The arrested subcritical crack tip damage zone from the core region of the specimen was diced off and prepared accordingly for optical microscopy (OM) and TEM observations.

For OM investigations, thin sections of the mid-section of the DN-4PB crack tip damage zone were obtained by sectioning and polishing to a thickness of ca. 40 μm. These thin sections were then examined using an Olympus BX60 optical microscope under the bright field mode.

For TEM imaging, a block with the crack tip damage zone was isolated from the specimen and embedded in Epo-Fix embedding resin for materialographic use (Electron Microscopy Sciences). After curing overnight at room temperature, the block was trimmed into a trapezoid shape at the tip with a cross section area of around 0.3 × 0.3 mm^2. Then, the trimmed block was faced off by a diamond knife, followed by microtoming and staining as aforementioned.

5.2.8. Tensile Tests

Room temperature tensile tests were conducted in accordance with ASTM D638 using an MTS servo-hydraulic test machine. Four crosshead speeds were utilized in order to cover a reasonable range of different tensile behavior transitions: 0.51, 5.08, 50.8 and 508 mm/min. The strain was measured by a calibrated MTS extensometer (Model 632.11B-20). Average values and standard deviations of Young's modulus and yield stress were calculated based on at least three specimens per sample type.

5.3. Results and Discussion

5.3.1. Morphology of BCP-Toughened Epoxy

Figure 5.1 shows the TEM micrograph of RuO_4-stained BCP-toughened epoxy. The BCP phase has been stained to appear as dark color and the light background is the epoxy phase. It is evident that the BCP has self-assembled into well-defined spherical micelles and is homogeneously dispersed in the epoxy matrix. No macro-phase separation was observed. The diameter of the nano-phase separated BCP is on average 15 nm.

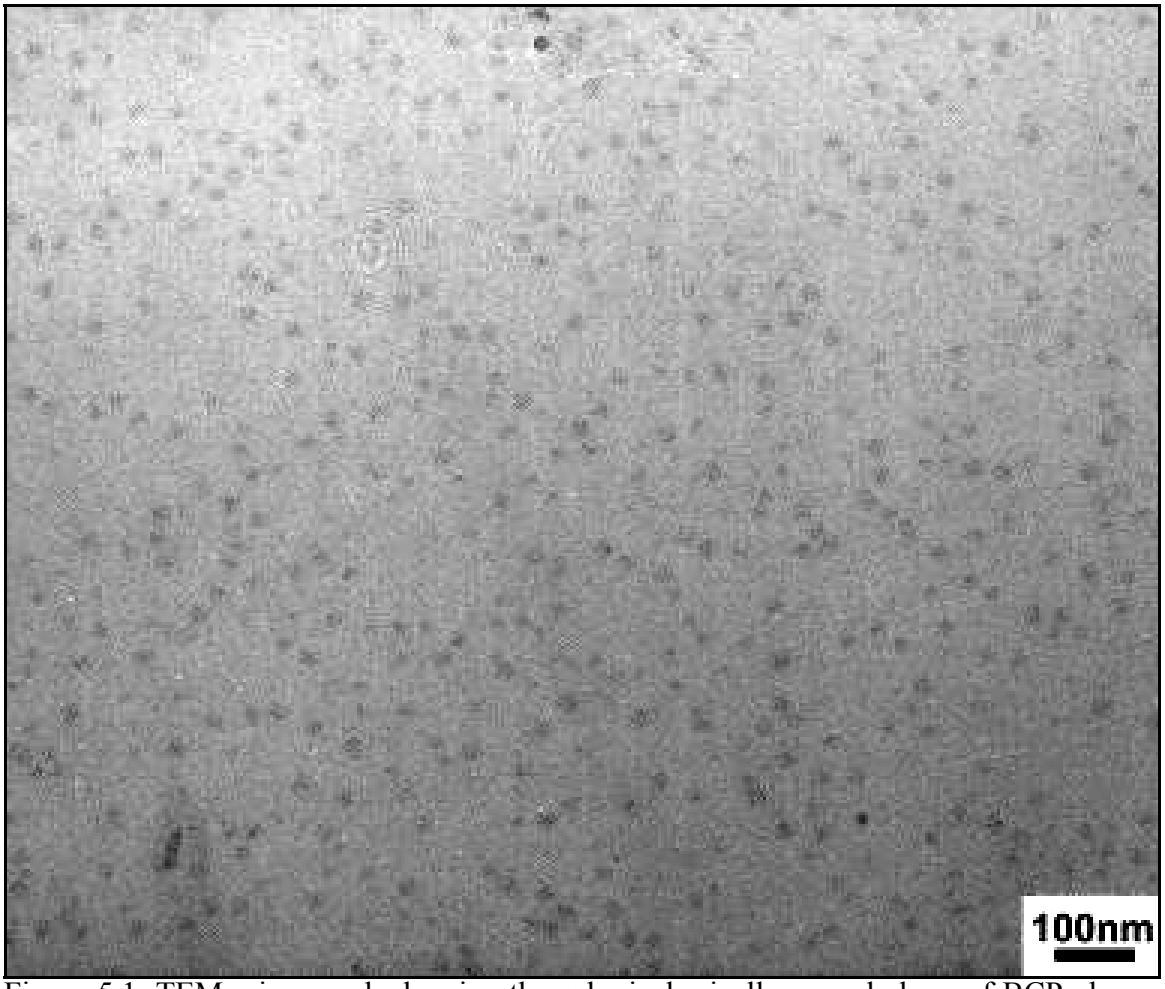

Figure 5.1. TEM micrograph showing the spherical micellar morphology of BCP phase in epoxy matrix.

5.3.2. Viscoelastic Damping Characteristics

The damping characteristics of neat epoxy and BCP-toughened epoxy were studied based on the tan δ curves obtained from DMA (see Figure 5.2). The spectra show a noticeable increase in the tan δ curve of epoxy after the incorporation of BCP at temperatures above 0°C. This indicates that the BCP causes some portion of the epoxy network to become more mobile at temperatures above 0 °C. One explanation for this behavior is mixing between the epoxy-philic corona blocks (PEO) at the boundary between the epoxy-phobic micelle core and the crosslinked epoxy matrix. PEO is estimated to have a glass transition temperature below -40 °C[166] and in the amorphous form this polymer will plasticize glassy epoxy. The wide temperature range over which tan δ is affected likely reflects a gradient in composition in the vicinity of the micelle corona. As a result, the BCP-toughened epoxy is likely to become more strain rate dependent when tested at room temperature. In this study, the strain rate effect on the mechanical behavior of BCP-toughened epoxy is therefore systematically investigated and compared against the unmodified equivalent.

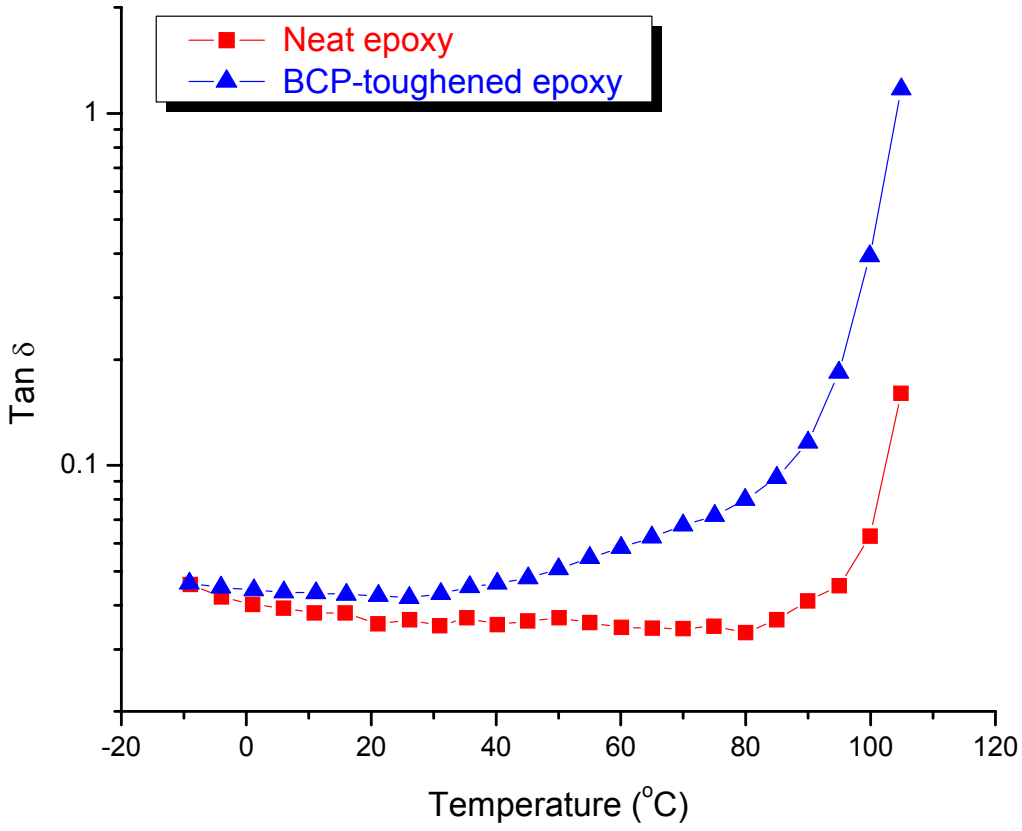

Figure 5.2. Tan δ traces of neat epoxy and BCP-toughened epoxy in a region leading up to their T_g.

5.3.3. Fracture Behavior

The K_{IC} values of neat epoxy and BCP-toughened epoxy are summarized in Table 5.1. Three different test rates of 0.51, 15.24, and 508 mm/min were chosen for the study. As shown in Table 5.1, the toughening effect for BCP-toughened epoxy is reduced significantly with an increase in the test rate. This indicates that the PEO block

of BCP has altered the epoxy network structure, making it more susceptible to strain rate dependence. It is also important to note that, although others have reported such a strain rate dependence in toughened polymeric systems,[10, 76, 164, 165] the rate dependence found in this study is much more prominent. One possible reason is that the PEO block might have participated in the network structure formation around the PEP phase, making it more effective in modifying the viscoelasticity of the epoxy network.

Table 5.1. Fracture toughness ($MPa \cdot m^{1/2}$) of neat epoxy and BCP-toughened epoxy at different test rates.

Test rate, mm/min	0.51	15.24	508
Neat epoxy	0.96±0.04	0.80±0.05	0.74±0.04
BCP-toughened epoxy	2.73±0.08	2.21±0.12	1.30±0.08
Relative toughening effect (toughened versus neat)	+184%	+176%	+76%

The fracture surface obtained from the SEN-3PB tested specimen was analyzed. A stress-whitening region is clearly shown on the fracture surface generated in the slowest test rate case (0.51 mm/min). When the test rate is increased, the whitening zone becomes smaller and smaller (see Figure 5.3). It is important to mention that no stress

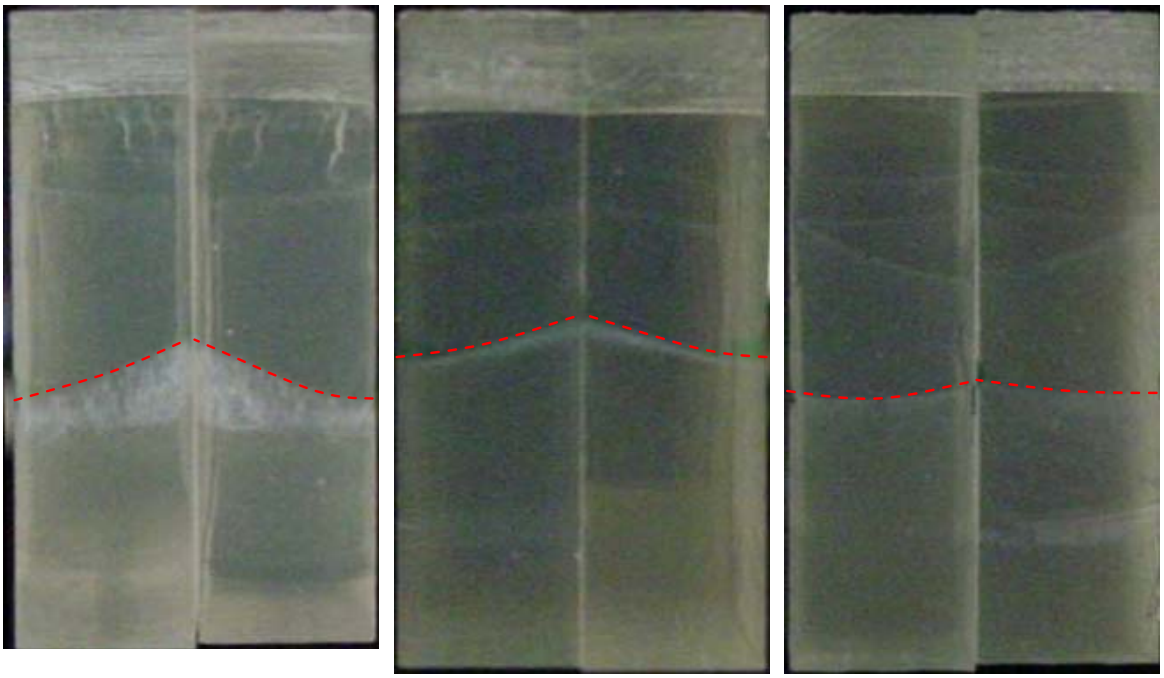

(a) (b) (c)

Figure 5.3. Fracture surfaces of BCP-toughened epoxy specimens after the SEN-3PB tests at test rates of (a) 0.51 mm/min, (b) 15.24 mm/min, and (c) 508 mm/min, respectively. The red dashed lines represent the initial crack fronts and the crack propagated from top to bottom.

whitening is expected in the neat epoxy regardless of the test rate. Because the stress-whitening phenomenon implies the presence of some form of cavitation, careful TEM observations in the crack tip region of the DN-4PB specimens were conducted to determine the source of the voiding phenomenon.

The fracture surfaces were also examined using SEM. Micrographs of BCP-toughened epoxy samples fractured at different rates are shown in Figures 5.4-5.6. For comparison purposes, the fracture surface of a neat epoxy fractured at 0.51 mm/min is shown in Figure 5.7. At a test rate of 0.51 mm/min, BCP-toughened epoxy exhibits a rough fracture surface in the crack tip region, suggesting a ductile fracture behavior. At higher test rates (i.e., 15.24 and 508 mm/min), only small-scale surface features were generated. In other words, the higher the test rate, the smoother the facture surface became. In contrast, neat epoxy fractured at 0.51 mm/min developed a featureless smooth surface as a typical brittle mode of fracture. Neat epoxy specimens tested at 15.24 and 508 mm/min showed no difference and, therefore, are not presented here.

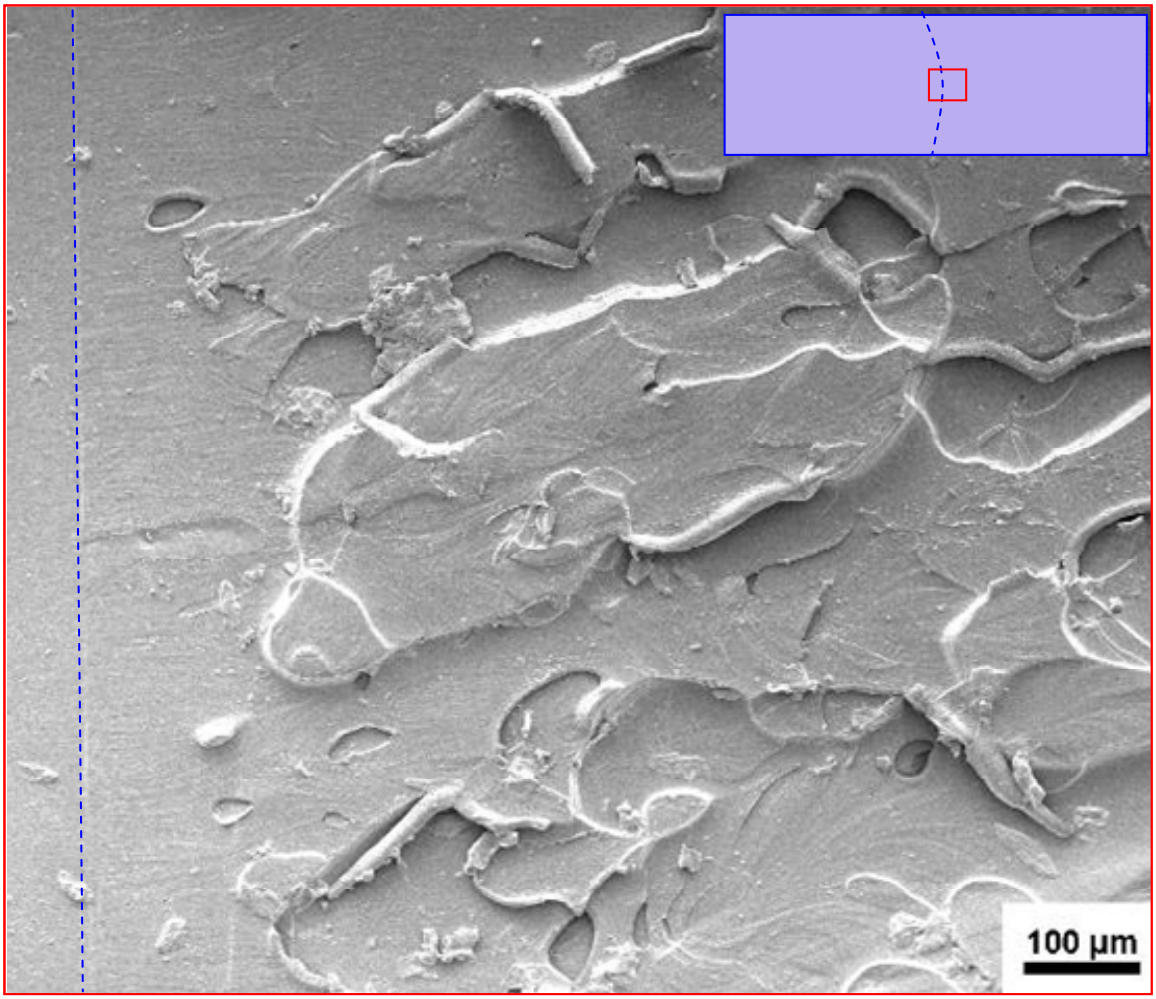

(a)

Figure 5.4. SEM micrographs showing the fracture surface of BCP-toughened epoxy fractured at 0.51 mm/min at a magnification of (a) 150× and (b) 600×. The insets show the spots where the micrographs were taken. The blue dashed lines represent the initial crack fronts and the crack propagates from left to right.

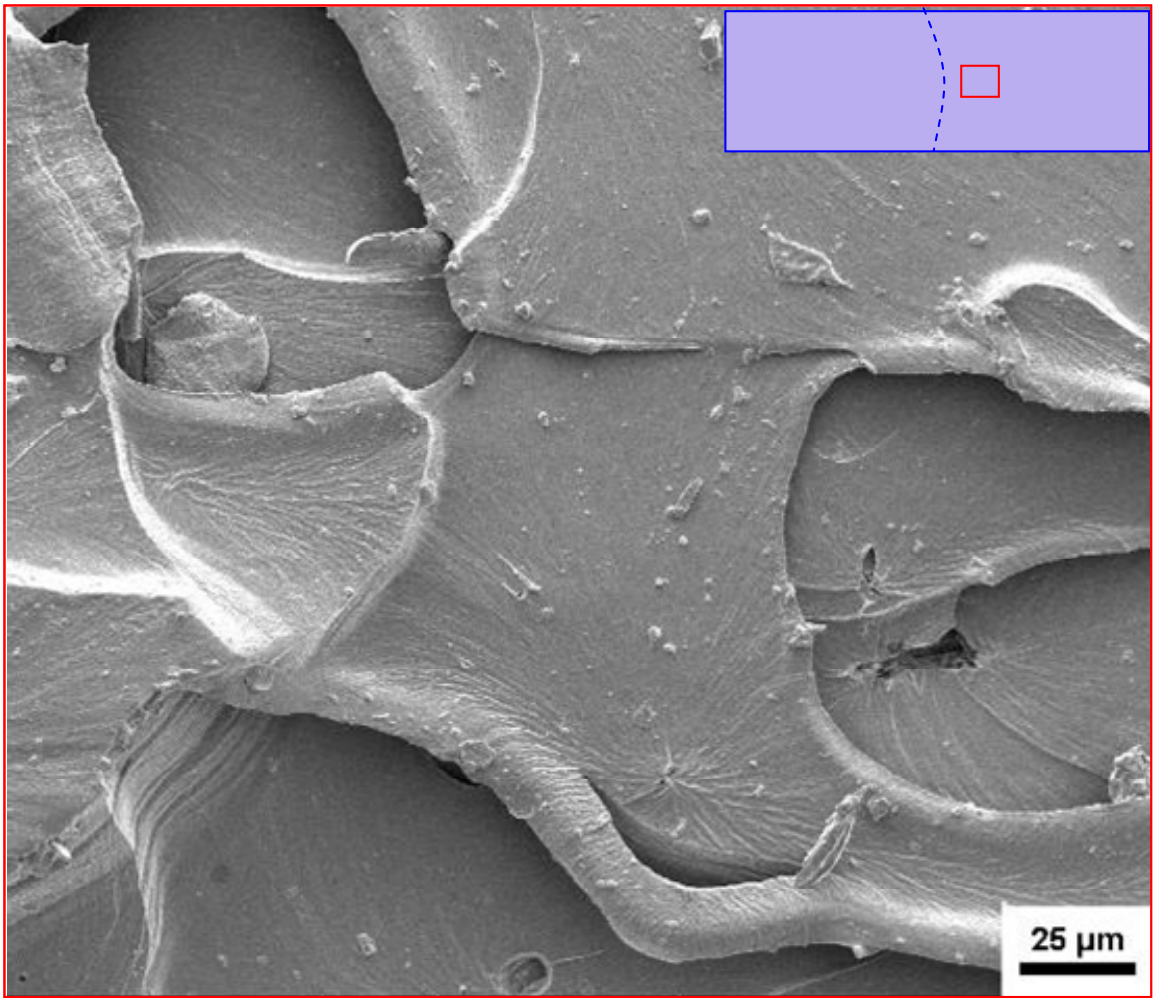

(b)

Figure 5.4. Continued.

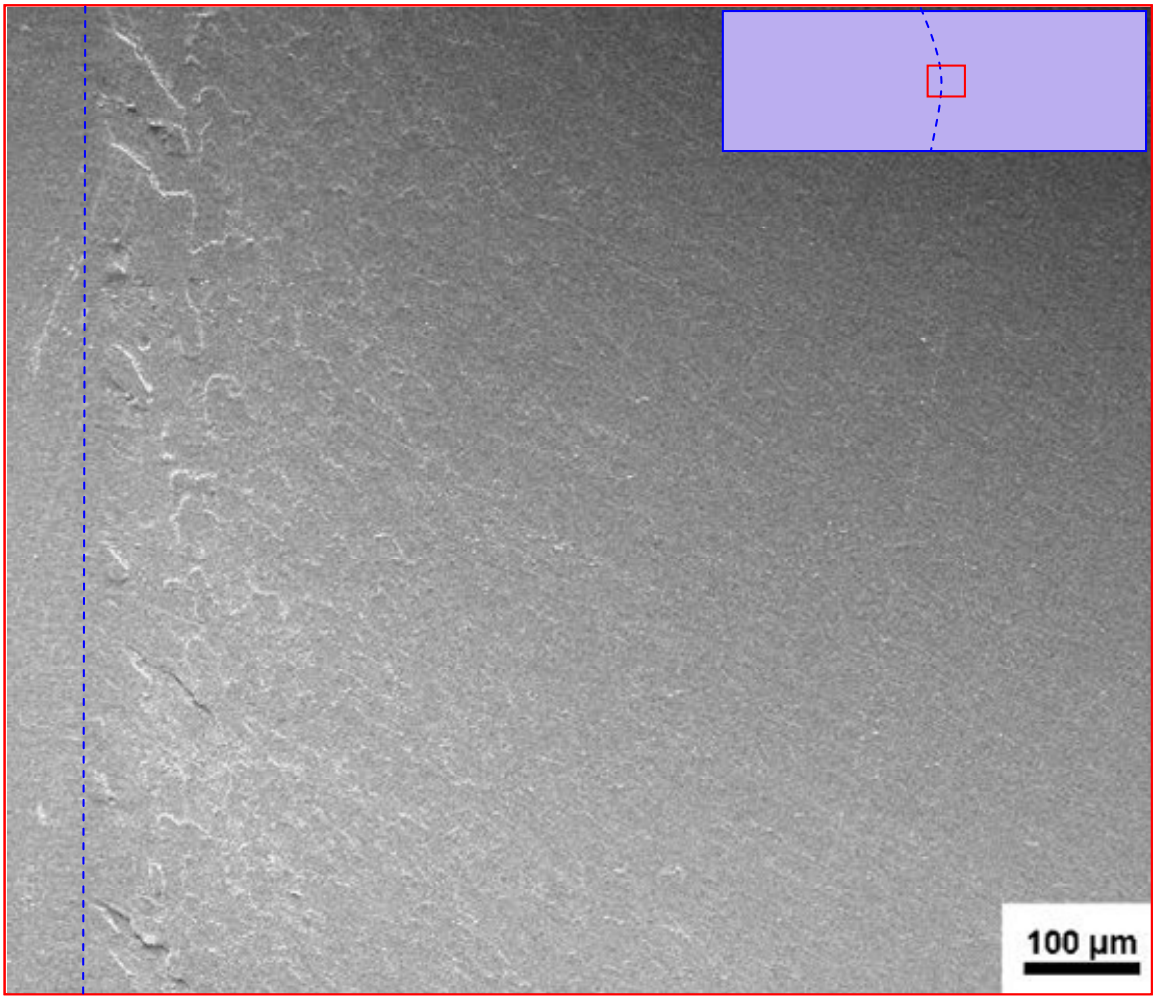

(a)

Figure 5.5. SEM micrographs showing the fracture surface of BCP-toughened epoxy fractured at 15.24 mm/min at a magnification of (a) 150× and (b) 600×. The insets show the spots where the micrographs were taken. The blue dashed lines represent the initial crack fronts and the crack propagates from left to right.

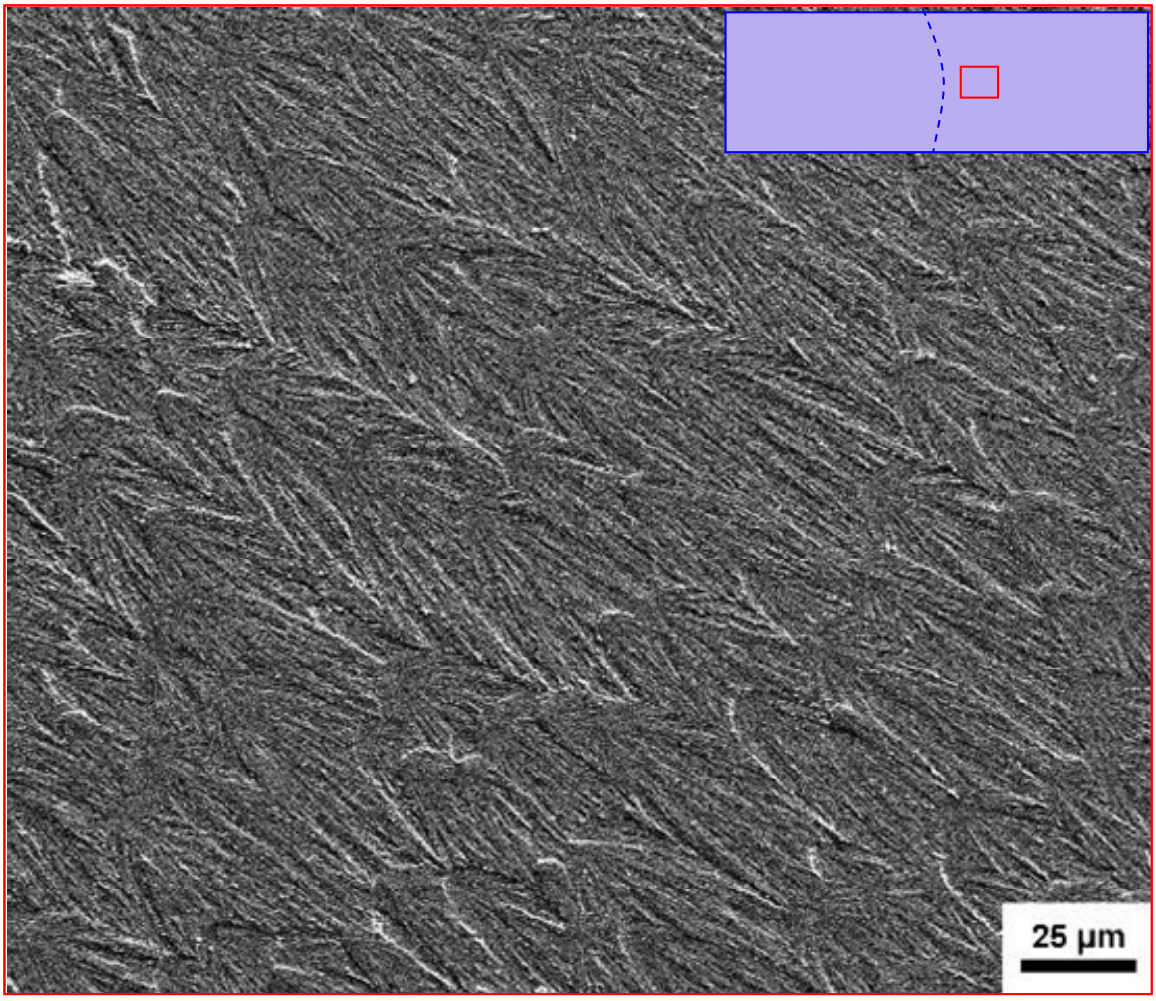

(b)

Figure 5.5. Continued.

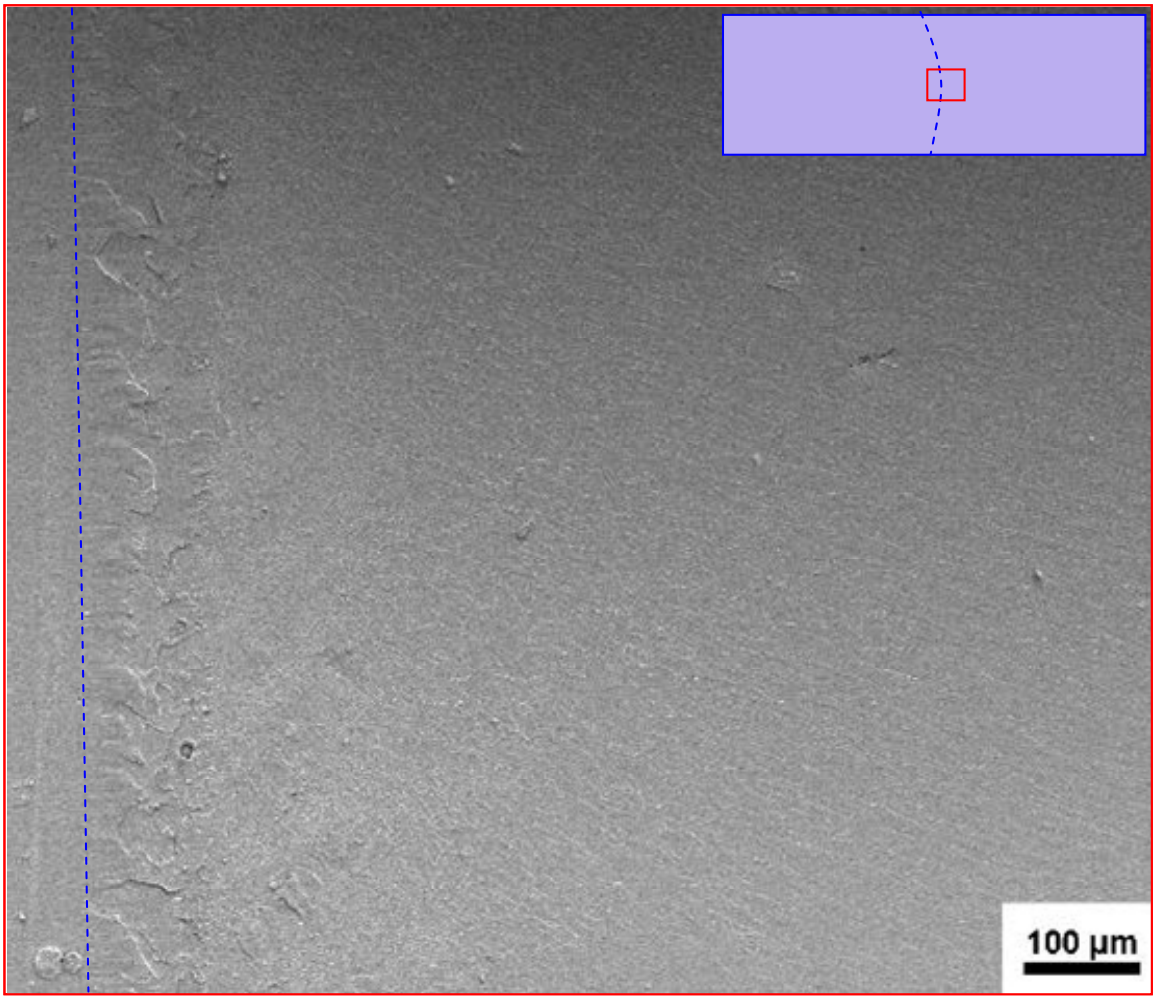

(a)

Figure 5.6. SEM micrographs showing the fracture surface of BCP-toughened epoxy fractured at 508 mm/min at a magnification of (a) 150× and (b) 600×. The insets show the spots where the micrographs were taken. The blue dashed lines represent the initial crack fronts and the crack propagates from left to right.

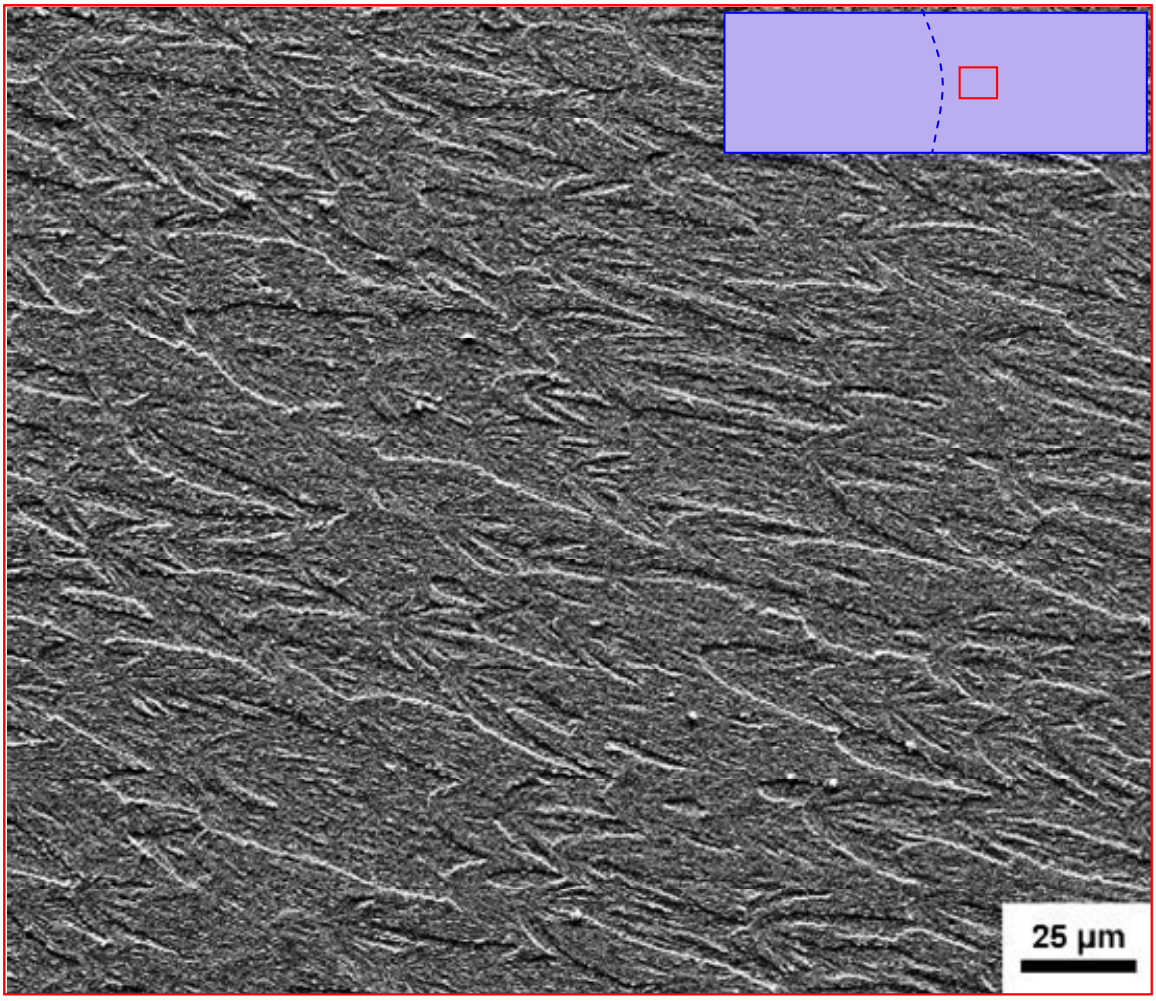

(b)

Figure 5.6 Continued.

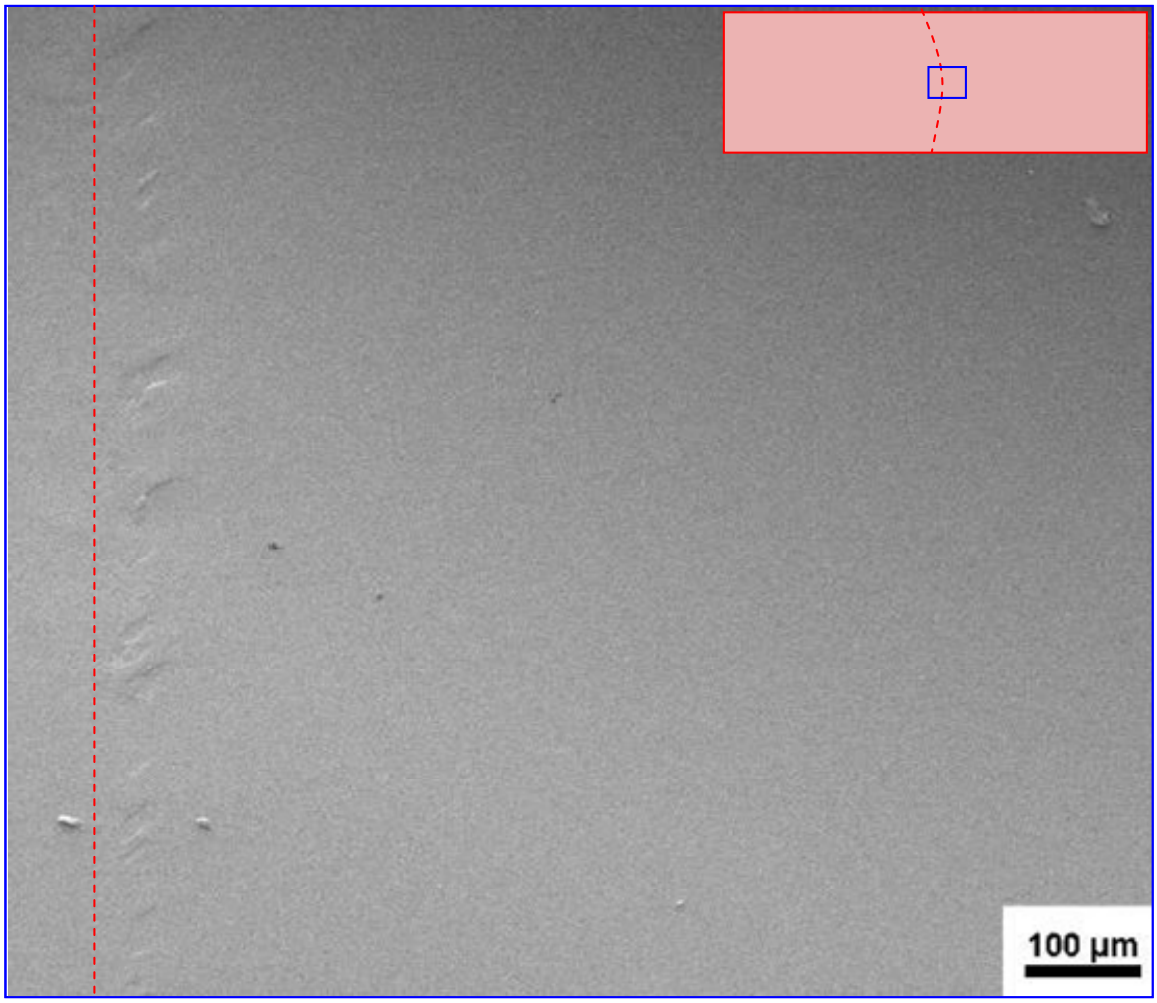

(a)

Figure 5.7. SEM micrographs showing the fracture surface of neat epoxy fractured at 0.51 mm/min at a magnification of (a) 150× and (b) 600×. The insets show the spots where the micrographs were taken. The red dashed lines represent the initial crack fronts and the crack propagates from left to right.

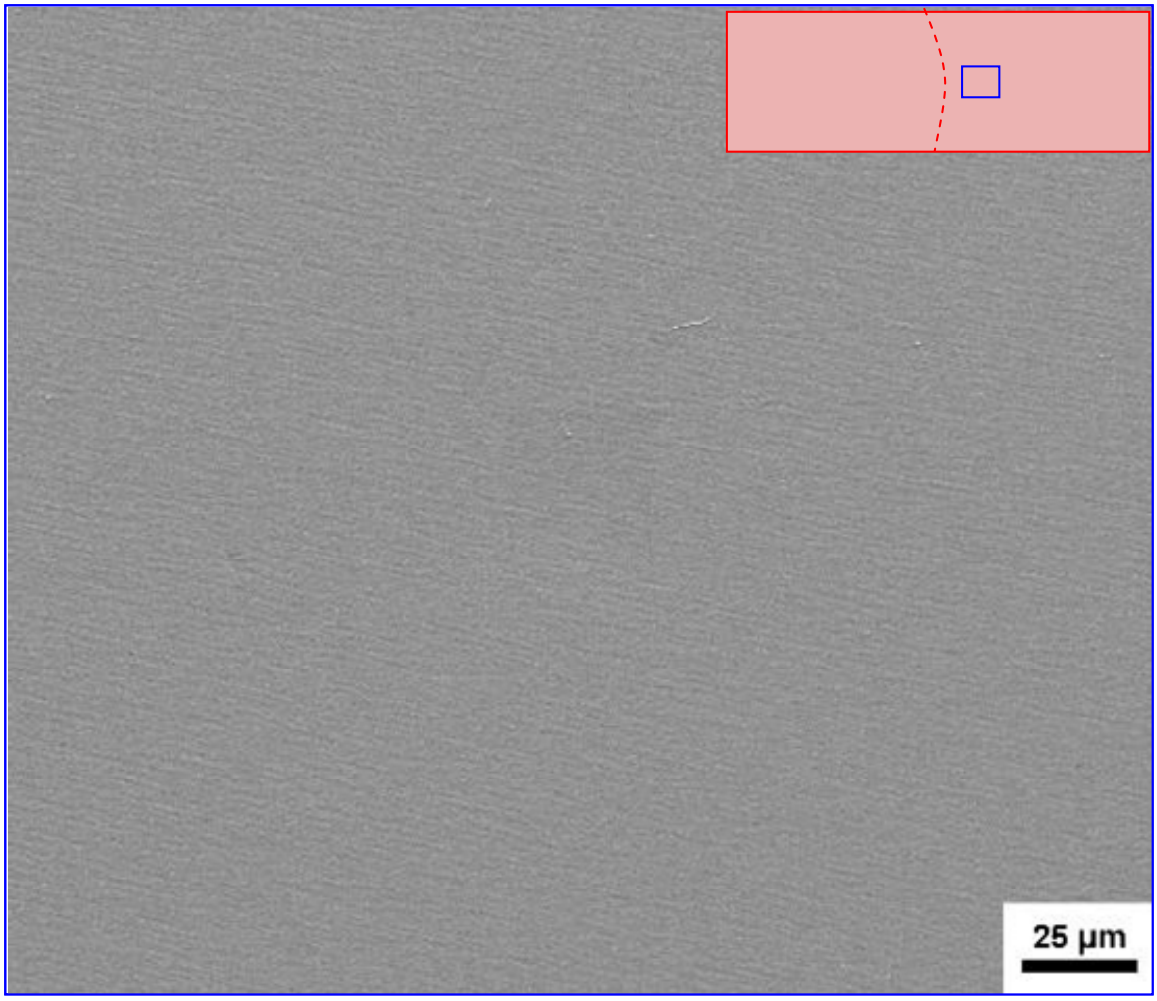

(b)

Figure 5.7. Continued.

5.3.4. Strain Rate Effect on Mechanical Properties and Toughening Mechanisms

The DN-4PB tests have revealed that one of the key toughening mechanisms in BCP-toughened epoxy is BCP micelle cavitation-induced matrix shear banding. The details regarding this toughening effect can be found in previous chapters. Herein we compare the toughening effect at different test rates.

Figure 5.8 presents the DN-4PB subcritical crack tip damage zones in BCP-toughened epoxy at different test rates, observed by OM under bright field. It is evident that the higher the strain rate, the smaller the damage zone size. At both 0.51 and 15.24 mm/min test conditions, dilatation bands[9-11, 17, 126] are generated at the crack tip with a noticeable difference in their sizes and intensities. At the highest test rate of 508 mm/min, the crack tip damage zone size becomes significantly reduced, forming just a slightly darker crack tip under OM without observable dilatation bands. The comparison demonstrates that the toughening effect is suppressed with increasing test rate.

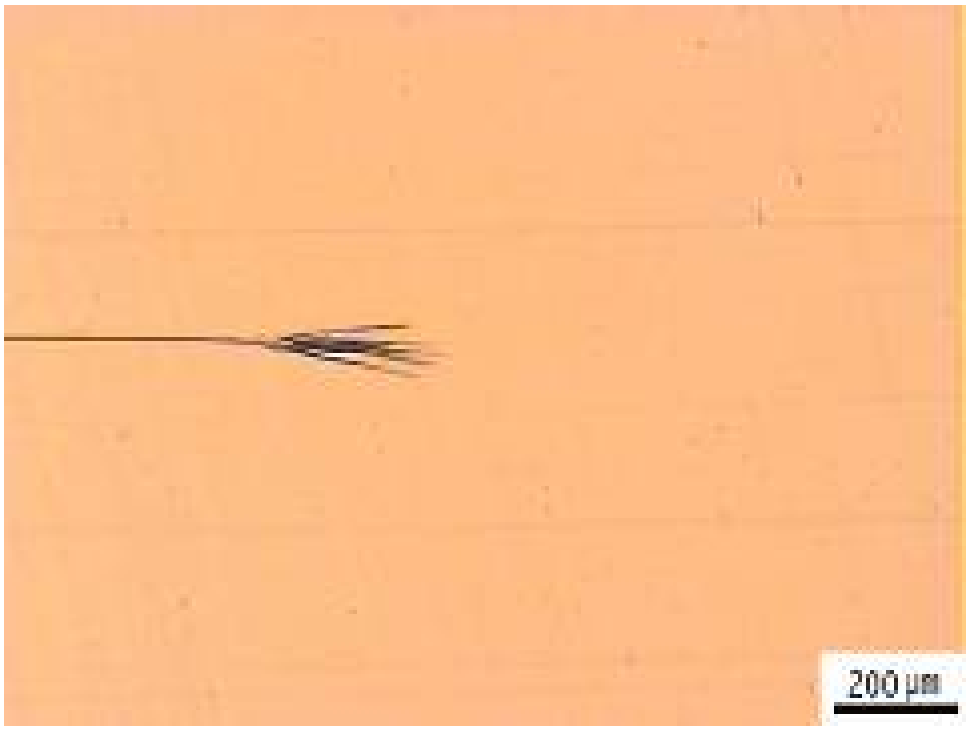

(a)

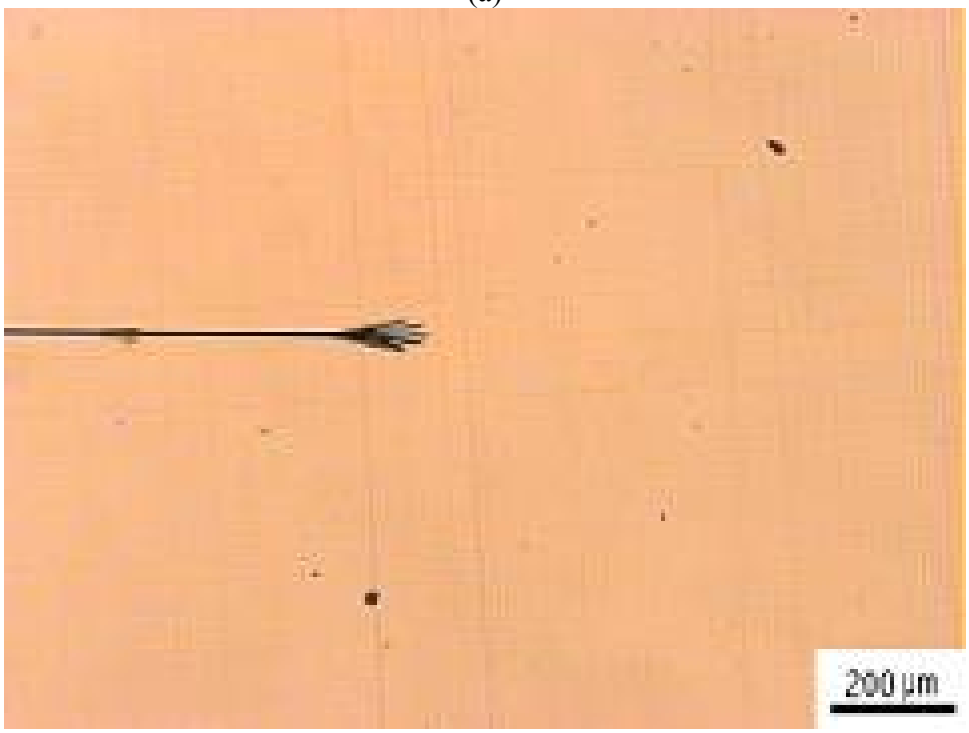

(b)

Figure 5.8. OM images showing the subcritical crack tip damage zones of BCP-toughened epoxy specimens after the DN-4PB tests at different rates of (a) 0.51 mm/min, (b) 15.24 mm/min, and (c) 508 mm/min. The crack propagates from left to right in each case.

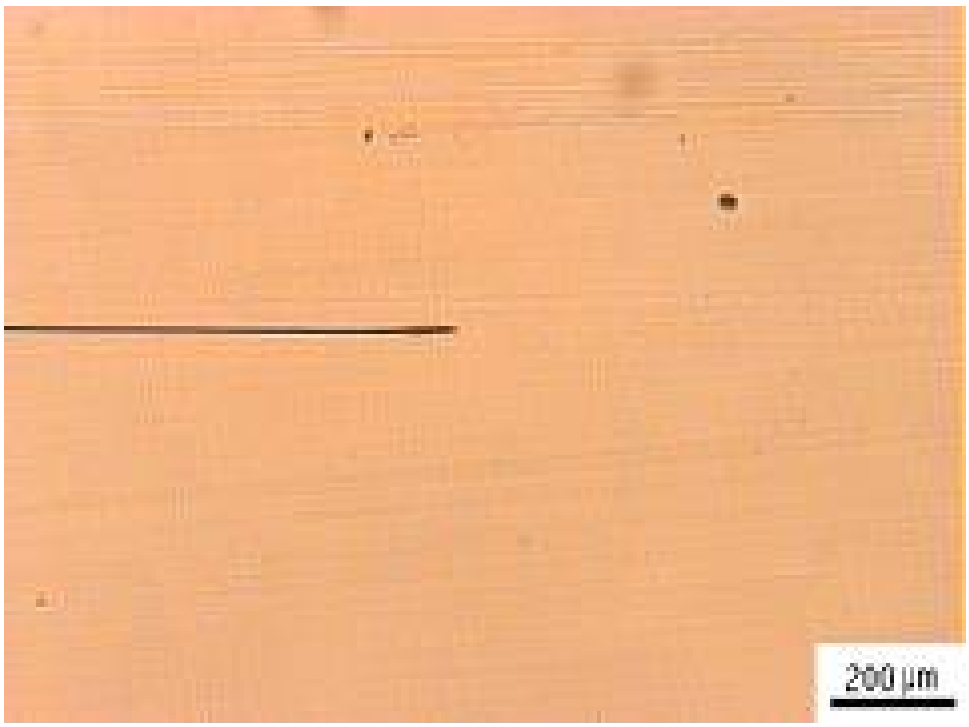

(c)

Figure 5.8. Continued.

In order to investigate the micromechanical deformation mechanisms of the materials upon cracking, TEM was used to examine the crack tip damage zone of the DN-4PB specimens at higher magnifications. Figures 5.9-5.11 show the TEM micrographs of BCP-toughened epoxy specimens taken at similar locations relative to the subcritical crack tip after the DN-4PB tests at different rates. Again, rubber particle cavitation-induced epoxy shear banding was the major toughening mechanism for the two relatively slow rate cases (0.51 and 15.24 mm/min). By comparing Figures 5.9 and 5.10, it is evident that a higher test rate produced a lesser degree of BCP cavitation and plastic deformation at the same relative locations. Accordingly, the sizes of the cavitation zone and the shear banding zone were also shrunk as the test rate was increased. In the highest test rate case (508 mm/min), no observable cavitation or deformation of the BCP particles was found anywhere in the specimen. Therefore, as expected, the capacity for BCP to help dissipate fracture energy was suppressed with increasing test rate, leading to a low K_{IC} value.

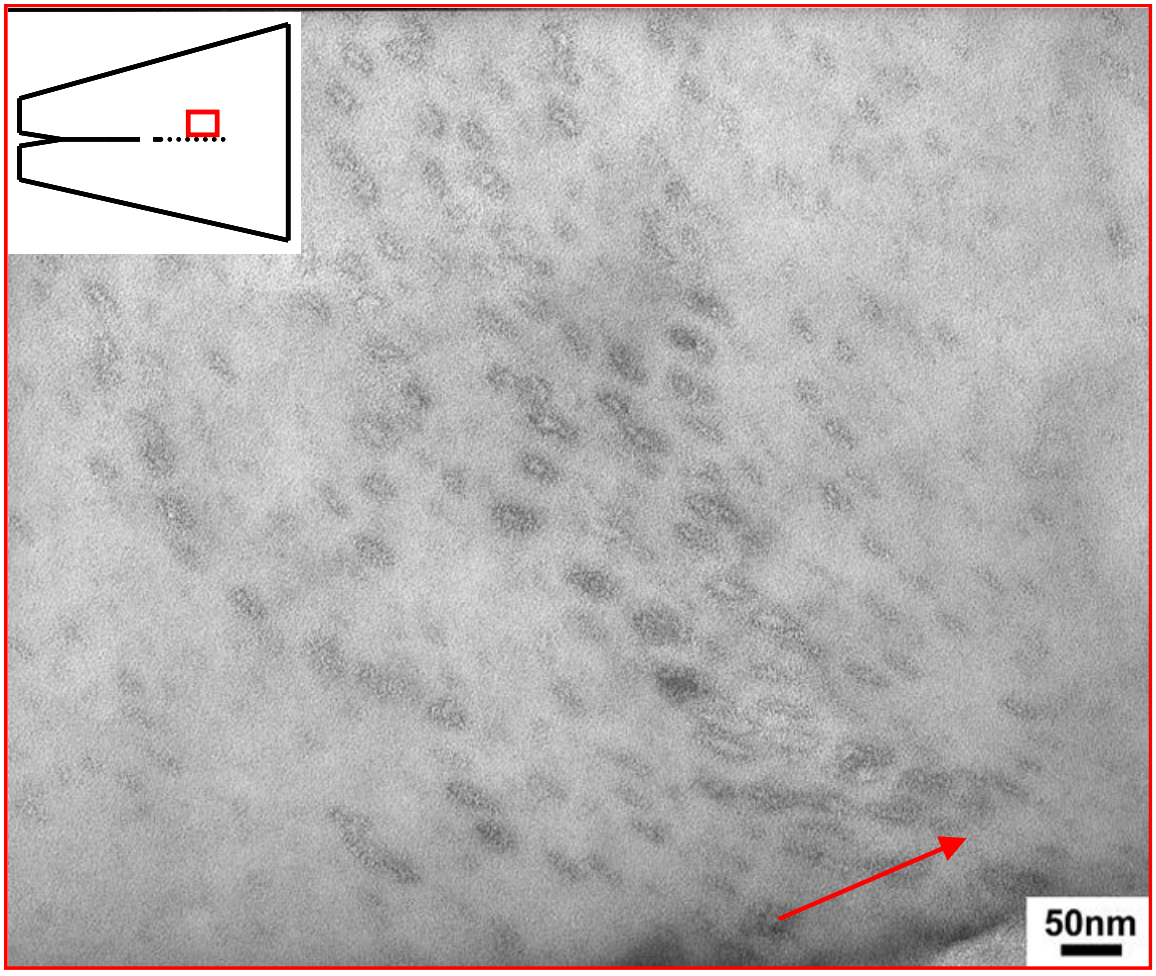

(a)

Figure 5.9. TEM micrographs of BCP-toughened epoxy after DN-4PB test at 0.51 mm/min at locations (a) close to the crack tip and (b) some distance away from the crack. The insets show the spots where the micrographs were taken. The arrows indicate the crack propagation direction.

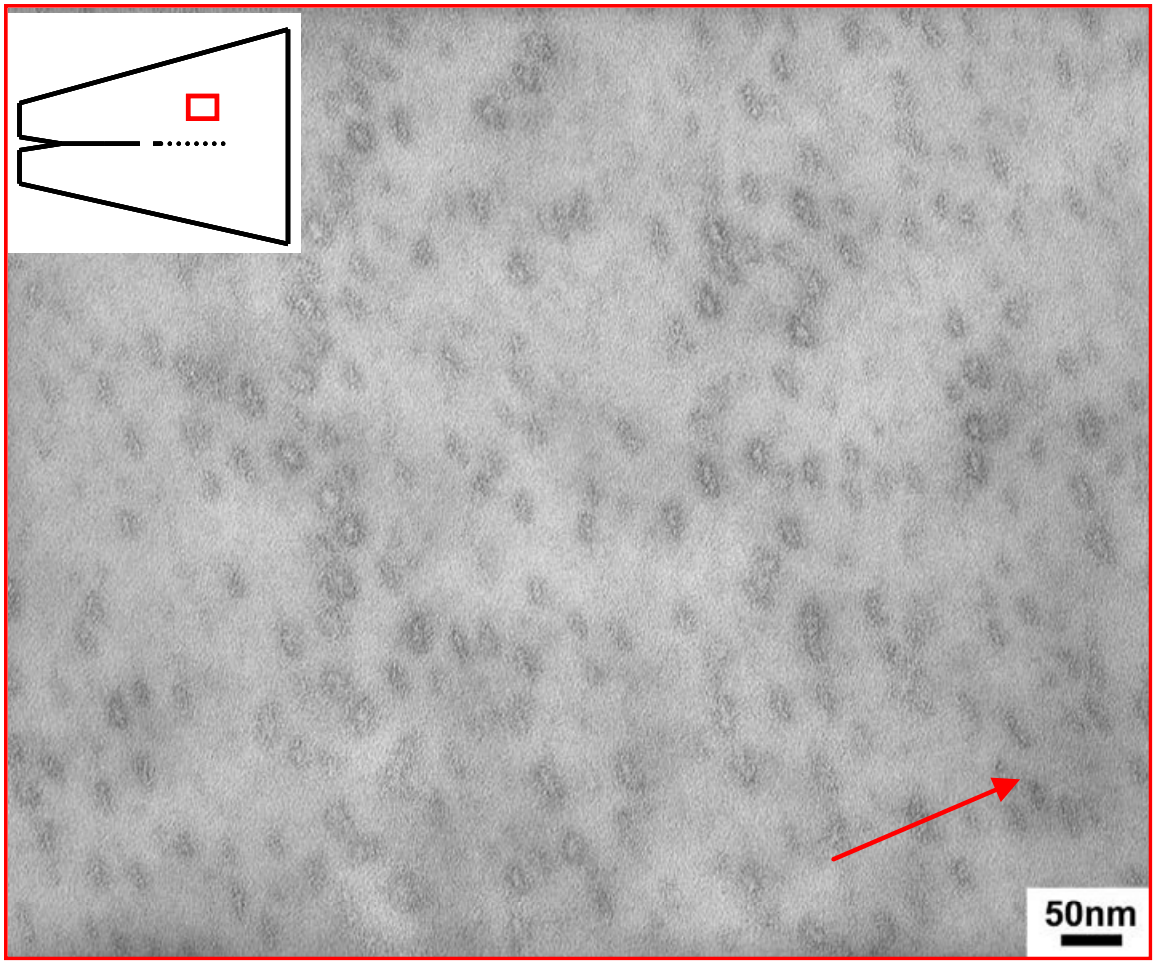

(b)

Figure 5.9. Continued.

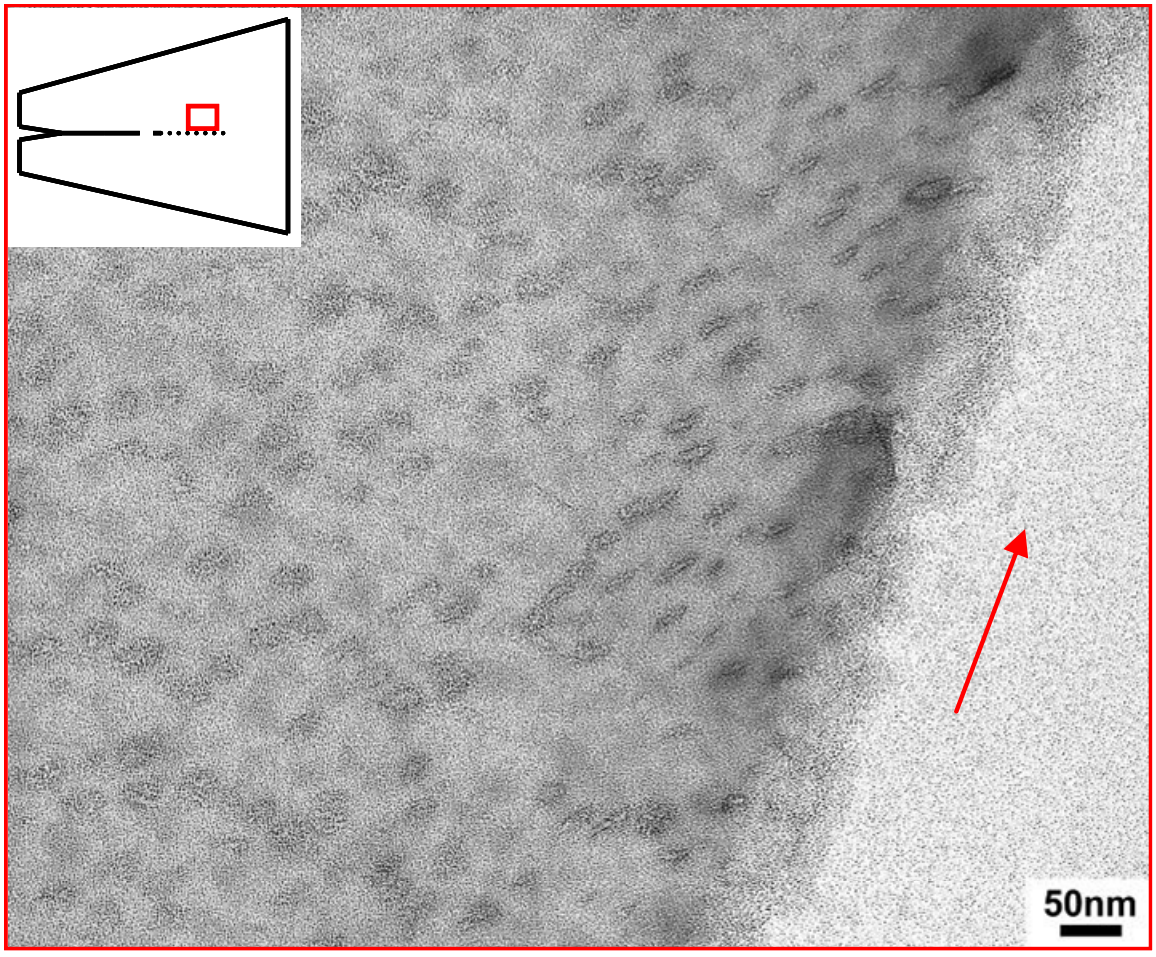

(a)

Figure 5.10. TEM micrographs of BCP-toughened epoxy after DN-4PB test at 15.24 mm/min at locations (a) close to the crack tip and (b) some distance away from the crack. The insets show the spots where the micrographs were taken. The arrows indicate the crack propagation direction.

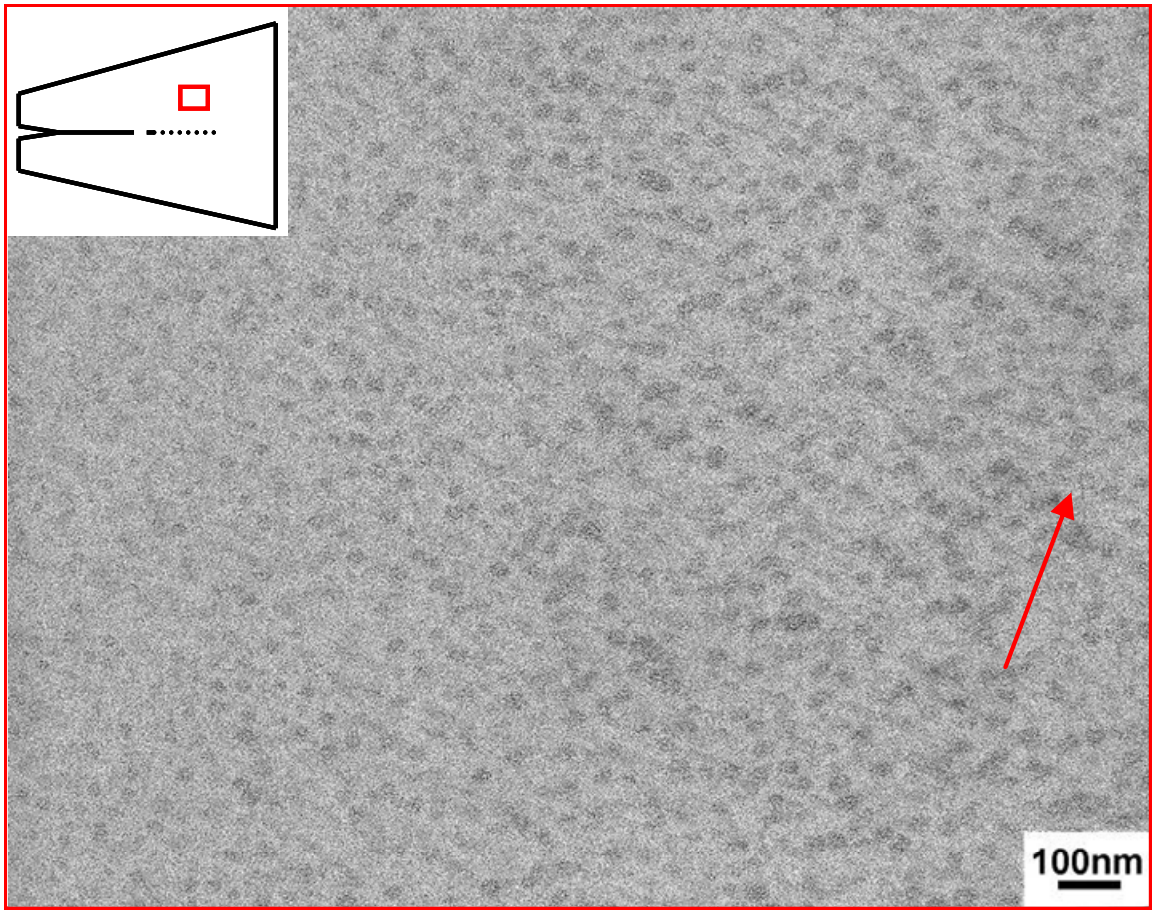

(b)

Figure 5.10. Continued.

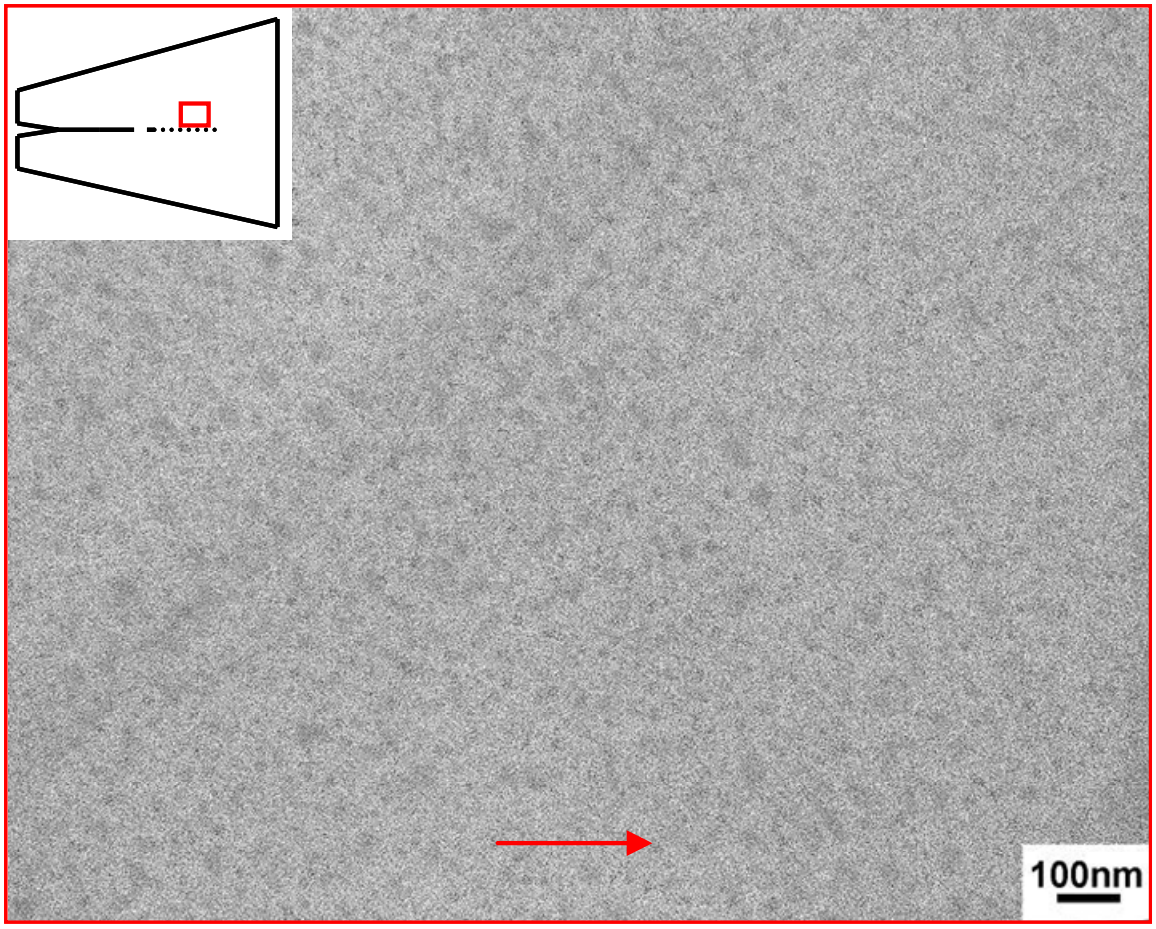

(a)

Figure 5.11. TEM micrographs of BCP-toughened epoxy after DN-4PB test at 508 mm/min at locations (a) close to the crack tip and (b) some distance away from the crack. The insets show the spots where the micrographs were taken. The arrows indicate the crack propagation direction.

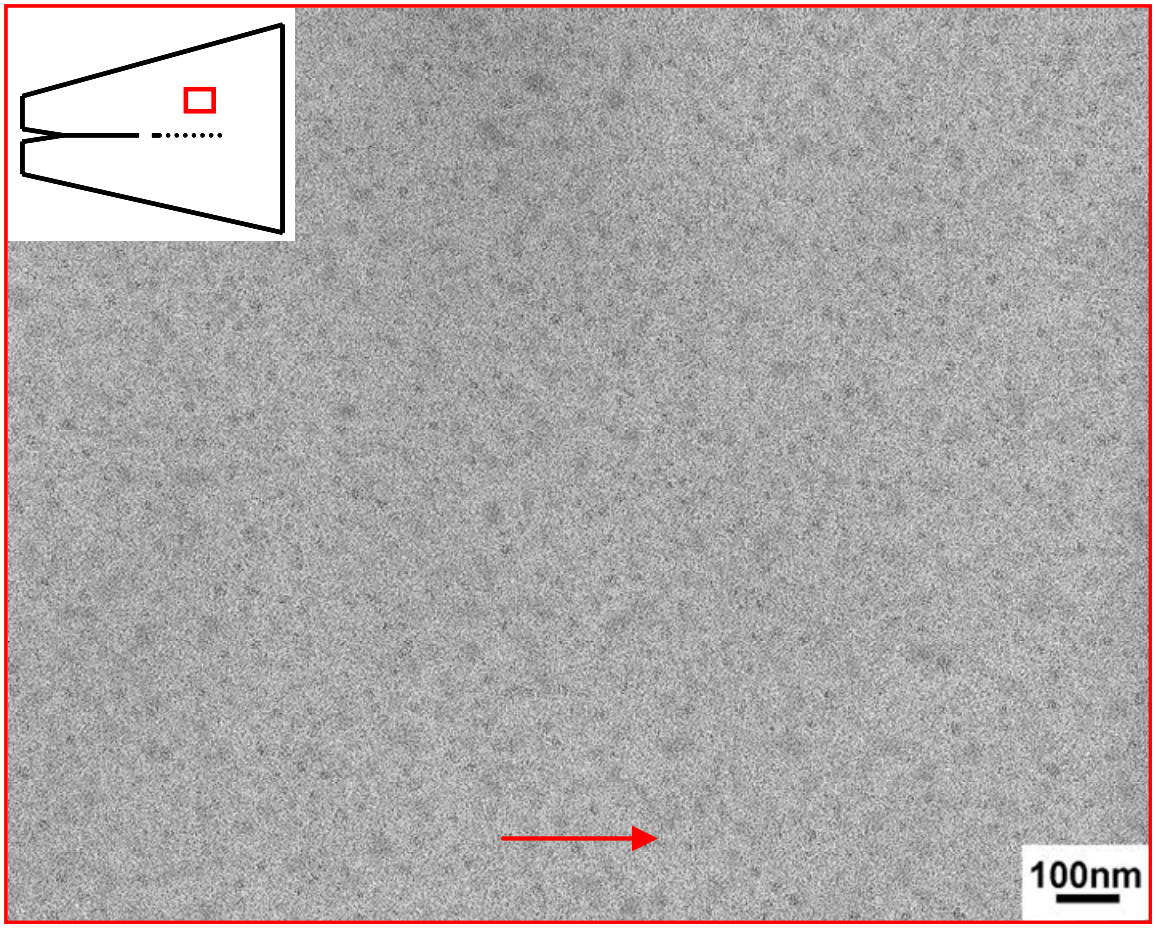

(b)

Figure 5.11. Continued.

In Chapter III, it is discussed that crack tip blunting plays an important toughening role in the slow test rate (i.e., 0.51 mm/min) case, corroborated by a lower yield stress after the addition of BCP. To show the possible contribution of crack tip blunting on toughening, tensile tests were performed and compared at different test rates of 0.51, 5.08, 50.8 and 508 mm/min. The stress-strain curves are displayed in Figure 5.12 and the key tensile properties are summarized in Table 5.2. As the test rate was increased, the yield stress increased and the ductility decreased. This implies that it is harder to undergo plastics deformation as the test rate is increased. This in turn results in a reduction of the crack tip blunting effect.

Here we note that yielding and localized necking were observed only at slow test rate conditions (0.51, 5.08 and 50.8 mm/min). Figure 5.12 shows that at a test rate of 508 mm/min, the specimen broke before yielding could occur. This behavior undermines the possibility of matrix shear banding or crack tip blunting at high test rates.

A possible explanation for the strain rate sensitivity of toughened polymers is the greatly increased damping characteristics of BCP-toughened epoxy (Figure 5.2). In a toughened polymeric system, the micromechanical deformation mechanism for fracture behavior involves a time-dependent process, which is related to the relaxation of the matrix molecules with respect to the applied strain rate of the test. At high test rates, the volumetric dilatation of the rubber particle remains too low when early brittle failure occurs in the matrix. Thus, no extensive cavitation can take place around the crack tip to trigger massive plastic deformation of the epoxy matrix. Meanwhile, the capability of

the matrix to undergo shear banding is also highly restricted at high rates due to greatly increased critical stress for yielding to take place.

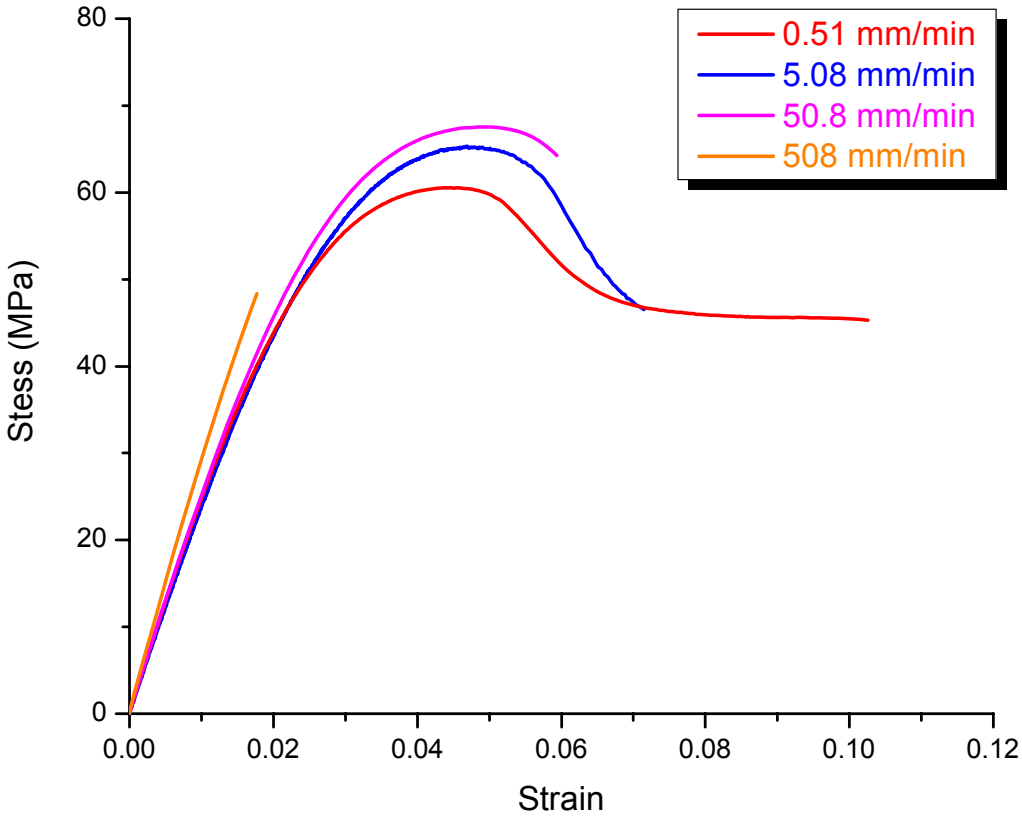

Figure 5.12. Stress-strain curves of BCP-toughened epoxy specimens at tensile test rates of 0.51, 5.08, 50.8 and 508 mm/min.

Table 5.2. Young's modulus and yield stress values of BCP-toughened epoxy specimens at different tensile test rates.

Test rate (mm/min)	0.51	5.08	50.8	508
Young's modulus (GPa)	2.51±0.07	2.58±0.05	2.54±0.06	2.82±0.08
Yield stress (MPa)	60.3±0.2	65.8±0.4	66.9±0.7	n/a

Different scenarios in mechanical behavior of toughened polymers at different loading rate conditions under the SEN-3PB unstable geometry condition are summarized in Figure 5.13. When the test rate is gradually increased, the material will go through a fully stable, mixed stable/unstable, and fully unstable transition.

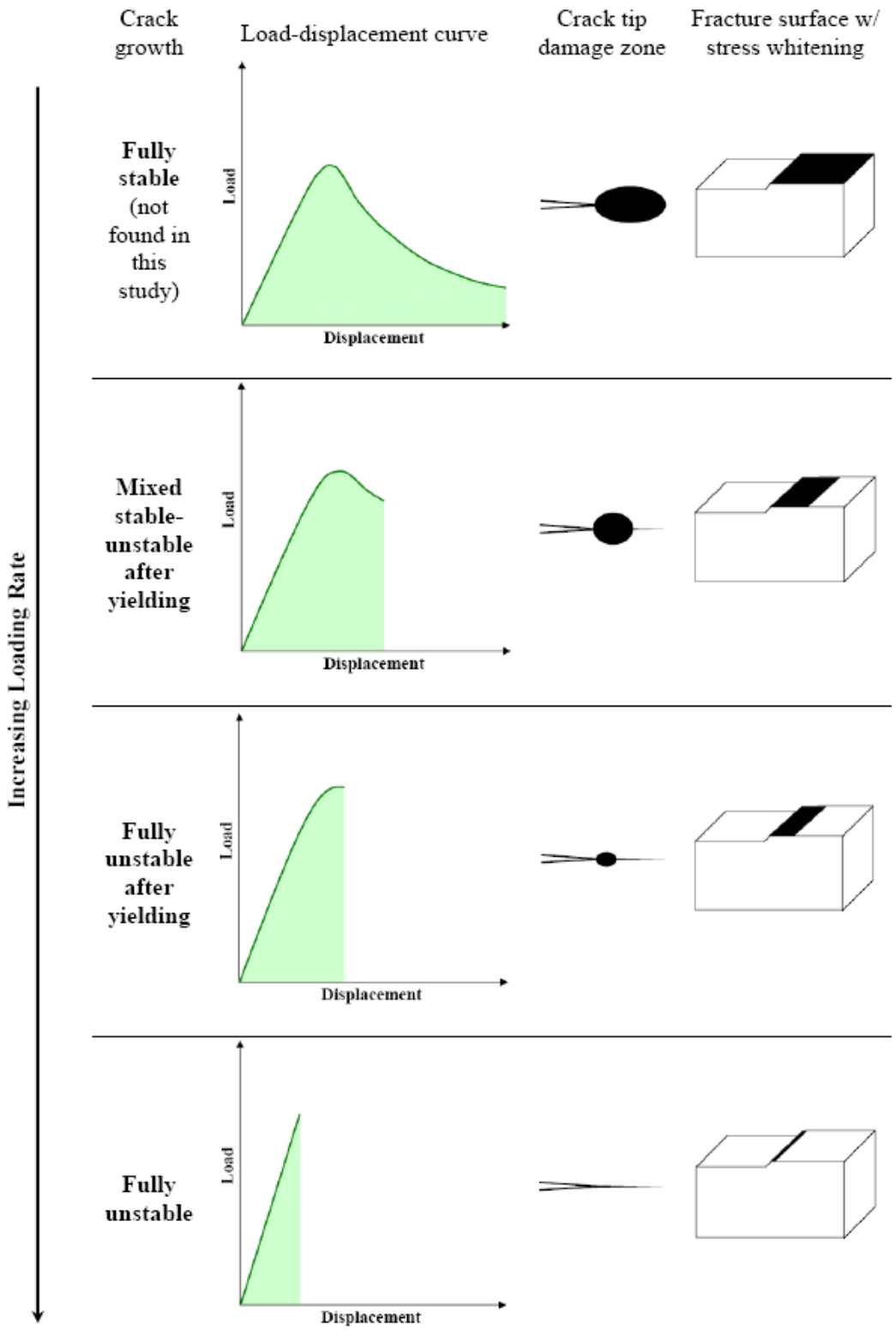

Figure 5.13. Schematic of stable-unstable transitions in mechanical behavior of toughened plastics as test rate increases.

Although the above viscoelastic behavior has been observed in other toughened polymeric systems, the strain rate dependence observed in BCP-toughened epoxy was found to be more pronounced than what were found in the literature.[76, 81, 165] The only systematic study on rate effect in toughened epoxy found in the literature is based on carboxyl-terminated butadiene acrylonitrile (CTBN)-modified epoxy.[76, 165] Figure 5.14 shows a comparison of the rate effect for the BCP-toughened epoxy performed in this study and the CTBN-toughened epoxy,[76] along with their unmodified counterparts. From the plots, it is apparent that K_{IC} is related in an inverse linear manner to the log of loading rate. According to the slopes of the plots, it is evident that the effect of rate dependence on fracture toughness of the BCP-toughened epoxy is more significant than that of the CTBN-toughened epoxy and their neat epoxy counterparts. A plausible explanation for this phenomenon is that the epoxy network in this study has been modified by the epoxy-philic PEO block. A detailed illustration of this unique modification is described in the next section. A point worth reiterating is that the fracture toughness improvement obtained with only 5 wt% of BCP is comparable to that produced with a much higher concentration of CTBN.

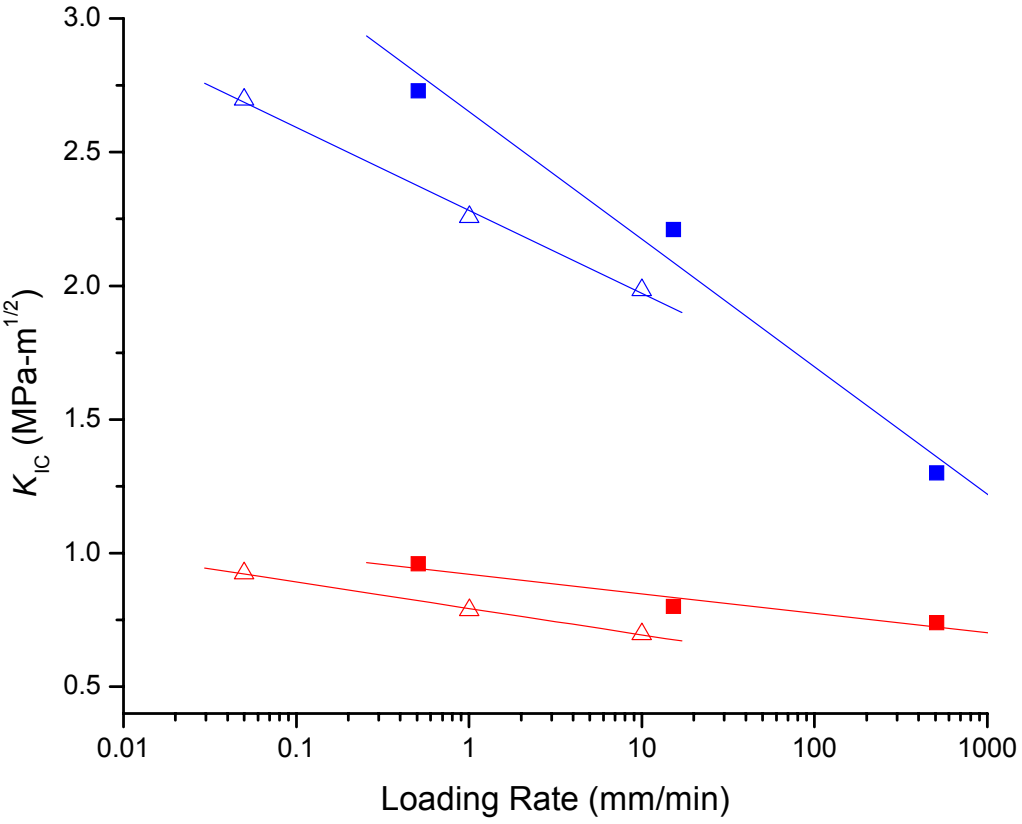

Figure 5.14. Fracture toughness, K_{IC}, plotted against loading rate for two sets of neat and toughened epoxies: the ones in the present work (■ unmodified and ■ 5 wt% BCP-modified), and in Ref. 50 (△ unmodified and △ 12.5 wt% CTBN-modified).

5.3.5. Effect of PEO Block on Epoxy Properties

Considering the fact that there is still a 76% increase in K_{IC} at a strain rate of 508 mm/min, we surmise that the PEO block of the PEP-PEO copolymer may have played a significant role in toughening, especially when the favorable rubber particle cavitation and matrix shear banding mechanisms are suppressed. The finding from DMA (Figure

5.2) demonstrates a greatly enhanced damping level above 0 °C due to the presence of PEO in the epoxy network. The modification of the epoxy network by PEO is believed to contribute to the significant strain rate dependence as well as toughening when compared with other toughened polymers.[10, 164, 165]

The unique micellar structure of the PEP-PEO amphiphilic BCP in the epoxy matrix originates from the interfacial curvature caused by the selective swelling of PEO chains in the epoxy.[43] There are no chemical reactions or ionic interactions between the epoxy and the PEO backbone.[43] Therefore, the epoxy polymerization kinetics[167, 168] should not be affected by the presence of BCP particles. However, the –OH groups generated through the epoxy curing reactions may interact by hydrogen bonding with the ether oxygen of PEO. This interaction has been confirmed by others based on the observed shift of associated hydroxyl band and the intensity ratio change between associated and free hydroxyl bands in Fourier transform infrared (FTIR) spectra.[39] Bellenger *et al.* have found that in epoxy-diamine systems, the higher nucleophilic character of the aliphatic nitrogen favors OH–N interaction, leaving fewer –OH groups free to form hydrogen bonds with –O– in PEO backbone.[169] Because the epoxy system utilized in this study does not contain nucleophilic nitrogen, the hydrogen bonding is expected to be strong, leading to an altered localized epoxy network around the BCP micelles. Bates and co-workers have reported the expulsion of PEO from the epoxy during curing,[43, 45] leading to the formation of a core-shell-like morphology, which may induce more complexity in identifying the effect of (partially) segregated PEO on epoxy network formation.

The literature reports[34, 39, 40, 170] on the changes in T_g and tensile properties with the addition of pure PEO to epoxy have been inconsistent. They generally show reasonable improvements in fracture toughness under various PEO loadings. This implies that PEO molecules can plasticize an epoxy matrix, making it more viscoelastic, thus more test rate dependent.

Another interesting phenomenon worth mentioning is that the rubbery plateau storage moduli obtained from DMA tests decrease with the incorporation of BCP micelles in the epoxy (see Chapter III). This suggests that the incorporation of BCP reduces crosslink density of the epoxy matrix.[154, 155] A drop in matrix crosslink density usually indicates an increase in the material intrinsic ability to undergo shear deformation, which can partially account for the significant toughening effect and high rate sensitivity. A detailed discussion of the crosslink density effect on epoxy toughenability has been given in Chapter IV.

The present study shows that PEP-PEO copolymer toughening of epoxy is effective. However, care should be taken when BCP-toughened epoxy experiences high loading rates in real-life applications. Fracture toughness evaluation of BCP-toughened epoxy under a range of test rates is advisable for applications where high rate performance is of primary concern.

5.4. Summary

The fracture and tensile behaviors of nano-sized PEP-PEO micelle-toughened epoxy were systematically investigated at test rates ranging from 0.51 to 508 mm/min.

BCP-toughened epoxy was found to exhibit an increased rate dependence compared to the same epoxy containing no BCP, and compared to the characteristics of CTBN-toughened epoxy. A higher strain rate leads to a lower fracture toughness and a more brittle behavior in tension. Clear evidence from the DN-4PB investigation demonstrates significant rate dependence on the observed toughening mechanisms. An increase in test rate suppresses the sizes and intensities of BCP particle cavitation and matrix shear banding zones. This reduction in damage zone size significantly hinders the fracture energy dissipation process, thus leading to much lower fracture resistance. A greatly increased damping level attributed to the plasticization of the epoxy network by the PEO blocks is found in BCP-modified epoxy, which appears to be responsible for the observed strain rate dependence effect. Care should be taken when toughened polymers are to be utilized for high rate applications.

CHAPTER VI

CONCLUSIONS AND RECOMMENDATIONS

6.1. Concluding Remarks

6.1.1. Epoxy Toughening with Nano-Sized Block Copolymer (BCP) Micelles

The objective of this research is to gain a fundamental knowledge of structure-property relationship in polymers containing nano-structures/nano-domains, and the focus of this dissertation is placed on the studies of nano-sized BCP micelle-toughened epoxies. An amphiphilic poly(ethylene-*alt*-propylene)-*b*-poly(ethylene oxide) (PEP-PEO, M_n = 9100 g/mol, w_{EO} = 0.40) diblock copolymer was incorporated into a liquid diglycidyl ether of bisphenol-A (DGEBA) based epoxy resin as a toughening agent. The BCP self-assembled into well-dispersed 15 nm spherical micelle particles in the epoxy matrix. The nano-sized BCP particles at 5 wt% loading can significantly improve the fracture toughness of epoxy (by a 180% increase in K_{IC}, critical stress intensity factor) without deteriorating other desirable properties, such as Young's modulus and glass transition temperature (T_g). Structure-property relationship of this nano-domain containing epoxy has been investigated.

6.1.2. Toughening Mechanisms in Epoxies Containing Nano-Sized BCP Micelles

The micromechanical deformation and toughening mechanisms in nano-sized BCP micelle-modified epoxies were investigated using the double-notch four-point-

bending (DN-4PB) technique. It has been found that the key operative toughening mechanism is BCP nanoparticle cavitation-induced epoxy matrix shear banding. The "nano-cavitation" of the 15 nm particles is believed to be the first reported in polymer toughening, which is far below the lower limit predicted by any existing physical models. The likely causes for the observed nano-scale cavitation phenomenon may include the unique BCP micelle structural characteristics and a possible influence of the surrounding epoxy network, which is significantly modified by the epoxy-philic PEO block. Other mechanisms, such as crack tip blunting, may also play a role in the toughening.

6.1.3. Crosslink Density Effect on Fracture Behavior of Epoxies Containing Nano-Sized BCP Micelles

The model DGEBA-based epoxy resins containing well-dispersed 15 nm PEP-PEO BCP micelles were prepared with variations in matrix crosslink density. The molecular weight between crosslinks (M_c) of the epoxies was varied *via* the controlled epoxy thermoset technology and estimated experimentally. As expected, it was found that the fracture toughness of BCP-modified epoxies is strongly influenced by the crosslink density of the epoxy matrix, with higher toughenability for lower crosslink density epoxies. Some major toughening mechanisms, i.e., nanoparticle cavitation and matrix shear banding, are evidenced to be highly restricted in tightly-crosslinked epoxy matrices. The nano-sized BCP particles were also found to be at least as effective as micro-sized CSR particles in toughening epoxies at various levels of crosslink densities.

6.1.4. Strain Rate Effect on Mechanical Properties of Epoxies Containing Nano-Sized BCP Micelles

Based on the dynamic mechanical analysis (DMA) results on BCP-modified epoxy, there existed a pronounced viscoelastic damping characteristic above room temperature in the modified epoxy, suggesting that its mechanical properties may be more strain rate dependent compared to the neat epoxy counterpart. Therefore, the fracture and tensile behavior of the BCP-modified epoxy were investigated at loading rates ranging from 0.51 to 508 mm/min. The mechanical properties of BCP-toughened epoxy were found to exhibit significantly higher rate dependent than the neat epoxy and the CTBN-toughened epoxy. As expected, a higher test rate leads to a more brittle behavior of the material and a lower fracture toughness value. Clear evidence from the DN-4PB investigation demonstrates significant rate dependence on the observed toughening mechanisms. An increase in the testing rate suppresses the sizes and intensities of BCP nanoparticle cavitation and matrix shear banding zones. This reduction in damage zone size significantly hinders the fracture energy dissipation process, thus leading to much lower fracture resistance. Plasticization of the epoxy network by the PEO block appears to be responsible for the observed strain rate dependence effect. Extreme care should be exercised when toughened polymers are to be used for high rate applications.

6.2. Recommendations and Challenges for Future Work

In order to have a complete understanding of the fundamental structure-property relationships and to fully expand the application scope of the technologies developed in this investigation, we believe at least several questions would be of interest to continue the pursuit, as presented in the following.

6.2.1. Other Important Factors in Epoxy Toughening

This dissertation addresses some critical issues in epoxy toughening based on nano-sized BCP micelles, such as toughening mechanisms, matrix crosslink density effect, strain rate dependence, etc. However, a few other important questions remain unanswered. One of them is the toughening agent concentration effect. The current research only studies the case with 5 wt% loading. The effectiveness of higher (or lower) concentrations would be of interest. Another important factor is the size effect. Although we have shown the effectiveness of 15 nm rubber toughening, we have not compared that with other particle sizes. To make this size effect investigation meaningful, one of the prerequisites is an independent control of the particle size without affecting the matrix characteristics and the dispersion of the toughening agent. We have initiated the study on the particle shape effect but have not completed it. Other than spherical micelles, wormlike micelles and vesicle structures are believed to be of great interest, as well. Conclusive toughening mechanisms for BCP-modified epoxies with different disordered morphologies are still awaiting experimental investigations.

6.2.2. Localized Interactions at Interface/Interphase

The interface/interphase property is a very important factor influencing the overall properties of filled materials, because the modification to the host material is realized through the interactions at the interface between matrix and fillers. In nano-sized BCP-modified epoxies, it is difficult to directly probe the properties of the PEO-epoxy intermixing phase due to the lack of the information of localized interactions in a nanometer scale. One suggestion is to examine the secondary relaxation (β-relaxation) peaks in BCP-modified epoxies to investigate how the presence of BCP micelles (the epoxy-miscible PEO block, to be specific) affects the local motion of the epoxy chain segments. It is worth mentioning that Bates et al.[43, 45] observed the expulsion of PEO from epoxy during cure, which created a core-shell like morphology (see Figure 6.1). That itself is an interesting phenomenon and may induce more complexity in indentifying the localized interactions at the PEO-epoxy interphase.

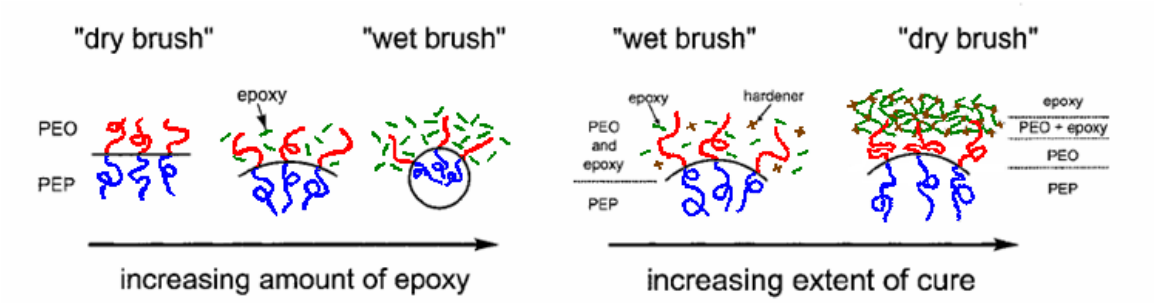

(a) (b)

Figure 6.1. (a) Illustration of swelling-induced change in the interfacial curvature for PEP-PEO and epoxy blends. PEO blocks extend from the neat PEO/PEP interface as a "dry brush". Epoxy selectively swells the PEO brush, creating a "wet brush" and the PEO/PEP interface curves to accommodate this change within the constraint of constant density while minimizing PEP and PEO chain distortions. (b) Illustration of PEO block expulsion as the epoxy matrix crosslinks and its molecular weight diverges. The system initially has a curved interface due to selective swelling of the PEO blocks by the epoxy. As the epoxy cures, the PEO blocks are expelled, transforming the "wet brush" to a "dry brush", thereby reducing the interfacial curvature. (After Bates et al.[43]).

6.2.3. Mechanics in Nanometer Scales

It is always difficult to address issues at nanometer scales, either from a molecular interaction point of view or a mechanics point of view. The localized interactions described in the last section are one example. Another example is the true onset of "nano-cavitation" phenomenon in BCP micelles. We have speculated that the nano-scale cavitation is originated from the expansion of the pre-existing transient nanovoids in a form of free volume. However, the stress states and free energy barriers at such a small scale are not yet understood. It is unclear whether continuum mechanics still applies at nanometer scales. Significant efforts, probably with the aid of molecular

dynamics simulations, are needed to unambiguously understand the nano-engineered materials.

6.2.4. Applications of Nano-Toughening Technique in Other Matrices

In Chapter IV, the nano-BCP toughening approach has been applied in model DGEBA type of epoxies with variations in crosslink density, but we do not know if this approach also works for other matrices. It has been demonstrated that epoxy resins with different chemistry or formulations may lead to different morphologies and different properties of the final BCP-toughened epoxies. It may not be easy to predict the morphology in different resins due to variations in curing kinetics and network development. The detailed nature of the morphology evolution that leads to well-defined nano-structures in a certain chemical environment is still unknown. Significant efforts are still needed to establish guidelines for the preparation of high performance thermosets with superior mechanical properties.

REFERENCES

(1) Mansoori, G. A., *Principles of Nanotechnology*. World Scientific Publishing Co. Pte. Ltd.: Singapore, 2005.

(2) Pham, H. Q.; Marks, M. J., *Epoxy Resins*. Wiley-VCH Verlag GmbH & Co. KGaA: Weinheim, Germany, 2006.

(3) Pearson, R. A.; Yee, A. F. *J. Mater. Sci.* **1986,** *21*, 2475.

(4) Yee, A. F.; Pearson, R. A. *J. Mater. Sci.* **1986,** *21*, 2462.

(5) Pearson, R. A.; Yee, A. F. *J. Mater. Sci.* **1989,** *24*, 2571.

(6) Pearson, R. A.; Yee, A. F. *J. Mater. Sci.* **1991,** *26*, 3828.

(7) Sue, H.-J. *Polym. Eng. Sci.* **1991,** *31*, 270.

(8) Sue, H.-J. *Polym. Eng. Sci.* **1991,** *31*, 275.

(9) Sue, H.-J. *J. Mater. Sci.* **1992,** *27*, 3098.

(10) Sue, H.-J.; Garcia-Meitin, E. I.; Orchard, N. A. *J. Polym. Sci., Part B: Polym. Phys.* **1993,** *31*, 595.

(11) Sue, H.-J.; Puckett, P. M.; Garcia-Meitin, E. I.; Bertram, J. L. *J. Polym. Sci., Part B: Polym. Phys.* **1995,** *33*, 2003.

(12) Sue, H.-J.; Yee, A. F. *Polym. Eng. Sci.* **1996,** *36*, 2320.

(13) Kim, D. S.; Cho, K.; Kim, J. K.; Park, C. E. *Polym. Eng. Sci.* **1996,** *36*, 755.

(14) Day, R. J.; Lovell, P. A.; Pierre, D. *Polym. Int.* **1997**, *44*, 288.

(15) Qian, J. Y.; Pearson, R. A.; Dimonie, V. L.; Shaffer, O. L.; El-Aasser, M. S. *Polymer* **1997,** *38*, 21.

(16) Lin, K. F.; Shieh, Y. D. *J. Appl. Polym. Sci.* **1998,** *70*, 2313.

(17) Sue, H.-J.; Puckett, P. M.; Bertram, J. L.; Walker, L. L.; Garcia-Meitin, E. I. *J. Polym. Sci., Part B: Polym. Phys.* **1999,** *37*, 2137.

(18) Becu-Longuet, L.; Bonnet, A.; Pichot, C.; Sautereau, H.; Maazouz, A. *J. Appl. Polym. Sci.* **1999,** *72*, 849.

(19) Gam, K. T.; Miyamoto, M.; Nishimura, R.; Sue, H.-J. *Polym. Eng. Sci.* **2003,** *43*, 1635.

(20) Sue, H. J.; Gam, K. T.; Bestaoui, N.; Clearfield, A.; Miyamoto, M.; Miyatake, N. *Acta Mater* **2004,** *8*, 2239.

(21) Sue, H.-J.; Pearson, R. A.; Yee, A. F. *Polym. Eng. Sci.* **1991,** *31*, 793.

(22) Konczol, L.; Doll, W.; Buchholz, U.; Mulhaupt, R. *J. Appl. Polym. Sci.* **1994**, *54*, 815.

(23) Kinloch, A. J.; Yuen, M. L.; Jenkins, S. D. *J. Mater. Sci.* **1994,** *29*, 3781.

(24) Sue, H.-J.; Garcia-Meitin, E. I.; Pickelman, D. M.; Bott, C. J. *Colloid. Polym. Sci.* **1996,** *274*, 342.

(25) Groleau, M. R.; Shi, Y. B.; Yee, A. F.; Bertram, J. L.; Sue, H.-J.; Yang, P. C. *Compos. Sci. Technol.* **1996,** *56*, 1223.

(26) Girodet, C.; Espuche, E.; Sautereau, H.; Chabert, B.; Ganga, R.; Valot, E. *J. Mater. Sci.* **1996,** *31*, 2997.

(27) Zheng, S.; Wang, J.; Guo, Q.; Wei, J.; Li, J. *Polymer* **1996,** *37*, 4667.

(28) Girard-Reydet, E.; Sautereau, H.; Pascault, J.-P. *Polymer* **1999,** *40*, 1677.

(29) Hofflin, F.; Konczol, L.; Doll, W.; Morawiec, J.; Mulhaupt, R. *J. Appl. Polym. Sci.* **2000,** *76*, 623.

(30) Okamatsu, T.; Ochi, M. *Polymer* **2002,** *43*, 721.

(31) Derkowski, B. J.; Sue, H.-J. *Polym. Compos.* **2003,** *24*, 158.

(32) Dean, J. M.; Lipic, P. M.; Grubbs, R. B.; Cook, R. F.; Bates, F. S. *J. Polym. Sci., Part B: Polym. Phys.* **2001,** *39*, 2996.

(33) Dean, J. M.; Grubbs, R. B.; Saad, W.; Cook, R. F.; Bates, F. S. *J. Polym. Sci., Part B: Polym. Phys.* **2003,** *41*, 2444.

(34) Dean, J. M.; Verghese, N. E.; Pham, H. Q.; Bates, F. S. *Macromolecules* **2003,** *36*, 9267.

(35) Ritzenthaler, S.; Court, F.; Girard-Reydet, E.; Leibler, L.; Pascault, J.-P. *Macromolecules* **2003,** *36*, 118.

(36) Girard-Reydet, E.; Pascault, J.-P.; Bonnet, A.; Court, F.; Leibler, L. *Macromol. Symp.* **2003,** *198*, 309.

(37) Rebizant, V.; Venet, A.-S.; Tournilhac, F.; Girard-Reydet, E.; Navarro, C.; Pascault, J.-P.; Leibler, L. *Macromolecules* **2004,** *37*, 8017.

(38) Wu, J.; Thio, Y. S.; Bates, F. S. *J. Polym. Sci., Part B: Polym. Phys.* **2005,** *43*, 1950.

(39) Larranaga, M.; Arruti, P.; Serrano, E.; de la Caba, K.; Remiro, P. M.; Riccardi, C. C.; Mondragon, I. *Colloid. Polym. Sci.* **2006,** *284*, 1419.

(40) Larranaga, M.; Serrano, E.; Martin, M. D.; Tercjack, A.; Kortaberria, G.; de la Caba, K.; Riccardi, C. C.; Mondragon, I. *Polym. Int.* **2007,** *56*, 1392.

(41) Hydro, R. M.; Pearson, R. A. *J. Polym. Sci., Part B: Polym. Phys.* **2007,** *45*, 1470.

(42) Hillmyer, M. A.; Lipic, P. M.; Hajduk, D.; Almdal, K.; Bates, F. S. *J. Am. Chem. Soc.* **1997,** *119*, 2749.

(43) Lipic, P. M.; Bates, F. S.; Hillmyer, M. A. *J. Am. Chem. Soc.* **1998,** *120*, 8963.

(44) Grubbs, R. B.; Broz, M. E.; Dean, J. M.; Bates, F. S. *Macromolecules* **2000,** *33*, 2308.

(45) Grubbs, R. B.; Broz, M. E.; Dean, J. M.; Bates, F. S. *Macromolecules* **2000,** *33*, 9522.

(46) Grubbs, R. B.; Dean, J. M.; Bates, F. S. *Macromolecules* **2001,** *34*, 8593.

(47) Guo, Q.; Dean, J. M.; Grubbs, R. B.; Bates, F. S. *J. Polym. Sci., Part B: Polym. Phys.* **2003,** *41*, 1994.

(48) Sumeet, J.; Bates, F. S. *Science* **2003,** *300*, 460.

(49) Bucknall, C. B., *Toughened Plastics*. Applied Science: London, UK, 1977.

(50) Kinloch, A. J.; Young, J., *Fracture Behavior of Polymers*. Applied Science: London, UK, 1983.

(51) Kinloch, A. J., In *Toughened Plastics*, Riew, C. K., Ed.; *Adv. Chem. Ser.* **1989**, *67*, 222.

(52) Bascom, W. D.; Cottington, R. L.; Jones, R. L.; Peyser, P. *J. Appl. Polym. Sci.* **1975,** *19*, 2545.

(53) Sultan, J. N.; McGarry, F. J. *J. Polym. Eng. Sci.* **1973,** *13*, 29.

(54) Huang, Y.; Kinloch, A. J. *Polymer* **1992,** *33*, 5338.

(55) Sue, H.-J.; Garcia-Meitin, E. I.; Pickelman, D. M., In *Elastomer Technology Handbook*, Cheremisinoff, N. P., Ed. CRC Press: Boca Raton, FL, 1993.

(56) Sue, H.-J.; Garcia-Meitin, E. I.; Pickelman, D. M.; Yang, P. C., In *Toughened Plastics*, Riew, C. K., Ed.; *Adv. Chem. Ser.* **1993**, *252*, 161.

(57) Sue, H. J.; Puckett, P. M.; Garcia-Meitin, E. I.; Bertram, J. L. *J. Polym. Sci., Part B: Polym. Phys.* **1995,** *33*, 2003.

(58) Borggreve, R. J. M.; Gaymans, R. J.; Eichenwald, H. M. *Polymer* **1989,** *30*, 78.

(59) Borggreve, R. J. M.; Gaymans, R. J.; Schuijer, J. *Polymer* **1989,** *30*, 71.

(60) Borggreve, R. J. M.; Gaymans, R. J.; Schuijer, J.; Ingen Housz, J. F. *Polymer* **1987,** *28*, 1489.

(61) Wu, S. *J. Appl. Polym. Sci.* **1998,** *35*, 549.

(62) Parker, D. S.; Sue, H.-J.; Huang, J.; Yee, A. F. *Polymer* **1990,** *31*, 2267.

(63) Yee, A. F. *J. Mater. Sci.* **1977,** *12*, 757.

(64) Chang, F. C.; Wu, J. S.; Chu, L. H. *J. Appl. Polym. Sci.* **1992,** *44*, 491.

(65) Bubeck, R. A.; Buckley, D. J.; Kramer, E. J.; Brown, H. R. *J. Mater. Sci.* **1991,** *26*, 6249.

(66) Breuer, H.; Haaf, F.; Stabenow, J. *J. Macromol. Sci. Phys.* **1977,** *14*, 387.

(67) Haaf, F.; Breuer, H.; Echte, A.; Schmitt, B. J.; Stabenow, J. *J. Sci. Ind. Res.* **1981,** *40*, 659.

(68) Tse, A.; Shin, E.; Hiltner, A.; Baer, E.; Laakso, R. *J. Mater. Sci.* **1991,** *26*, 2823.

(69) Hourston, D. J.; Lane, S.; Zhang, H. X. *Polymer* **1991,** *32*, 2215.

(70) Azimi, H. R.; Pearson, R. A.; Hertzberg, R. *J. Mater. Sci.* **1996,** *31*, 3777.

(71) Lazzeri, A.; Bucknall, C. B. *J. Mater. Sci.* **1993,** *28*, 6799.

(72) Bucknall, C. B.; Karpodinis, A.; Zhang, X. C. *J. Mater. Sci.* **1994,** *29*, 3377.

(73) Lazzeri, A.; Bucknall, C. B. *Polymer* **1995,** *26*, 2895.

(74) Gaymans, R. J.; Borggreve, R. J. M.; Oostenbrink, A. J. *Makromol. Chem. Macromol. Symp.* **1990,** *38*, 125.

(75) Sultan, J. N.; Liable, R. C.; McGarry, F. J. *Polym. Symp.* **1971,** *16*, 127.

(76) Kinloch, A. J.; Shaw, S. J.; Tod, D. A.; Hunston, D. L. *Polymer* **1983,** *24*, 1341.

(77) Kinloch, A. J.; Shaw, S. J.; Hunston, D. L. *Polymer* **1983,** *24*, 1355.

(78) Garg, A. C.; Mai, Y.-W. *Compos. Sci. Technol.* **1988,** *31*, 179.

(79) Garg, A. C.; Mai, Y.-W. *Compos. Sci. Technol.* **1988,** *31*, 225.

(80) Personal communication with H.-J. Sue.

(81) Xiao, K.; Ye, L. *Polym. Eng. Sci.* **2000,** *40*, 70.

(82) Kojima, Y.; Usuki, A.; Kawasumi, M.; Okada, A.; Fukushima, Y.; Kurauchi, T.; Kamigaito, O. *J. Mater. Res.* **1993,** *8*, 1185.

(83) Kojima, Y.; Usuki, A.; Kawasumi, M.; Okada, A.; Kurauchi, T.; Kamigaito, O. *J. Polym. Sci. Polym. Chem.* **1993,** *31*, 983.

(84) Usuki, A.; Kojima, Y.; Kawasumi, M.; Okada, A.; Fukushima, Y.; Kurauchi, T.; Kamigaito, O. *J. Mater. Res.* **1993,** *8*, 1179.

(85) Yano, K.; Usuki, A.; Okada, A.; Kurauchi, T.; Kamigaito, O. *J. Polym. Sci. Polym. Chem.* **1993,** *31*, 2493.

(86) Liu, J.; Boo, W. J.; Clearfield, A.; Sue, H. J. *Materials and Manufacturing Processes* **2006,** *21*, 143.

(87) Boo, W. J.; Liu, J.; Sue, H. J. *Mater. Sci. Technol.* **2006,** *22*, 829.

(88) Hajduk, D. A.; Harper, P. E.; Gruner, S. M.; Honeker, C. C.; Thomas, E. L.; Fetters, L. J. *Macromolecules* **1995,** *28*, 2570.

(89) Matsen, M. W.; Bates, F. S. *Macromolecules* **1996,** *29*, 1092.

(90) Schulz, M. F.; Khandpur, A. K.; Bates, F. S.; Almdal, K.; Mortensen, K.; Hajduk, D. A.; Gruner, S. M. *Macromolecules* **1996,** *29*, 2857.

(91) Bates, F. S.; Fredrickson, G. H. *Physics Today* **1999,** *52*, 32.

(92) Kinning, D. J.; Winey, K. I.; Thomas, E. L. *Macromolecules* **1988,** *21*, 3502.

(93) Kinning, D. J.; Thomas, E. L.; Fetters, L. J. *Macromolecules* **1991,** *24*, 3893.

(94) Koizumi, S.; Hasegawa, H.; Hashimoto, T. *Makromol. Chem. Macromol. Symp.* **1992,** *62*, 75.

(95) Matsen, M. W. *Macromolecules* **1995,** *28*, 5765.

(96) Bates, F. S.; Maurer, W. W.; Lipic, P. M.; Hillmyer, M. A.; Almdal, K.; Mortensen, K.; Fredrickson, G. H.; Lodge, T. P. *Phys. Rev. Lett.* **1997,** *79*, 849.

(97) Zhang, L.; Eisenberg, A. *Science* **1995,** *268*, 1728.

(98) Hajduk, D. A.; Kossuth, M. B.; Hillmyer, M. A.; Bates, F. S. *J. Phys. Chem. B* **1998,** *102*, 4269.

(99) Alexandridis, P.; Spontak, R. J. *Current Opinion in Colloid & Interface Science* **1999,** *4*, 130.

(100) Discher, B. M.; Won, Y. Y.; Ege, D. S.; Lee, J. C.-M.; Bates, F. S.; Discher, D. E.; Hammer, D. A. *Science* **1999,** *284*, 1143.

(101) Discher, B. M.; Hammer, D. A.; Bates, F. S.; Discher, D. E. *Current Opinion in Colloid & Interface Science* **2000,** *5*, 125.

(102) Lodge, T. P.; Pudil, B.; Hanley, K. J. *Macromolecules* **2002,** *35*, 4707.

(103) Won, Y. Y.; Brannan, A.; Davis, H. T.; Bates, F. S. *J. Phys. Chem. B* **2002,** *106*, 3354.

(104) Mijovic, J.; Shen, M.; Sy, J. W.; Mondragon, I. *Macromolecules* **2000,** *33*, 5235.

(105) Guo, Q.; Thomann, R.; Gronski, W.; Thurn-Albrecht, T. *Macromolecules* **2002,** *35*, 3133.

(106) Kosonen, H.; Ruokolainen, J.; Nyholm, P.; Ikkala, O. *Macromolecules* **2001,** *34*, 3046.

(107) Kosonen, H.; Ruokolainen, J.; Nyholm, P.; Ikkala, O. *Polymer* **2001,** *42*, 9481.

(108) Kosonen, H.; Ruokolainen, J.; Torkkeli, M.; Serimaa, R.; Nyholm, P.; Ikkala, O. *Macromol. Chem. Phys.* **2002,** *203*, 388.

(109) Bates, F. S.; Fredrickson, G. H. *Annu. Rev. Phys. Chem.* **1990,** *41*, 525.

(110) Bates, F. S.; Schulz, M. F.; Khandpur, A. K.; Forster, S.; Rosedale, J. H.; Almdal, K.; Mortensen, K. *Faraday Discuss* **1994,** *98*, 1.

(111) Forster, S.; Khandpur, A. K.; Zhao, J.; Bates, F. S.; Hamley, I. W.; Ryan, A. J.; Bras, W. *Macromolecules* **1994,** *27*, 6922.

(112) Zhao, J.; Majumdar, B.; Schulz, M. F.; Bates, F. S.; Almdal, K.; Mortensen, K.; Hajduk, D. A.; Gruner, S. M. *Macromolecules* **1996,** *29*, 1204.

(113) Rosoff, M., *Vesicles*. Marcel Dekker: New York, NY, 1996.

(114) Ding, J.; Liu, G. *Macromolecules* **1997,** *30*, 655.

(115) Konak, C.; Oupicky, D.; Chytry, V.; Ulbrich, K. *Macromolecules* **2000,** *33*, 5318.

(116) Nardin, C.; Hirt, T.; Leukel, J.; Meier, W. *Langmuir* **2000,** *16*, 1035.

(117) Shen, H.; Eisenberg, A. *Angew. Chem. Int. Ed.* **2000,** *39*, 3310.

(118) Ritzenthaler, S.; Court, F.; David, L.; Girard-Reydet, E.; Leibler, L.; Pascault, J. P. *Macromolecules* **2002,** *35*, 6245.

(119) Hillmyer, M. A.; Bates, F. S. *Macromolecules* **1996,** *29*, 6994.

(120) Lesser, A. J.; Crawford, E. *J. Appl. Polym. Sci.* **1997,** *66*, 387.

(121) Nielsen, L. E. *J. Macromol. Sci.* **1969,** *C3*, 69.

(122) Nielsen, L. E.; Landel, R. F., *Mechancial Properties of Polymers and Composites*. 2 ed.; Marcel Dekker: New York, NY, 1994.

(123) Sue, H.-J.; Pearson, R. A.; Parker, D. S.; Huang, J.; Yee, A. F. *Polym. Prepr.* **1988,** *29*, 147.

(124) Sue, H.-J.; Yee, A. F. *J. Mater. Sci.* **1993,** *28*, 2975.

(125) Holik, A. S.; Kambour, R. P.; Hobbs, S. Y.; Fink, D. G. *Microstruct. Sci.* **1979,** *7*, 357.

(126) Sue, H.-J.; Yang, P. C.; Garcia-Meitin, E. I.; Bishop, M. T. *J. Mater. Sci. Letters* **1993,** *12*, 1463.

(127) Kinloch, A. J.; Williams, J. G. *J. Mater. Sci.* **1980,** *15*, 987.

(128) Dompas, D.; Groeninckx, G. *Polymer* **1994,** *35*, 4743.

(129) Fond, C.; Lobbrecht, A.; Schirrer, R. *Int. J. Fract.* **1996,** *77*, 141.

(130) Smit, R. J. M.; Brekelmans, W. A. M.; Meijer, H. E. H. *J. Mater. Sci.* **2000,** *35*, 2869.

(131) Bucknall, C. B., In *The Physics of Glassy Polymers*, 2 ed.; Haward, R. N.; Young, R. J., Eds. Chapman & Hall: London, UK, 1997; p 363.

(132) Hasan, O. A.; Boyce, M. C.; Berko, S. *J. Polym. Sci., Part B: Polym. Phys.* **1993,** *31*, 185.

(133) Hristov, H. A.; Bolan, B.; Yee, A. F.; Xie, L.; Gidley, D. W. *Macromolecules* **1996,** *29*, 8507.

(134) Bartos, J.; Bandzuch, P.; Sausa, O.; Kristiakova, K.; Kristiakova, J.; Kanaka, T.; Jenninger, W. *Macromolecules* **1997,** *30*, 6906.

(135) Bucknall, C. B. *J. Polym. Sci., Part B: Polym. Phys.* **2007,** *45*, 1399.

(136) Gent, A. N. *J. Polym. Sci. Symp.* **1974,** *48*, 1.

(137) Harper, C. A., *Handbook of Plastics and Elastomers*. McGraw-Hill Book Company: New York, NY, 1975.

(138) Jho, J. Y.; Yee, A. F. *Macromolecules* **1991,** *24*, 1905.

(139) Xiao, C.; Jho, J. Y.; Yee, A. F. *Macromolecules* **1994,** *27*, 2761.

(140) Lee, P. L.; Kowalewski, T.; Poliks, M. D.; Schaefer, J. *Macromolecules* **1995,** *28*, 2476.

(141) Menard, K. P., *Dynamic Mechanical Analysis: A Practical Introduction*. CRC Press: Boca Raton, FL, 1999.

(142) Wendorf, J. H.; Fischer, E. W. *Kolloid-Zeitschrift & Zeitschrift für Polymere* **1973,** *251*, 876.

(143) David, L.; Vigier, G.; Etienne, S.; Faivre, A.; Soles, C. L.; Yee, A. F. *J. Non-Cryst. Solids* **1998,** *235*, 383.

(144) Yang, L.; Hristov, H. A.; Yee, A. F.; Gidley, D. W.; Bauchiere, D.; Halary, J. L.; Monnerie, L. *Polymer* **1995,** *36*, 3997.

(145) Iijima, T.; Yoshioka, N.; Tomoi, M. *Eur. Polym. J.* **1992,** *28*, 573.

(146) Iijima, T.; Miura, S.; Fukuda, W.; Tomoi, M. *Eur. Polym. J.* **1993,** *29*, 1103.

(147) Lu, F.; Plummer, C. J. G.; Cantwell, W. J.; Kausch, H. H. *Polym. Bull.* **1996,** *37*, 399.

(148) Lu, F.; Kausch, H. H.; Cantwell, W. J.; Fischer, M. *J. Mater. Sci. Letters* **1996,** *15*, 1018.

(149) Kishi, H.; Shi, Y. B.; Huang, J.; Yee, A. F. *J. Mater. Sci.* **1997,** *32*, 761.

(150) Kishi, H.; Shi, Y. B.; Huang, J.; Yee, A. F. *J. Mater. Sci.* **1998,** *33*, 3479.

(151) Kang, B. U.; Jho, J. Y.; Kim, J. K.; Lee, S. S.; Park, M.; Lim, S.; Choe, C. R. *J. Appl. Polym. Sci.* **2001,** *79*, 38.

(152) Sue, H. J.; Bertram, J. L.; Garcia-Meitin, E. I.; Wilchester, J. W.; Walker, L. L. *Colloid. Polym. Sci.* **1994,** *272*, 456.

(153) Ferry, J. D., *Viscoelastic Properties of Polymers*. 3 ed.; John Wiley & Sons: New York, NY, 1980.

(154) Nielsen, L. E. *J. Macromol. Sci.* **1969,** *C3*, 69.

(155) Timm, D. C.; Ayorinde, A. J.; Foral, R. F. *Br. Polym. J.* **1985,** *17*, 227.

(156) Webb, T. W.; Aifantis, E. C. *Mech. Res. Comm.* **1997,** *24*, 115.

(157) Barry, D. B.; Delatycki, O. *J. Appl. Polym. Sci.* **1989,** *38*, 339.

(158) Karger-Kocsis, J.; Czigany, T. *Polym. Eng. Sci.* **2000,** *40*, 1809.

(159) Imasawa, Y.; Matsuo, M. *Polym. Eng. Sci.* **1970,** *10*, 261.

(160) Kusaka, T.; Hojo, M.; Mai, Y.-W.; Kurokawa, T.; Nojima, T.; Ochiai, S. *Compos. Sci. Technol.* **1998,** *58*, 591.

(161) Todo, M.; Takahashi, K.; Beguelin, P.; Kausch, H. H. *Compos. Sci. Technol.* **2000,** *60*, 763.

(162) Jiang, W.; Tsang, F. F. Y.; Tjong, S. C.; Li, R. K. Y.; Kim, J. K.; Mai, Y.-W. *Appl. Compos. Mater.* **2001,** *8*, 361.

(163) Jacob, G. C.; Starbuck, J. M.; Fellers, J. F.; Simunovic, S.; Boeman, R. G. *J. Appl. Polym. Sci.* **2006,** *100*, 695.

(164) Julien, O.; Beguelin, P.; Monnerie, L.; Kausch, H. H., In *Toughened Plastics II*, Riew, C. K.; Kinloch, A. J., Eds.; *Adv. Chem. Ser.* **1996**, *252*, 233.

(165) Raghavan, D.; He, J.; Hunston, D.; Hoffman, D. *J. Adhesion* **2002,** *78*, 723.

(166) Mark, J. E., *Polymer Data Handbook*. Oxford University Press: New York, NY, 1999.

(167) Barton, J. M. *Adv. Polym. Sci.* **1985,** *72*, 112.

(168) Rozenberg, B. A. *Adv. Polym. Sci.* **1986,** *75*, 115.

(169) Bellenger, V.; Verdu, J.; Francillette, I.; Hoarau, P.; More, E. *Polymer* **1987,** *28*, 1079.

(170) Larranaga, M.; Mondragon, I.; Riccardi, C. C. *Polym. Int.* **2007,** *56*, 426.

VITA

Dr. Jia (Daniel) Liu obtained his B.S. in polymer materials and engineering from Fudan University (Shanghai, China) in 2002, and M.Phil. in mechanical engineering from The Hong Kong University of Science and Technology (Kowloon, Hong Kong) in 2004. He has completed the Ph.D. program in materials science and engineering at Texas A&M University (College Station, Texas, United States) in 2009. His research interests include polymers and polymer nanocomposites, structure-property relationship, mechanical and fracture behaviors, and polymer toughening and strengthening. He is a current member of Sigma Xi, Society of Plastics Engineers (SPE), Materials Research Society (MRS), American Society of Mechanical Engineers (ASME), and International Microelectronics and Packaging Society (IMAPS). Dr. Liu's permanent email address is danieljliu@gmail.com.

SELECTED JOURNAL PUBLICATIONS

1. **J. Liu**, H.-J. Sue, Z.J. Thompson, F.S. Bates, M. Dettloff, G. Jacob, N. Verghese, H. Pham, "Strain Rate Effect on Toughening of Nano-Sized PEP-PEO Block Copolymer Modified Epoxy," *Acta Materialia*, In press (2009).
2. L. Sun, **J. Liu**, S. Kirumakki, E.D. Schwerdtfeger, R.J. Howell, K. Al-Bahily, S.A. Miller, A. Clearfield, H.-J. Sue, "Polypropylene Nanocomposites Based on Designed Synthetic Nanoplatelets," *Chemistry of Materials*, In press (2009).
3. **J. Liu**, H.-J. Sue, Z.J. Thompson, F.S. Bates, M. Dettloff, G. Jacob, N. Verghese, H. Pham, "Effect of Crosslink Density on Fracture Behavior of Model Epoxies Containing Block Copolymer Nanoparticles," *Polymer*, Submitted (2009).
4. **J. Liu**, H.-J. Sue, Z.J. Thompson, F.S. Bates, M. Dettloff, G. Jacob, N. Verghese, H. Pham, "Nano-Cavitation in Self-Assembled Amphiphilic Block Copolymer-Modified Epoxy," *Macromolecules*, 41, 7616-7624 (2008).
5. **J. Liu**, W.-J. Boo, A. Clearfield, H.-J. Sue, "Intercalation and Exfoliation: A Review on Morphology of Polymer Nanocomposites Reinforced by Inorganic Layer Structures," *Materials and Manufacturing Processes*, 20, 143-151 (2006).
6. W.-J. Boo, **J. Liu**, H.-J. Sue, "Fracture Behaviour of Nanoplatelet Reinforced Polymer Nanocomposites," *Materials Science and Technology*, 22, 829-834 (2006).